Fundamental Studies of Enzymes: From Single Molecule Kinetics to Conformational Studies

A dissertation submitted by

Marcin J. Rojek

In partial fulfillment of the requirements for the degree of

Doctor of Philosophy

In

Chemistry

TUFTS UNIVERSITY

February 2015

Advisor: Professor David R. Walt

Acknowledgements

There are many people who contributed to this thesis and supported me during my doctorate training. Without the help and guidance of my advisor, committee members, friends, and family it would have never been possible for me to obtain this degree.

I would like to thank my advisor, Dr. David R. Walt, who gave me the opportunity to pursue my dreams and guided me in graduate school. As a mentor, he taught me the importance of having well-designed experiments and how to approach intractable problems with new ideas and solutions. I appreciate the freedom that I had in his lab as well as the comfort of being able to pursue new ideas.

I would like to thank Professors Elena Rybak-Akimova and Krishna Kumar for their guidance and patience and for serving as my research committee members. I would like to thank Professor Dagmar Ringe for serving as an independent examination committee on my thesis.

I would like to thank my fellow group members, past and present, especially Professor Hans Gorris, who introduced me to fundamental enzymology research. I would like to give a special thanks to my friends outside of the lab as well as to those who helped me with my research projects: Pratyusha Mogalisetti, Shonda Gaylord, Milena Milutinovic, Elena Benito-Peña, Maël Manesse, Stephanie Schubert, Shuai Nie, Shazia Baig, and the rest of the lab members. Special thanks also go to Venkata Subramanian Raman from the Kumar lab for his support and help.

I would like to thank the Haggett family for their support and for giving me the opportunity to live and study in the United States.

Finally, I would like to thank my family, especially my mom and my dad for their support and encouragement, and my girlfriend Ania Frackowiak for her understanding, patience, and support. All of you helped make my life enjoyable during my time in the PhD program.

Abstract

This thesis covers the usage of fiber optic arrays developed in the Walt lab for sensitive detection of individual molecules. We were able to apply the fiber optic platform to study the activities and conformational changes of individual enzymes. For this purpose, we developed a heating stage to introduce heat pulses, as described in the following chapters.

Chapter 1 describes the current detection approaches used to study single enzyme molecules. Recent advances in technology have promoted the development of many new techniques for single molecule studies; however, this thesis focuses only on fluorescent based studies. Chapter 1 only covers general approaches. Detailed descriptions of all currently used fluorescent techniques would be impossible to cover within the scope of this thesis.

Chapter 2 describes in detail the development and the basic principles of the platform used in our single molecule research. In addition to the previously described fiber bundles and sealing techniques, this section also describes the implementation of a heating stage. The heating platform allows us to study single enzymes with respect to temperature variations. Precise control of the temperature during the experiments allows us to measure the activities of enzymes at different temperatures as well to study conformational changes and denaturation.

In Chapter 3 we attempted to unearth the origins of the stable heterogeneity in activities of individual enzymes. We performed heated pulse experiments and found that the activities of individual enzymes changed after heating pulses were applied, but the average activity remained constant. From this experiment we concluded that enzyme conformation must play the leading role in the distribution in activity.

In Chapter 4 we used a temperature ramp to calculate the activation energies of individual enzymes. We were able to monitor the activities of individual β-galactosidase enzymes with respect to increased temperature. In addition to activation energy, we were able to obtain both entropy and enthalpy values by using the Eyring-Polanyi equation. We showed that the activation energy is greatly distributed amongst the enzyme molecules.

In Chapter 5 we performed single molecule experiments on different β-glucuronidase mutants. By using the heating platform, we demonstrated that at the single molecule level a fraction of individual enzymes behave as thermal switches. These enzymes lack activity at room temperature, but become active when treated with a heating pulse. “Thermal switches” could be beneficial for developing specific drug carriers, where a thermal pulse would trigger downstream enzymatic reactions.

Finally, Chapter 6 describes the thermal denaturation of monomeric enzymes as well as refolding studies performed at the single molecule level. Gaining a more fundamental understanding of how individual enzymes fold and work within a population can provide insight into how they affect downstream biochemical processes as well as how folding and mis-folding occur.

Table of Contents

Chapter 6: Single Molecule Anfinsen Experiment. Refolding Studies of Single RNase A Enzyme

Chapter 1: Fluorescence Based Analysis of Enzymes at the Single Molecule Level

1.1 Introduction

Enzymes play a vital role in living organisms, catalyzing nearly all of the biological reactions that take place. The activity of enzymes has been studied extensively for over a century and many important principles have been described, such as Michaelis-Menten (MM) kinetics. The MM model describes the kinetics of enzymes at steady state. In short; a substrate (S) combines with the enzyme to yield the enzyme substrate complex (ES), which can be turned over to either the product enzyme complex (EP) or dissociate back into the enzyme and substrate. This process is described in Eq 1.1, where k_1, k_2 and k_{-1} are rate constants for each reaction step.

$$E + S \underset{k_{-1}}{\overset{k_1}{\rightleftarrows}} ES \overset{k_2}{\rightarrow} EP \rightarrow E + P \quad \text{(Eq. 1.1)}$$

When the enzyme concentration is much lower than the substrate concentration, the reaction can reach steady state where:

$$\frac{d[ES]}{dt} = 0 \quad \text{(Eq. 1.2)}$$

The reaction velocity can be obtained from Eq 1.3:

$$v = \frac{v_{max}[S]}{K_M + [S]} \qquad \text{(Eq. 1.3)}$$

This equation is known as the Michaelis-Menten equation, where v_{max} is the maximum velocity of the reaction and K_M is defined as the Michaelis-Menten constant an apparent dissociation

constant of the enzyme-substrate complex (ES).(*1*) The MM equation holds for most enzymatic reactions, including more complex reactions with several intermediates along the reaction pathway. However, classical bulk experiments involve large quantities of enzyme molecules and only provide an average rate constant for the entire enzyme population and any fluctuations in activity within a single enzyme or between two different enzyme molecules are easily masked. To fully understand protein dynamics and behavior, new approaches based on single molecule analysis must be developed. Single molecule techniques enable the study of stochastic events pertaining to individual molecules as well as the ability to directly observe individual steps or intermediates in biochemical reactions.(*2*) In the simplest case, it can be expected that bulk and single molecule experiments performed on a homogeneous enzyme population would have similar results. Theoretically, each molecule should produce the same number of product molecules over time within the limit of the expected distribution of the square root of the number of product molecules, due to the stochastic nature of the event. However, single molecule studies have revealed that the activity of individual enzymes is heterogeneous. The goals of the single molecule experiments described in this thesis are to understand this observed heterogeneity and to determine the origins of this behavior.

1.2 Historical perspective

The first single molecule experiments were developed by Rotman and coworkers in 1961.(*3*) In these experiments, a dilute aqueous solution of the enzyme β-galactosidase was dispersed within an oil medium. The resulting water-in-oil emulsion contained water droplets with individually encapsulated β-galactosidase molecules. Upon cleavage of the substrate, a fluorescent product was generated and measured over time (Figure 1.1).

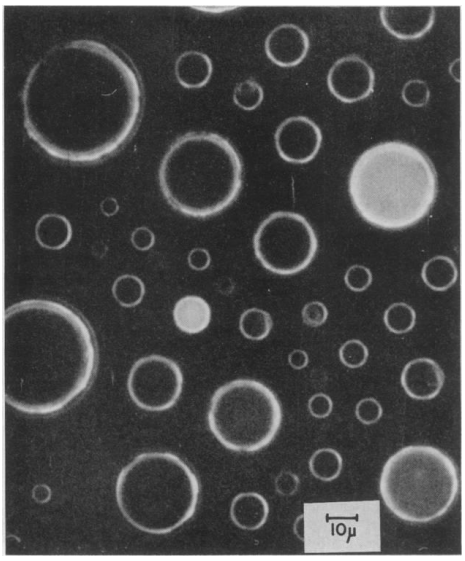

Figure 1.1. Emulsion of water droplets containing β-galactosidase substrate in oil. Some of the droplets contain single enzyme molecules, which over time turnover the non-fluorescent substrate to produce fluorescent product.(*3*)

This new single molecule method was also used to investigate heat shock effects on enzymes.(*3*) Researchers observed that upon heat shock, individual enzymes either retained full activity or were completely inactivated. This result could only be obtained from the examination of individual enzymes and would have been impossible using traditional ensemble measurements. The previously described experiments were completed approximately 30 years ago. With the development of new instrumentation and techniques, more advanced experiments have been performed. In 1995, single molecule studies on lactate dehydrogenase (LDH) were carried out. In this study, researchers used narrow capillaries to isolate individual enzyme molecules.(*4*) Through experimentation it was discovered that the turnover numbers from individual LDH molecules were distinct and stable over long periods of time. The existence of a long-lived conformational state, later called static heterogeneity, was hypothesized.

The next advance in single molecule research was the ability to monitor one substrate turnover at a time. For example, Figure 2A, B shows studies performed on single cholesterol oxidase enzymes where the reduction of the flavin adenine dinucleotide (FAD) coenzyme was monitored.(*5*, *6*)

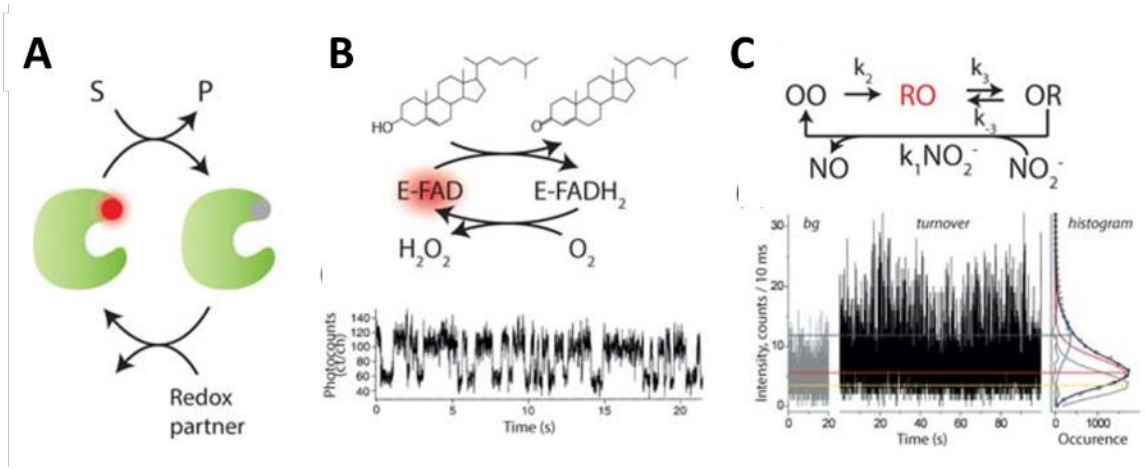

Figure 1.2. (A) General description of fluorescent cofactor based assays. (B) Real time observation of turnover cycles for cholesterol oxidase using the cofactor FAD as a fluorescent reporter.(*5*) (C) Direct observation of individual nitrite reductase turnovers using a chemically attached chromophore.(*7*, *8*)

FAD is naturally fluorescent when oxidized and is non-fluorescent upon reduction. In these experiments, a redox reaction was performed to study cholesterol oxidase, where the oxidation of cholesterol was accompanied by the reduction of the FAD coenzyme. The real time observation of individual substrate turnovers for single enzymes showed that enzyme molecules exhibit a 'memory effect", where the consecutive substrate turnovers are not independent. Despite the appeal of this technique, the use of cofactors as fluorescent reporters has several drawbacks, including very low quantum yields and photostabilities. To overcome these limitations, Kuznetsova *et al*. used the photostable chromophore Atto-655 attached covalently to a nitrate reductase enzyme. Nitrate reductase has two copper centers per monomer in which the transfer

of electrons occurs for every turnover. The copper cofactors are not fluorescent; however, in an oxidized state they can efficiently quench the attached chromophore (Figure1. 2, A, C).(*8*)

Today, single enzyme studies are not limited to solely measuring the activity of single enzymes. Single molecule techniques have been developed to study conformational changes,(*9, 10*) folding,(*11, 12*) and protein-protein interactions(*13*) among other applications. This chapter focuses briefly on fluorescence based techniques as all of the experiments described in this thesis are based on fluorescence microscopy.

1.3 Fluorescent reporter systems

Although many different fluorescent techniques are used for studying single enzymes, they can be separated with respect to the different fluorescent reporters used for single enzyme detection. Four different reporter types can be distinguished; however, multiple different versions of each type can also be described.

1. *Fluorescent substrates*

   Fluorescent substrates are used to report binding and dissociation events at the single molecule level. However, they do not provide information regarding the enzymatic reaction, such as the conversion of substrate to the product. Fluorescent substrates contain fluorescent dyes that do not interfere with the enzyme activity. Funatsu *et al*. studied ATP cleavage reactions via the molecular motor protein myosin using Cy3 labeled ATP molecules as a fluorescent substrate.(*14*)

2. *Fluorogenic substrates*

Fluorogenic substrates result in increased fluorescence signal upon enzymatic reaction. They are the most common enzymatic reporters and have been successfully used for single molecule studies of multiple enzymes, such as proteases,(*15*) lipases,(*16*) and glycosidases.(*17*) Several fluorogenic substrates for oxidoreductases also exist, where the non-fluorescent substrate becomes fluorescent upon oxidation or reduction.(*18*)

3. *Fluorescent cofactors*

Several enzyme cofactors, such as flavin mononucleotide (FMN) and flavin adenine dinucleotide (FAD), are fluorescent in an oxidized state and non-fluorescent in a reduced state. Enzyme cofactors can be used as a enzymatic reaction reporters for flavoenzymes, where they undergo redox cycles. The advantage of these reporters is that they are naturally occurring molecules; however, their low quantum yield and poor photostability limit the number of turnovers that can be observed. These drawbacks challenge both statistical analysis and interpretation.

4. *Förster resonance energy transfer (FRET) substrates*

Förster resonance energy transfer (FRET) involves the transfer of non-radiative energy from an excited donor to a ground state acceptor chromophore via long-range dipole-dipole coupling.(*19-21*) FRET pairs are sensitive reporters for distance changes between chromophores on a length scale between 2 to 8 nm. They are also very useful as reporters when studying enzymatic conformational changes.(*22*)

Single molecule studies are not limited to the reporter systems described above. Only the most important and most commonly used systems for single molecule studies were mentioned. In the Walt lab, several of the systems presented above have been explored, such as fluorescent cofactors (NADH), fluorogenic substrates (resorufin based substrates), and FRET substrates. The majority of the work described in this thesis was performed using fluorogenic (**Chapter 3-5**) and FRET substrates (**Chapter 6**).

1.4 Assays and Encapsulation

In typical single molecule assays, the enzyme in question is diluted and the assay volume is reduced to the point where there is a high probability that only one enzyme molecule is contributing to the observed reaction. There are currently two different assays used for single enzyme studies. The first assay type records individual turnovers from single molecules and the second type records multiple turnovers per single enzyme (Figure 1.3, A, B). In the single turnover assay, it is possible to observe individual events. For example, the fluorescent substrate can be distinguished when it is bound to the enzyme. The time period where the substrate is bound to the enzyme can provide a direct measure of the turnover rate. In this approach, the stochastic nature of enzymatic activity is evident. Although it takes many observations to build up the average behavior of the enzyme, this method is an excellent tool for studying the dynamic heterogeneity in activities.

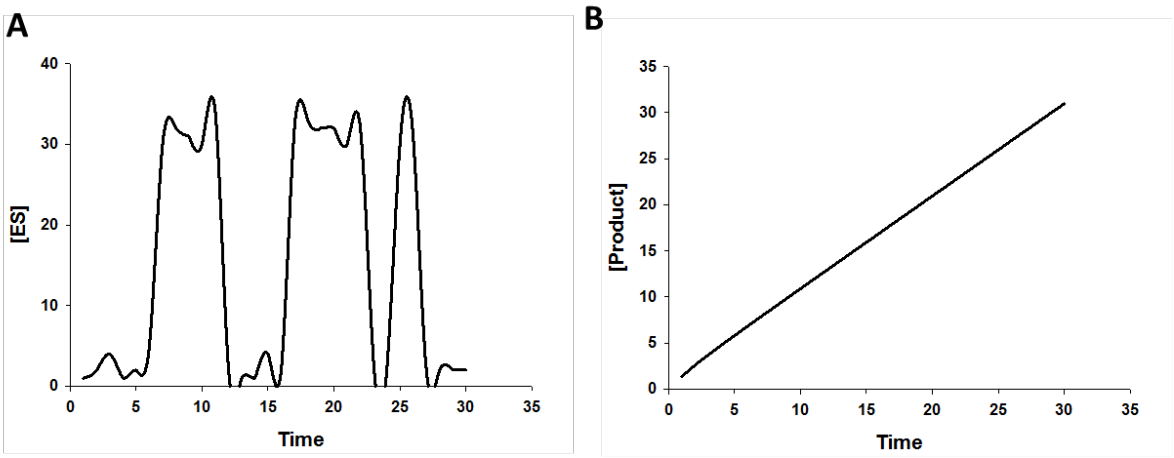

Figure 1.3. Schematic representation of different single enzyme assays. (A) The output of the single substrate turnover, where the fluorescence bursts are visible due to enzymatic activity. (B) The product formation measured for only one enzyme molecule in the multiple turnover assay.

In assays with multiple turnovers per single enzyme, individual enzymes turn over multiple substrate molecules within the enclosed volume. The activity of the enzyme is then averaged over time. This approach has several advantages compared to single turnover techniques. First, the detection system does not require single substrate molecule detection sensitivity and hence observations can be obtained using a standard fluorescence microscope. Moreover, this method does not require that the studied enzyme be immobilized on the surface. Thus, the observed heterogeneity in activity is unambiguously related to the intrinsic behavior of the enzyme and is not influenced by surface enzyme immobilization.

In order to observe enzyme reactions that involve multiple turnovers per single enzyme molecule, several requirements must be met. First, the enzyme must be enclosed with a sufficient quantity of substrate. Second, the volume of the reaction vessel must be small enough such that a high local concentration of fluorescence product is generated. Finally, a large number of individual vessels must fit within the field of view so that proper statistics can be obtained.

Several different confinement techniques are used across single enzyme research. For example, enzyme confinement has been performed inside of virus capsids using horseradish peroxidase.(*23*) Another method discussed previously involves the confinement of enzymes inside emulsion droplets.(*3, 24*) Individual enzymes have also been separated successfully using a capillary method based on capillary electrophoresis.(*4, 25-27*)

The last confinement method discussed in this chapter utilizes femtoliter arrays. The wells within such arrays have been prepared using various materials, such a glass and PDMS. Compared to experiments using droplets, well sizes within an array are extremely uniform. The wells are filled by pipetting a solution containing dilute enzyme and highly concentrated substrate. The enzyme concentration is chosen such that at least 90% of the wells do not contain an enzyme and the rest are filled with only one enzyme molecule. The wells can be sealed using various methods, creating individual reaction chambers and enabling the study of single enzyme activity.(*28, 29*) Due to the intrinsic rigidness and simplicity of the femtoliter array system, this method is commonly used for single enzyme studies. This thesis presents single molecule studies obtained using optical fiber bundle arrays, which are described in detail in Chapter 2.

1.5 Summary

In this chapter, we have described the different techniques used for studying single enzyme molecules. We introduced the fluorescence-based techniques, which are commonly used for single molecule experiments and the different ways to confine individual enzymes. By employing a single molecule approach, in following chapters we will attempt to answer some of the most recurring questions related to single enzyme experiments: what are the origins of the

static heterogeneity observed in single enzyme experiments and how do changes in primary structure affect enzymatic activity?

1.6 References

1. A. Fersht, *Structure and mechanism in protein science: a guide to enzyme catalysis and protein folding*. (Macmillan, 1999).
2. X. S. Xie, H. P. Lu, Single-molecule enzymology. *Journal of Biological Chemistry* **274**, 15967 (Jun 4, 1999).
3. B. Rotman, Measurement of Activity of Single Molecules of Beta-D-Galactosidase. *P Natl Acad Sci USA* **47**, 1981 (1961).
4. Q. F. Xue, E. S. Yeung, Differences in the Chemical-Reactivity of Individual Molecules of an Enzyme. *Nature* **373**, 681 (Feb 23, 1995).
5. H. P. Lu, L. Y. Xun, X. S. Xie, Single-molecule enzymatic dynamics. *Science* **282**, 1877 (Dec 4, 1998).
6. H. P. Lu, L. Y. Xun, X. S. Xie, Single-molecule spectroscopic study of protein conformational and enzymatic dynamics. *Biophys J* **76**, A136 (Jan, 1999).
7. S. K. H. N. S. Jorgensen, *Biophysical Reviews and Letters* **8**, 137 (2013).
8. S. Kuznetsova *et al*., The enzyme mechanism of nitrite reductase studied at single-molecule level. *P Natl Acad Sci USA* **105**, 3250 (Mar 4, 2008).
9. M. J. Rojek, D. R. Walt, Observing Single Enzyme Molecules Interconvert between Activity States upon Heating. *Plos One* **9**, (Jan 21, 2014).
10. N. S. Hatzakis, Single molecule insights on conformational selection and induced fit mechanism. *Biophys Chem* **186**, 46 (Feb, 2014).
11. L. Edman, R. Rigler, Memory landscapes of single-enzyme molecules. *Proc Natl Acad Sci U S A* **97**, 8266 (Jul 18, 2000).
12. M. Pirchi *et al*., Single-molecule fluorescence spectroscopy maps the folding landscape of a large protein. *Nat Commun* **2**, (Oct, 2011).
13. A. Mashaghi, G. Kramer, D. C. Lamb, M. P. Mayer, S. J. Tans, Chaperone action at the single-molecule level. *Chemical reviews* **114**, 660 (Jan 8, 2014).
14. T. Funatsu, Y. Harada, M. Tokunaga, K. Saito, T. Yanagida, Imaging of Single Fluorescent Molecules and Individual Atp Turnovers by Single Myosin Molecules in Aqueous-Solution. *Nature* **374**, 555 (Apr 6, 1995).
15. A. Y. Chen, A. S. Jani, L. F. Zheng, P. J. Burke, J. P. Brody, Microfabricated Arrays of Cylindrical Wells Facilitate Single-Molecule Enzymology of alpha-Chymotrypsin. *Biotechnology progress* **25**, 929 (Jul-Aug, 2009).
16. J. Tang, Exploring fluorescence intermittency in enzyme reactions of single lipase molecules. *Chem Phys Lett* **458**, 363 (Jun 17, 2008).
17. D. M. Rissin, D. R. Walt, Digital concentration readout of single enzyme molecules using femtoliter arrays and Poisson statistics. *Nano letters* **6**, 520 (Mar, 2006).
18. H. H. Gorris, D. R. Walt, Mechanistic Aspects of Horseradish Peroxidase Elucidated through Single-Molecule Studies. *J Am Chem Soc* **131**, 6277 (May 6, 2009).

19. P. Tinnefeld, M. Sauer, Branching out of single-molecule fluorescence spectroscopy: Challenges for chemistry and influence on biology. *Angew Chem Int Edit* **44**, 2642 (2005).
20. R. Roy, S. Hohng, T. Ha, A practical guide to single-molecule FRET. *Nat Methods* **5**, 507 (Jun, 2008).
21. K. Blank, G. De Cremer, J. Hofkens, Fluorescence-based analysis of enzymes at the single-molecule level. *Biotechnology journal* **4**, 465 (Apr, 2009).
22. T. Ha *et al*., Single-molecule fluorescence spectroscopy of enzyme conformational dynamics and cleavage mechanism. *Proc Natl Acad Sci U S A* **96**, 893 (Feb 2, 1999).
23. M. Comellas-Aragones *et al*., A virus-based single-enzyme nanoreactor. *Nature nanotechnology* **2**, 635 (Oct, 2007).
24. A. I. Lee, J. P. Brody, Single-molecule enzymology of chymotrypsin using water-in-oil emulsion. *Biophys J* **88**, 4303 (Jun, 2005).
25. D. B. Craig, E. A. Arriaga, J. C. Y. Wong, H. Lu, N. J. Dovichi, Studies on single alkaline phosphatase molecules: Reaction rate and activation energy of a reaction catalyzed by a single molecule and the effect of thermal denaturation - The death of an enzyme. *J Am Chem Soc* **118**, 5245 (Jun 5, 1996).
26. G. K. Shoemaker, D. H. Juers, J. M. L. Coombs, B. W. Matthews, D. B. Craig, Crystallization of beta-galactosidase does not reduce the range of activity of individual molecules. *Biochemistry* **42**, 1707 (Feb 18, 2003).
27. E. R. Nichols, D. B. Craig, Single Molecule Assays Reveal Differences Between In Vitro and In Vivo Synthesized beta-Galactosidase. *Protein J* **27**, 376 (Sep, 2008).
28. D. M. Rissin, H. H. Gorris, D. R. Walt, Distinct and long-lived activity states of single enzyme molecules. *J Am Chem Soc* **130**, 5349 (Apr 16, 2008).
29. H. B. Zhang, S. Nie, C. M. Etson, R. M. Wang, D. R. Walt, Oil-sealed femtoliter fiber-optic arrays for single molecule analysis. *Lab on a chip* **12**, 2229 (2012).

Chapter 2: Fiber Optic Arrays and Optical Fiber Platform for Fundamental Studies of Single Enzymes

2.1 Abstract

In this chapter I will describe the methods and platforms that we have developed to study single enzyme molecules. I will describe optical fibers, imaging systems, a heating stage, and experimental considerations related to heating studies.

2.2 Fibers and Optical Fiber Arrays

Optical fibers are used as a platform for the single enzyme kinetics experiments employed in this thesis. An optical fiber consists of a transparent core with a refractive index of n_1 surrounded by a cladding that has a refractive index of n_2 (where $n_2 < n_1$).(*1*) The fiber transmits light by a phenomenon called the total internal reflection (TIR). For total internal reflection to occur, the core and the cladding need to have different refractive indices, and the light needs to enter the fiber at a specific angle called the critical angle (Θ). The core of the fiber is made of silica doped with barium, boron and lanthanum; the cladding is made of silica doped with lead. The differences in glass composition make the two components have different refractive indices: n_1 = 1.69 for the core and n_2 = 1.56 for the cladding in our fibers. The critical angle (Θ) can be obtained from Equation 2.1:

$$\Theta_3 = sin^{-1}\left(\frac{n_2}{n_1}\right) \qquad \text{(Eq 2.1)}$$

The critical angle is related to the entering angle of the ray, called the angle of acceptance. A light ray enters the core at an angle of Θ_1, and travels through the core until it reaches the core-

cladding boundary. As long as the light ray intersects the core-cladding boundary at a small angle (< Θ_2), the ray will be reflected. Total internal reflection occurs only when the angle of incidence at the core-cladding boundary is greater than the critical angle Θ_3 (Figure 2.1). The maximum acceptance angle Θ_1 can be calculated from Equation 2.2:

$$\sin \Theta_1 = \frac{\sqrt{{n_1}^2+{n_2}^2}}{n_0} \quad \text{(Eq. 2.2)}$$

or

$$NA = \sqrt{{n_1}^2 + {n_2}^2} \quad \text{(Eq.2.3)}$$

where n_0, n_1, and n_2 are the refractive indices of air, the fiber core, and the fiber cladding respectively, and NA is defined as the numerical aperture. The higher the NA, the more light will be collected by the fiber.

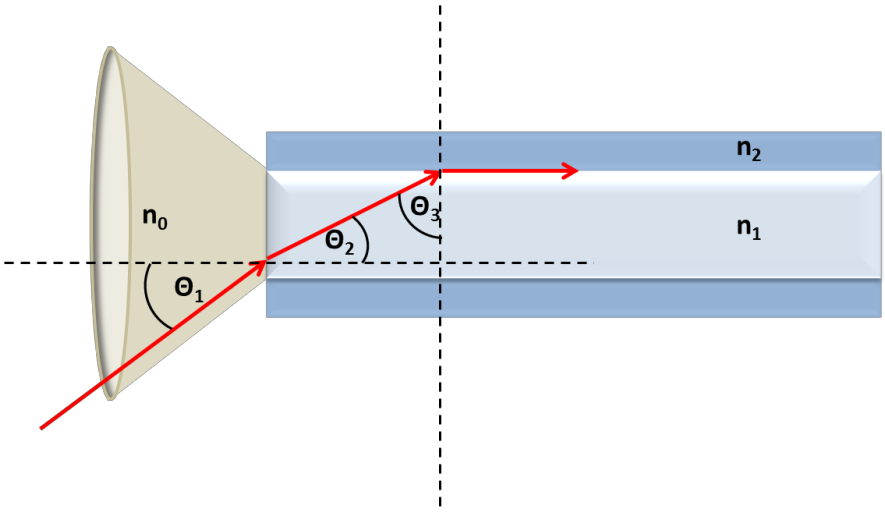

Figure 2.1. Schematic representation of the fiber. The incident light (red) enters the fiber core at angle Θ_1. The light is refracted due to the difference in the refractive indices of air and the fiber core. Only if the angle is greater than Θ_3 will the light be totally reflected and travel through the fiber. The gray cone corresponds to the acceptance angle for the fiber.

Fibers can be categorized according to their modal dispersion and effective pathway. The modal dispersion is determined by the difference in the path length of the light ray due to a difference in the incident angle. Light with a smaller incidence angle Θ_1 will travel a shorter distance than light with a larger Θ_1 because it goes through fewer reflections along the length of the fiber. The modal dispersion also depends on the fiber diameter as well as the incident light wavelength. Depending on the characteristics of the modal dispersion, fibers can be divided into single mode, multimode graded–index, and multimode step-index fibers. A detailed description is beyond the scope of this thesis.

A major advantage of the particular optical fibers described above is their ability to transmit a wide spectrum of light from 400 nm up to 1000 nm (Figure 2.2) with little loss of light intensity. Therefore, these fibers are well suited for fluorescence-based single molecule assays.

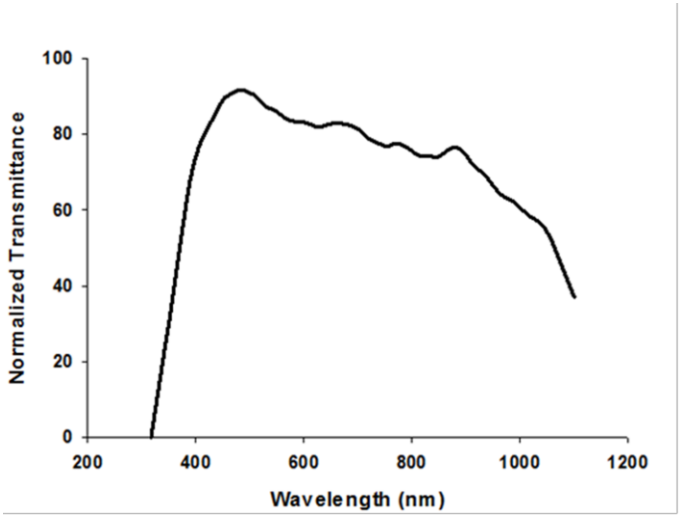

Figure 2.2. Transmittance spectrum of 4.5 cm long fiber performed on the Beckman DU 530 UV/VIS spectrophotometer.

To increase the ability to measure a relatively large population of events, we utilize fiber bundles. Each fiber bundle contains 50,000 hexagonally packed individual fibers (Figure 2.3 A, B). Each fiber bundle includes six fiducial fluorescent fibers located at the center of each face. They are used as reference points for future fiber image alignment or analysis (Figure 2.3 B).

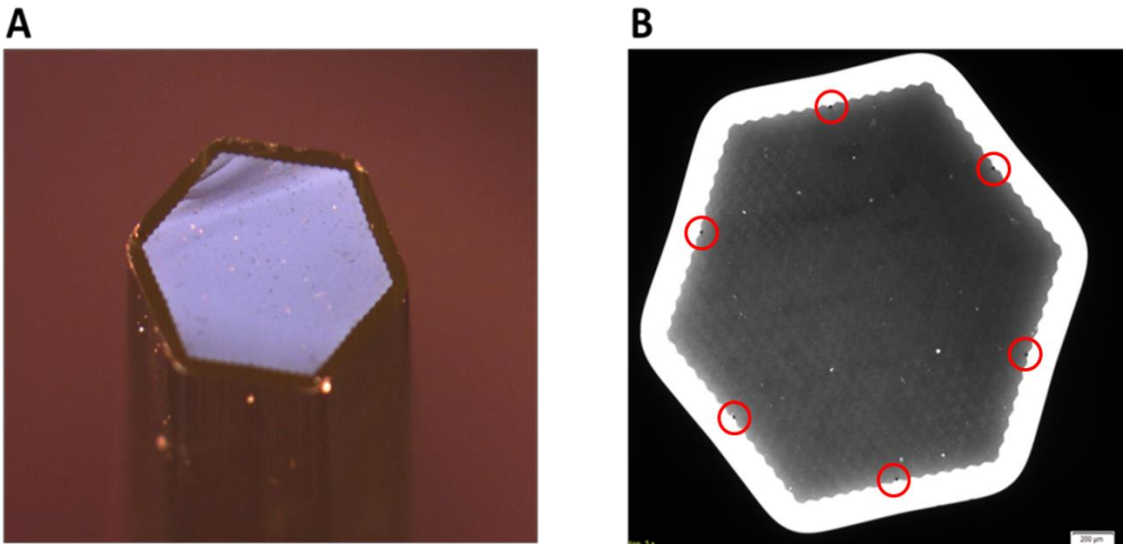

Figure 2.3. Images of the fiber bundle. (A) Side image of the fiber taken by Olympus SZX 16 stereoscope. (B) White light image obtained from the epi-fluorescence microscope (Olympus BX 61). Fiducials are circled in red.

Each individual fiber in the bundle is 4.5 μm in diameter. Because the core and the cladding of the fiber are composed of different materials, it is possible to selectively etch the core to create femtoliter volume reaction chambers (Figure 2.4).

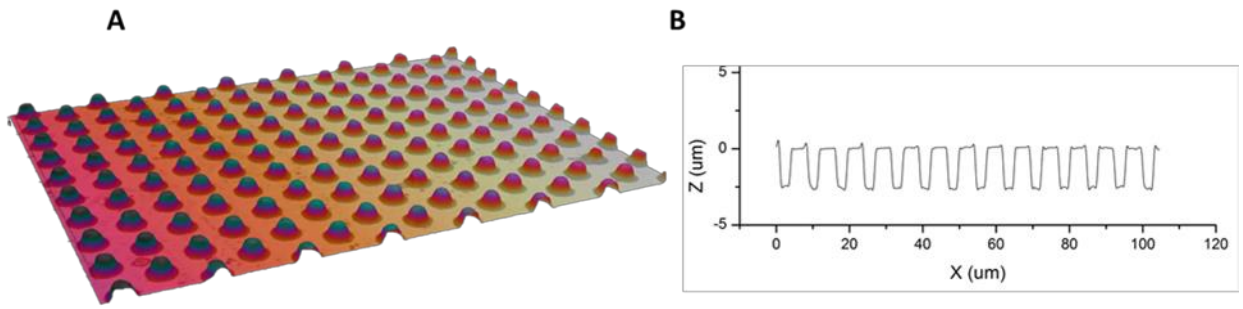

Figure 2.4. Fiber array images. (A) Inverted view of the fiber array and (B) line profile of the well depths. The data were obtained using an optical profiler and the variations in the diameter, area and volume are 0.9%, 1.3% and 3.9%, respectively. (Courtesy of Dr. Eli Zhang from Tufts University and Ben Garland from Zeta Instruments, Inc.)

2.3 Application of Fiber Arrays to Fundamental Studies of Single Enzymes

By taking advantage of fiber bundles' ability to transmit light within a wide spectral range and their ability to create arrays of individual wells, we can use the wells as individual reaction vessels and measure reaction progress via a generated fluorescent signal. A single enzyme trapped within a well can generate locally concentrated product; hence, in the femtoliter wells, a small number of product molecules is sufficient to produce a detectable fluorescent signal. This feature increases the sensitivity of the assay and allows us to study a reaction's progress within a relatively short time. The reaction vessels used throughout this thesis are 46 fL in volume (Figure 2.4); hence, a concentration of 36 pM of enzyme would theoretically yield one molecule per well. However, statistically, the molecules will be normally distributed among the wells, meaning that some vessels would contain multiple molecules and others would be empty(*2*). To ensure that only one molecule is present within any given well, the concentration needs to be significantly lower. For low enzyme concentrations, the Poisson distribution applies, which is

used for predicting the probable distribution of a series of events. By using a large number of wells and a very low concentration of the target molecule (low femtomolar range), we are able to trap individual molecules in the wells. We can precisely calculate the desired number of target molecules per well by using the Poisson distribution (2.4):

$$P_{\mu}(\nu) = e^{-\mu}\left(\frac{\mu^{\nu}}{\nu!}\right) \quad \text{(Eq. 2.4)}$$

where the probability of observing ν events is based on the expected average number μ per trial.(*3*) Table 2.1 presents the probability of having 0, 1, and 2 molecules per well for different analyte concentrations. The optimal concentration of 3.6 pM was used throughout this thesis. The calculated percentage of empty wells is 90% and the percentage of wells containing only one molecule is 9.5 %.

Target (pM)	**P(0) in %**	**P(1) in %**	**P(2) in %**
0.5	94.18	5.65	0.17
1	88.69	10.64	0.64
5	54.88	32.93	9.88

Table 2.1. Probabilities of having 0, 1, or 2 molecules per well for three different analyte concentrations(pM). The values were obtained from Eq. 2.4.

2.4 Custom Imaging System

In this thesis, I used two different custom imaging systems. Both imaging systems are based on fluorescence microscopy. They both include a custom fiber bundle holding stage, which allows us to detect fluorescent signals through the fiber. The imaging systems both measure fluorescence, and include a light source, filter sets, and a CCD camera. In the following section I will introduce the concept of fluorescence and describe the major components of both imaging systems.

2.4.1 Fluorescence

To monitor the progress of reactions we exploited the ability of optical fibers to transmit fluorescence signals. All of the work presented in this thesis is based on the detection of a fluorescent product (fluorophore) generated by an enzymatic reaction.

A fluorophore can absorb a photon when the photon's energy matches the energy needed for an electron to be promoted from the ground state (S_0) to a vibrational level of the first electronic state (S_1).(*4*) The electronic transition takes approximately 10^{-15} s, which is too short for the displacement of nuclei to occur. It takes a few picoseconds for the molecule to reach a new equilibrium. A molecule in this vibrationally-excited state can return to the ground state (S_0) by releasing energy. This process happens through a variety of different pathways. First, an internal non-radiative conversion occurs (k_{is}), in which the electron relaxes to the lowest vibrational level of the first electronic state (S_1). This process takes typically 10^{-12} s.(*5*) From the first excited electronic state (S_1), three major de-excitation processes are possible. First is radiative relaxation, where the fluorophore emits a photon of lower energy than the absorbed photon. This

fluorescence emission has typical lifetimes near 10^{-8} s. The loss of energy is due to the previous vibrational relaxation and causes the photon to have a longer wavelength (Stokes shift).(*5*, *6*)

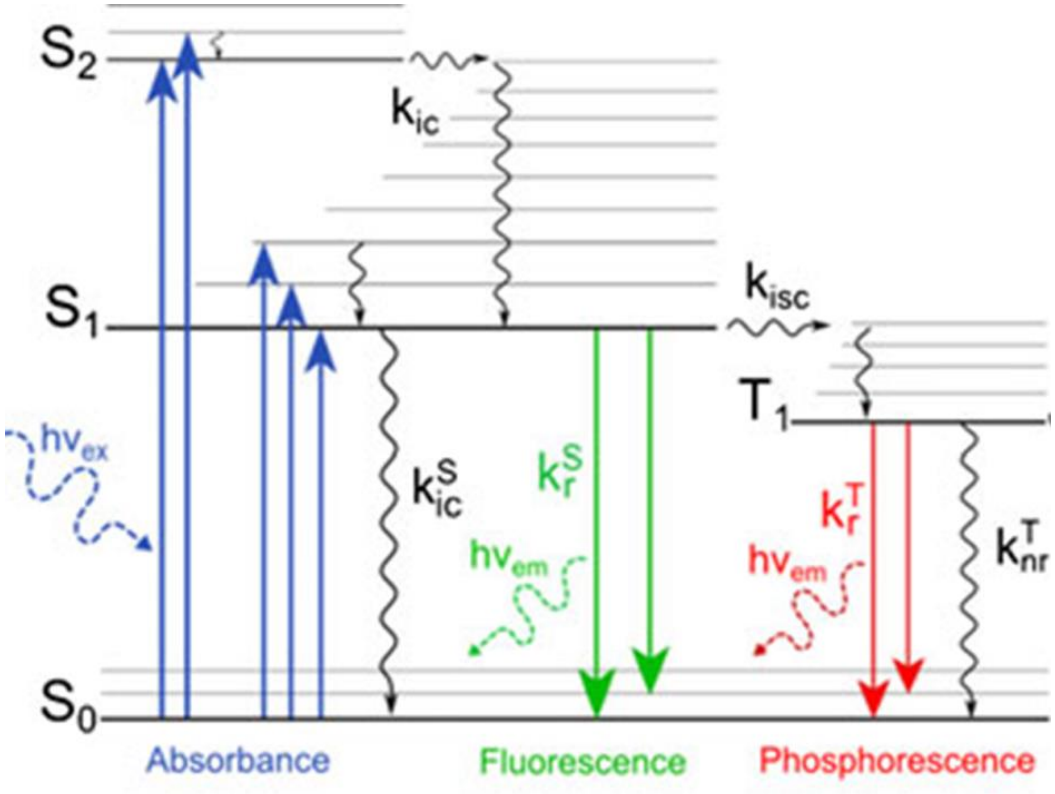

Figure 2.5. Perrin-Jablonski diagram**.** Different energy states of electrons during excitation (blue), emission (green) and emission via intersystem crossing (red).(*7*)

(This wavelength shift enables us to measure fluorescence by filtering excitation light from the detector.) The other two possibilities for the molecule to return to the ground state are non-radiative relaxation and intersystem crossing. Non-radiative relaxation takes place when the energy of the excited species is released through vibrational relaxation (k^S_{ic}). Intersystem crossing (k_{isc}) occurs when the excited species crosses to the excited triplet state by electron spin change.

Fluorophores can be characterized by their fluorescence lifetime (τ) and quantum yield (QY). The lifetime is defined as the average time the molecule spends in the excited state (Eq. 2.5);

$$\tau = \frac{1}{\Gamma + k_{nr}} \qquad \text{(Eq. 2.5)}$$

where Γ and k_{nr} are rate constants of the emissive and non-radiative decay respectively. In the absence of non-radiative decay, the lifetime is defined as an intrinsic or natural lifetime τ_n

$$\tau_n = \frac{1}{\Gamma} \qquad \text{(Eq. 2.6)}$$

and can be determined from the absorption, emission, and extinction of the fluorophore. The quantum yield (QY) is defined as a ratio of the number of emitted photons to the number of absorbed photons. (Eq. 2.7)

$$QY = \frac{\#\ photons_{\ emitted}}{\#\ photons_{absorbed}} \qquad \text{(Eq. 2.7)}$$

The quantum yield for the most efficient fluorophores such as rhodamines can approach unity. Quantum yield can also be defined with respect to the rate constants of emissive and non-radiative decay (Eq. 2.8).

$$QY = \frac{\Gamma}{\Gamma + k_{nr}} \qquad \text{(Eq. 2.8)}$$

The high sensitivity of fluorescence measurements make them very powerful tools for chemical sensing or biological detection. However, fluorescence-based measurements have several disadvantages. The most common disadvantages are intensity fluctuations or photobleaching of

fluorophores. With proper experimental design, these disadvantages can be easily minimized.(*5*, *8*)

2.4.2 Upright epi-fluorescence microscope system

The upright epi-fluorescence microscope system used in all heating studies integrated an Olympus BX-61 microscope, CCD camera, and light source. The Olympus BX-61 microscope is designed for fluorescence detection. A schematic of the microscope is provided in Figure 2.6. The microscope contains UIS2 optics and three different objectives were installed: 5x, 10x, and 20x UMPlanFl objectives with NAs of 0.15, 0.30, and 0.75 respectively. The majority of the images obtained for this thesis were done with the 10x objective.

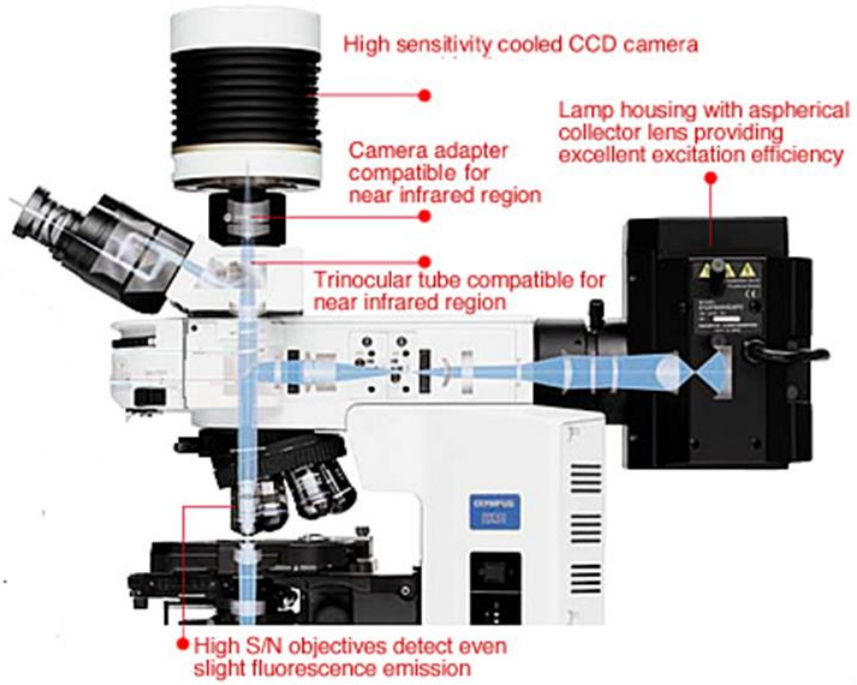

Figure 2.6. Schematic representation of the BX microscope. The lamp housing contains a short arc mercury lamp. The light travels through adjustment objectives to the filter cube. The light is filtered by the excitation filter and reflected by the dichroic mirror. The excitation light reaches the sample, where the excitation of the fluorophore occurs. The emitted light travels through the dichroic mirror and the emission filter and is collected by the CCD camera. Image from Olympus America.(*9*)

Light Source

Several different light sources can be applied to fluorescence microscopy. Light sources can have continuous or line emission spectra. Common light sources employed in fluorescence microscopy are halogen lamps, mercury lamps, xenon arc lamps and lasers. For our applications, where different fluorophores are used, the best light source would be one with a broad emission spectrum with high intensity. The best-suited lamp for our experiments was a mercury arc lamp from Ushio Inc. (Tokyo, Japan).

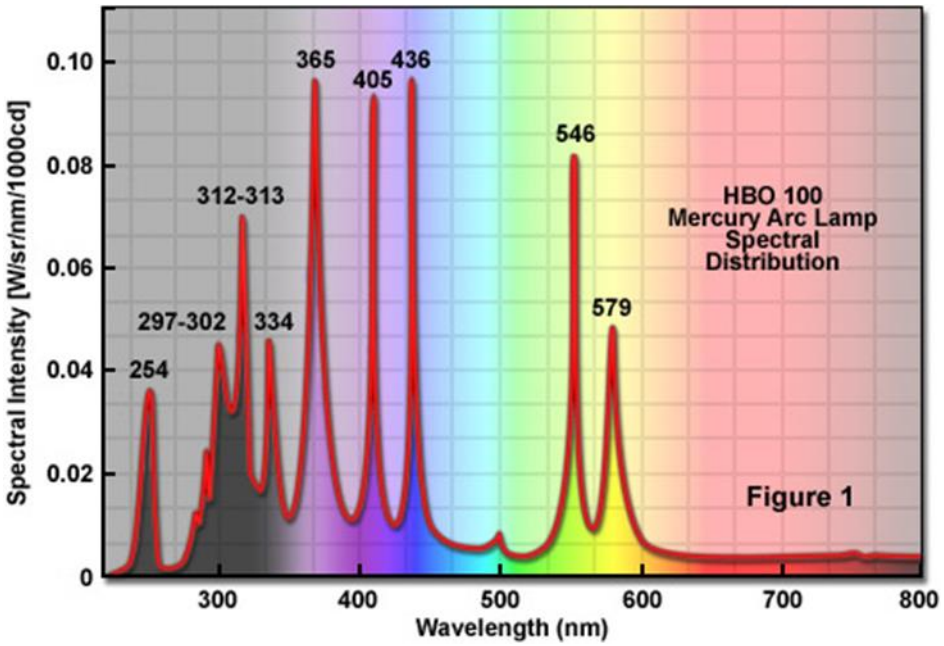

Figure 2.7. The intensity spectrum of the mercury arc lamp. The lamp emits high intensity light across the visible spectrum. (*10*)

Mercury vapor arc lamps are brighter than incandescent lamps (such as tungsten-halogen) and can provide intense illumination across the visible spectral region. They are highly reliable and stable. However, the drawback associated with the mercury arc lamp is the inconvenience of mechanical alignment due to temporal and spatial heterogeneity of the light intensity. Homogenous illumination intensity across the fiber bundle is necessary for precise measurements of product formation and the kinetics of individual enzymes (Figure 2.8, Figure 2.9).

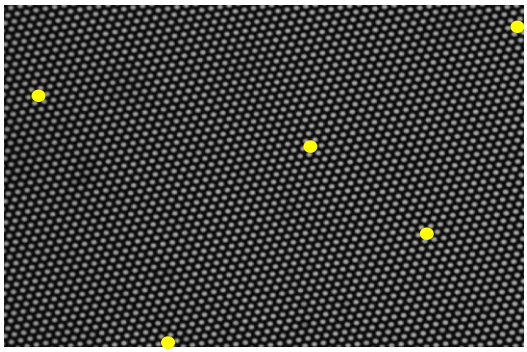

Figure 2.8. Image of the fiber with wells containing 100 μM concentration of the fluorescent product. The fluorescence intensities of five random wells were measured as follows: 657, 655, 657, 654, 662 a.u. (ImageJ Software). The small variation among the values suggests that the excitation light is uniform across the entire fiber bundle. Because the intensities correspond to the number of fluorescent product molecules within individual wells, this demonstration also illustrates the nearly identical well volumes.

Intensity variations could also alter the photobleaching rates in different sections of the fiber bundle. Another disadvantage of the mercury arc lamp is its shorter lifetime compared with different light sources. The lamp bulb must be changed every 200 to 300 hours depending on how often the lamp was turned on and off.

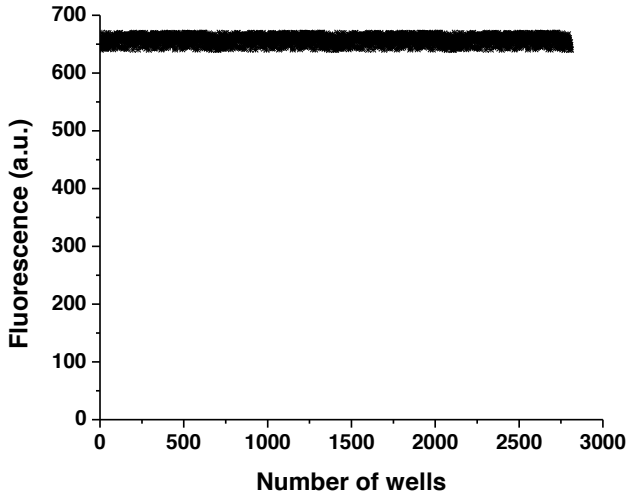

Figure 2.9. Fluorescence intensity of 100 μM of fluorescent product measured over the fiber array for more than 2000 wells. The average intensity measured is 659 arbitrary fluorescence units (a.u. and SD is 16 a.u. The intensities suggest nearly identical well volumes as well as uniform light intensity over the full fiber array.

Filter sets

Optical filters are an important part of fluorescence microscopy. The epi-fluorescence microscope system utilizes filter cubes containing both excitation and emission filters as well as a dichroic mirror. The Olympus BX-61 has a special housing for the filter sets. It can hold up to six different cubes. Each cube contains excitation and emission filters as well as a dichroic mirror (Figure 2.10). Each filter set is selected for a particular fluorescent dye; hence, the maximum fluorescence efficiency and signal transparency can be obtained.

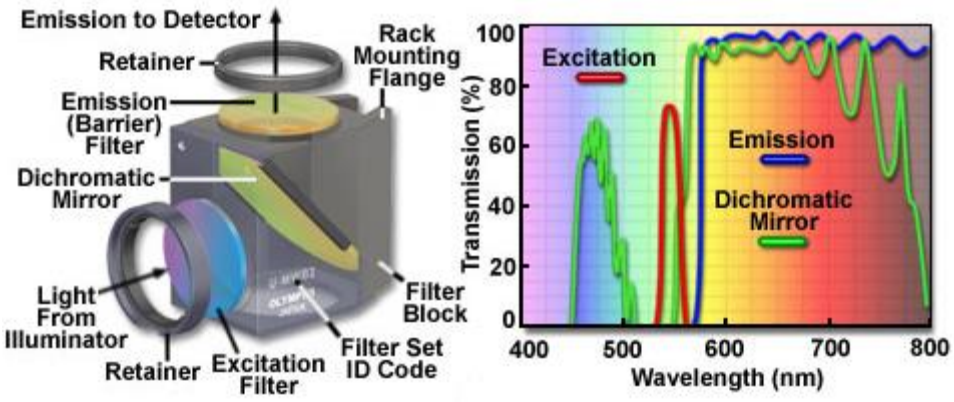

Figure 2.10. Schematic representation of a filter cube and transmission spectra of each filter. Image from Olympus America.(*9*)

Cameras

For our upright system we used charge-coupled device (CCD) cameras. A charge-coupled device is an integrated circuit incorporating a silicon surface, which is divided into light sensitive units called pixels. The applied photon flux generates a charge that can be transferred through the array to the final pixel row where the electronics of the camera measure the voltage and transform it into a digital image. In the experiments described in Chapters 3 and 4, we used the Sensicam QE from Cooke Corporation. It is a 12-bit high performance CCD camera. The CMOS Orca 4.0. Flash camera from Hamamatsu was used in the experiments described in Chapters 5 and 6. It is a 16 bit CMOS camera with a wider field of view compared to Sensicam QE. Compared with the CCD camera, in CMOS each pixel has its own charge to voltage conversion, allowing for high-speed imaging.(*11, 12*)

Stage

The microscope has a custom-built fiber bundle holder that allows us to install and lock a fiber bundle in a vertical position (Figure 2.11). The etched side containing the microwells is placed distal to the objective.

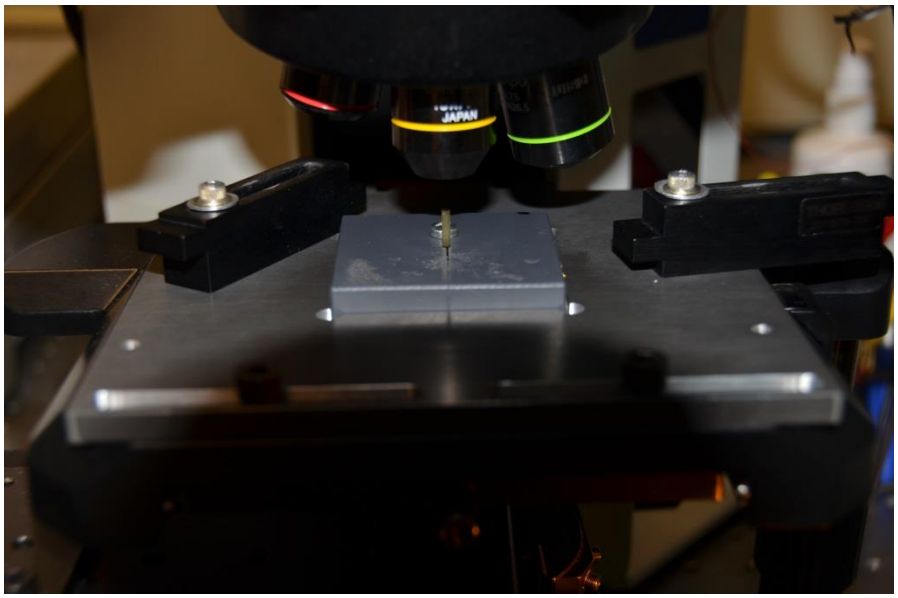

Figure 2.11. Photograph of the fiber holder with the installed fiber.

To seal the wells an additional stage is used. This stage is attached to a horizontal arm controlled by a z-translation stage. A small platform covered with a silicone sheet is placed on the stage directly under the fiber. By using the vertical motion of the arm we can press the silicone seal against the fiber to seal the reaction wells. The sealing is manually operated (Figure 2.12).

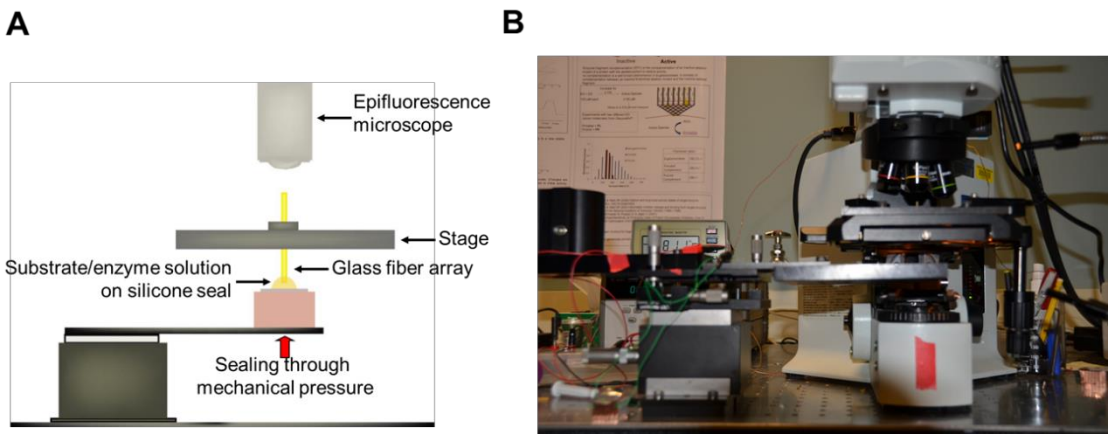

Figure 2.12. Custom built upright microscope stage (A) Cartoon representing the major components of the microscope stage. (B) Photograph of the horizontal arm under the BX-61 microscope.

2.4.5 Custom 8-fiber imager

The custom 8-fiber imager was developed by Quanterix Corporation. Eight-fiber strips are prepared by placing short fibers into a pre-grooved fiber holder (Figure 2.13). First, OP-4-20632 Dynamax epoxy is applied to the grooves. The individual fibers are placed inside the grooves and aligned using a custom made holder. The epoxy is cured by UV light for 40 s. Next, extra epoxy is applied to the holder and fibers are sandwiched with another flat strip (Sylgard 184 Silicone Elastomer). After overnight curing under UV light, the strip is carefully polished.

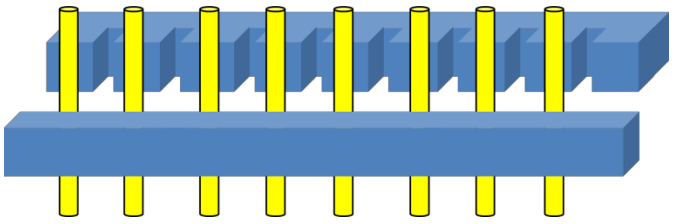

Figure 2.13. Schematic illustration of the components of the fiber strip.

The custom built stage of the 8-fiber imager uses mechanical sealing of the fibers. Pressure transducers are used under each fiber to allow a consistent force to be applied. Figure 2.14 shows the fiber strip placed in the holder with the pressure transducers placed under the strip. The fibers are stationary during image acquisition. The imager is designed in such a way that the each strip is initially aligned and the camera can then move from one fiber bundle to another. This design gives us the ability to image all eight fibers in one experiment. Disadvantages of this platform include image drift due to camera movement and low time resolution between images.

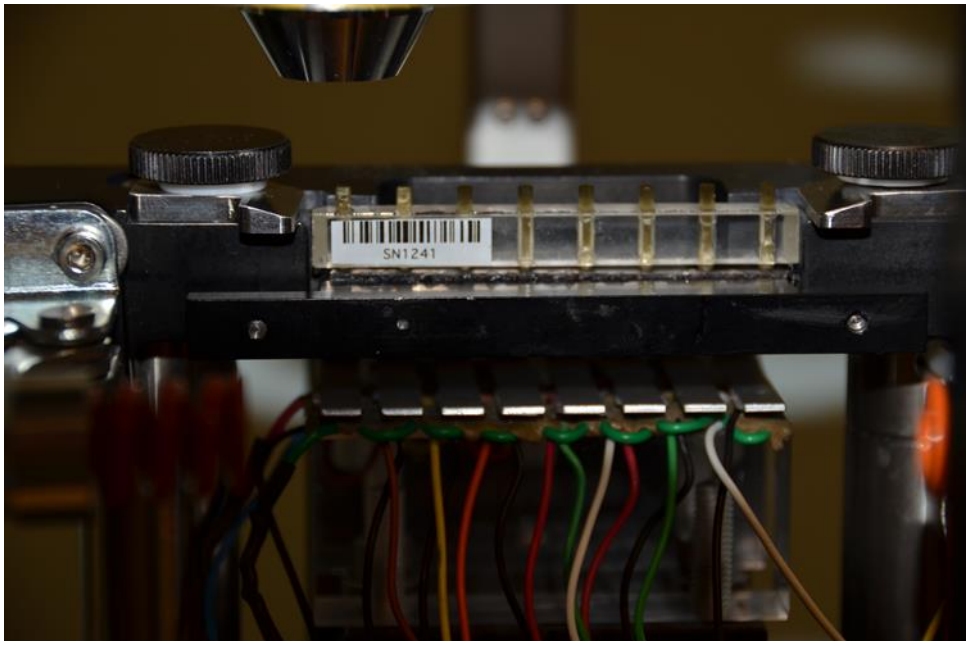

Figure 2.14. Photograph of the fiber strip placed in the holder with the pressure transducers placed under the strip. The fibers are stationary during image acquisition.

2.5 Heating stage development

The addition of a heating stage allows us to study single molecule activities with respect to changes in temperature. This approach was used to study conformational changes as described in Chapter 3. We were also able to obtain values of activation energies (E_a) of individual molecules. These studies are described in detail in Chapter 4. The heating stage was used for studies of thermal switching of activities of β-glucuronidase mutants in Chapter 5, and denaturation experiments as described in Chapter 6. In this section, we will describe the Peltier effect, thermolelectric plate and the heating stage development.

2.5.1 Introduction to Peltier effect and thermolelectric plate

Different forms of energy such as chemical, mechanical and electrical can be easily transformed into thermal energy. For example, Joule heating is a process where the transfer of electrical current through a conductor releases heat. A similar effect, called the Peltier effect, can be observed when current is transferred through different types of material and a temperature difference is created at the junction between materials. A typical thermoelectric plate contains conductive electrodes and two types of semiconductors—*n* and *p* type. Heat is absorbed by the flowing electrons or holes (cold side) and removed on the hot side on the junction between conductor and semiconductor (Figure 2.15).

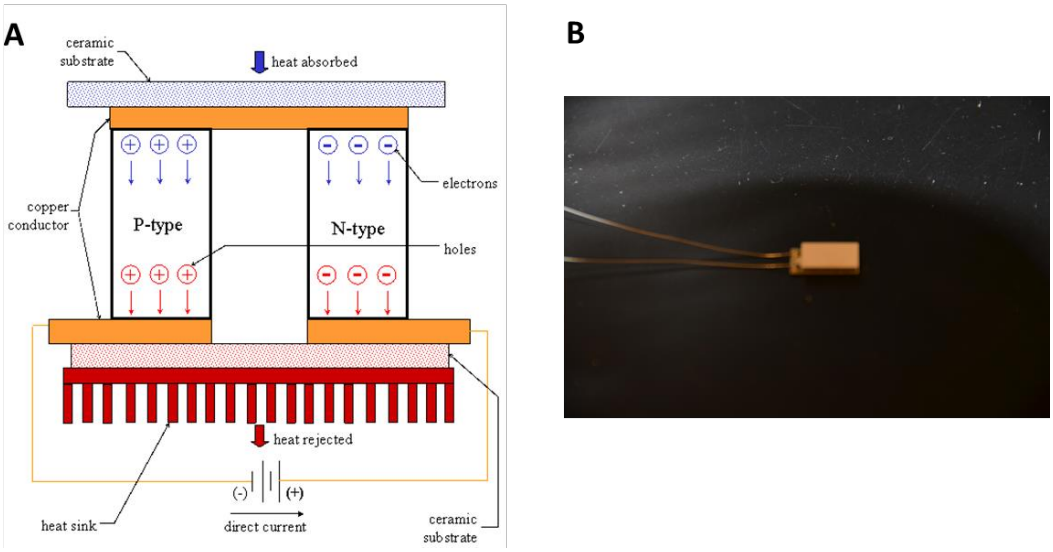

Figure 2.15. (A) Schematic representation of the Peltier plate. Electrons and holes flow through two different semiconductors (n and p). They absorb heat at one conductor/semiconductor junction and release heat at the other semiconductor/conductor junction. (B) Photograph of the 10 x 5 mm Peltier plate used in our heating experiments. Image from TE Technology Inc.(*13*)

When the current is reversed, the hot and cold sides reverse as well, expanding the temperature range below room temperature. The temperature change is proportional to the current applied to the Peltier plate.

Heating stage

The small heating plate (Figure 2.15, B) has been evaluated for the maximum temperature output. Depending on the voltage, the plate could reach from 4°C up to 98°C; however, due to low heat dispersion the temperatures were fluctuating over a prolonged time. To decrease fluctuations in temperature, the heating plate was attached to a copper heat sink by the Arctic Silver™ thermal adhesive, (Arctic Silver Inc, Visalia, CA) showed in figure 2.16, B. The copper heat sink allows the heating plate to reach stable temperatures from 10°C to 85°C with very low

fluctuations (max 0.2°). The heating stage was attached to an Agilent E3646A dual output DC power supply (Figure 2.16, A).

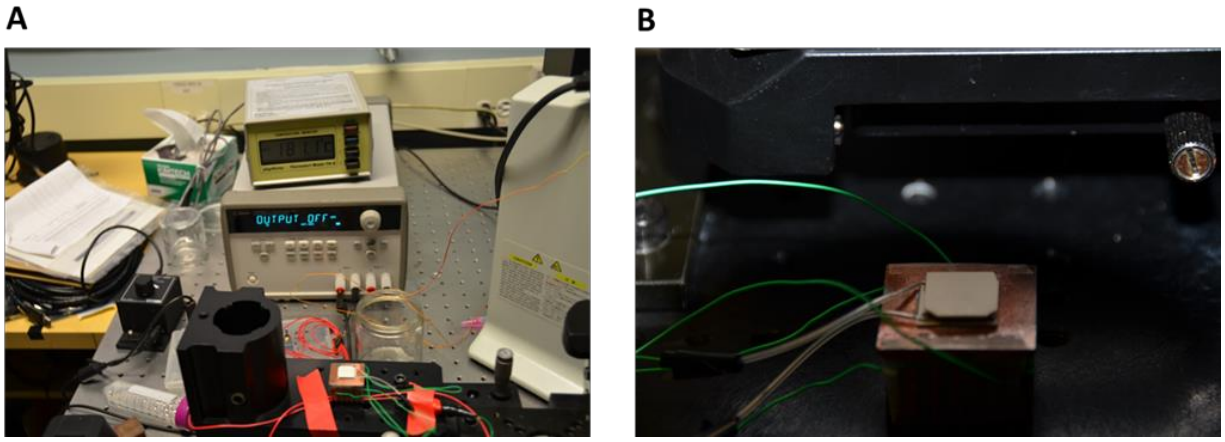

Figure 2.16. (A) Photograph of the Agilent E3646A dual output DC power supply with attached temperature monitor (Thermalert TH-8) and J-type thermocouple. (B) The Peltier plate attached to the heat sink.

During the preliminary fluorescent experiments with the heating stage, we discovered high background fluorescence coming from the ceramic composition of the heating plate. To minimize any fluorescence interference from the plate we used aluminum foil as a support for the PDMS sealing sheet (Figure 2.17).

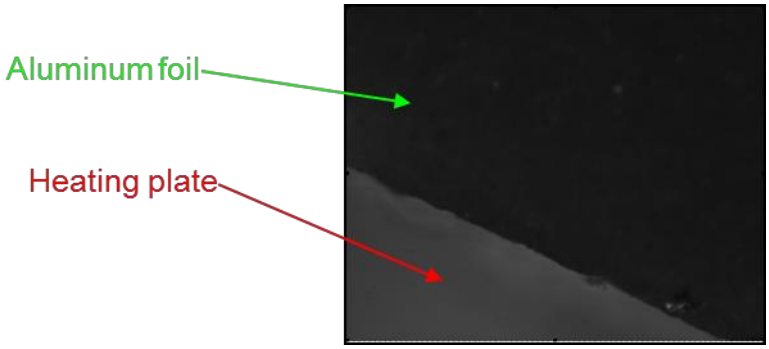

Figure 2.17. Image taken of the heating plate (Peltier plate) half covered with aluminum foil. The image was taken using the resorufin filter cube. The high intensity autofluorescence of the Peltier plate can be easily blocked with the aluminum foil.

Temperature control system

To control the temperature we integrated the thermocouple with the power supply via CPU. We developed a LabView interface where we could control the camera and the heating stage (Figure 2.18).

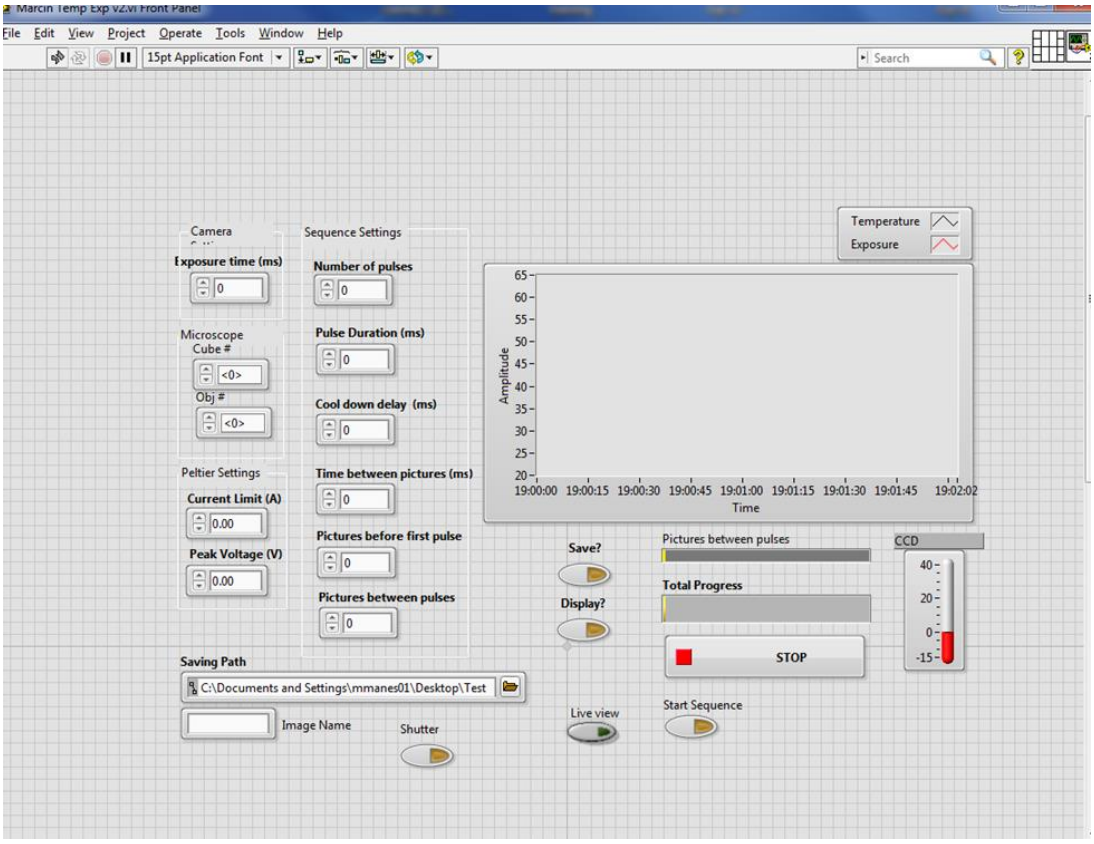

Figure 2.18. Screenshot of the LabView interface. By using a LabView program we were able to automate and combine the camera, microscope, voltage applied to the Peltier plate, and temperature sensor.

To correctly estimate the temperature on the fiber we tried three different approaches: a calibration method, real-time temperature sensing, and fluorescence intensity change measurements.

Calibration method: This method was successfully used in most of the experiments however it did not give the most accurate temperature values. The fiber was placed in the fiber holder and the thermocouple was inserted between the fiber and PDMS sheet. The thermocouple was

connected to the temperature reader while current was sent through the heating stage. The current was adjusted to produce a specific temperature. Temperature vs. current was recorded and measurements were repeated three times. An identical current corresponding to the desired temperature was applied during the experiment without real-time temperature measurement. After the experiment, the calibration was repeated on the same fiber and compared with that taken before the experiment. The experiment was excluded from further analysis if the differences in the two calibrations were greater than 0.5°C for a given voltage. However this was an unusual occurrence.

Temperature sensor: Because the temperature of the heating Peltier plate is uniform across the surface, we attached the short fiber with the thermocouple inserted between the fiber and the PDMS sheet atop the Peltier plate next to the imaged fiber during heating experiments (Figure 2.18). This method was as effective as the previously-described method and allowed us to measure real time temperatures during the experiment.

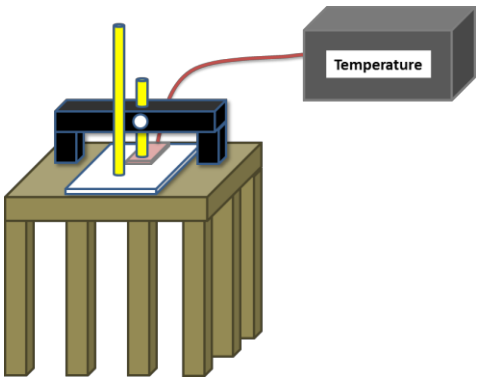

Figure 2.19. Schematic representation of the heating stage with a temperature sensor. The short fiber (yellow) is placed next to the imaged fiber (yellow) in custom made holder (black). The temperature sensor (pink) is inserted between the short fiber and Peltier plate (white).

Fluorescence intensity change: This method takes advantage of the phenomenon of fluorescence intensity decline with increasing temperature. We attempted to use the background fluorescence intensity of unoccupied wells to monitor the temperature in each individual well. However, due to very small changes in intensities with respect to temperature, obtaining a reliable calibration curve was impossible.

For all heating experiments described in this thesis we alternately used the calibration method and the temperature sensor method.

Temperature patterns

We were able to design different temperature patterns depending on the experiment to be performed. Here we will present three different temperature setups; however, the stage was not limited to only those three setups. Figure 2.20 shows temperature readings for some typical heating pulses. This graph represents pulses that were introduced during the experiments focused on conformational changes as described in detail in Chapter 3. The maximum temperature of those studies did not exceed 47°C, which is below the denaturation temperature of the studied enzyme.(*14-16*)

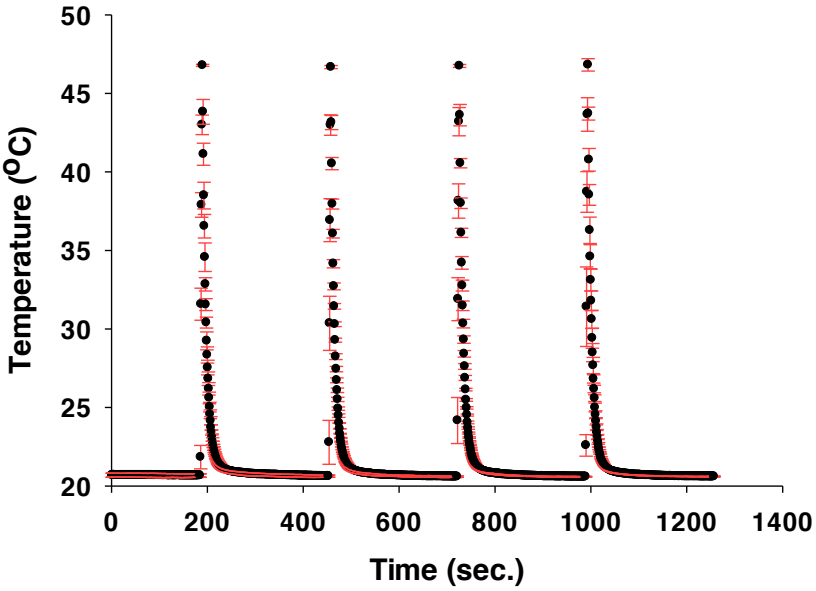

Figure 2.20. A plot of temperature pulses over the time span recorded by a thermocouple sensor used for the conformational studies described in Chapter 3.

For the calculations of activation energy (E_a) described in Chapter 4, we used a temperature ramp pattern (Figure 2.21). We chose six different temperatures (11ºC, 22ºC, 36ºC, 41ºC, 50ºC, 65ºC), stabilizing the system at each temperature for a minimum of two minutes. The relatively large temperature span allowed us to measure thermodynamic constants more precisely than other single molecule techniques.(*17*)

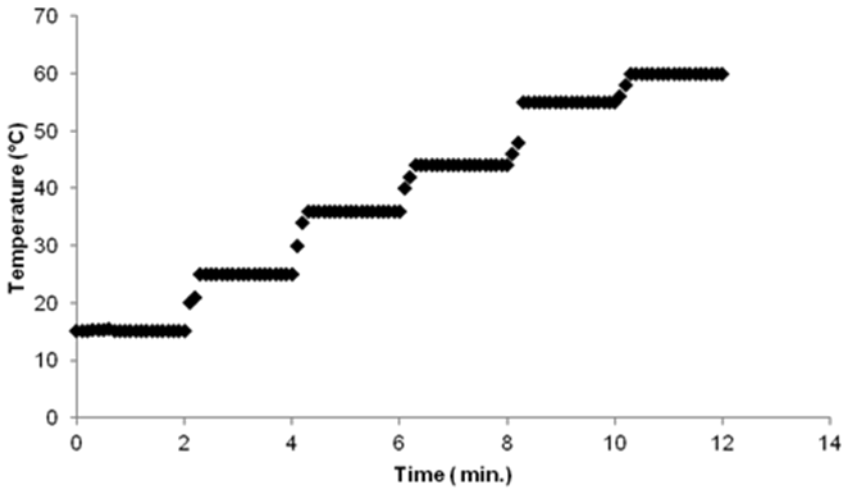

Figure 2.21. Temperature ramp used for determination of thermodynamic constants as described in Chapter 4.

We also performed different types of heating patterns for other experiments. For example, we measured the activity of mutant enzymes at 37°C as described in Chapter 5, and we carried out several temperature-dependent denaturation and folding experiments as described briefly in Chapter 6 (Figure 2.22).

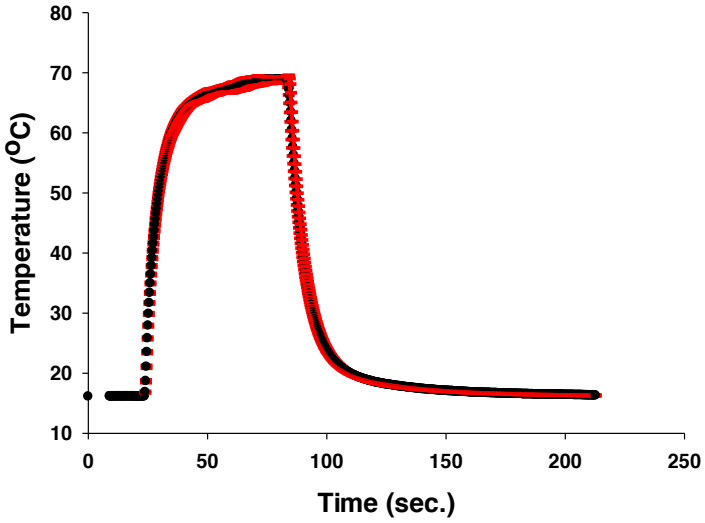

Figure 2.22. Temperature pattern for denaturation experiments performed on RNase A and described in Chapter 6.

2.5.2 Fiber bundle preparation and modifications

For single molecule kinetics studies, it is very important to properly prepare and modify the fiber bundles. Especially when temperature changes are introduced, special care needs to be taken to be sure that microwell sealing can withstand temperature fluctuations, and that the particular modification used for the fiber is thermally stable and does not interfere with the studied enzyme.

Fiber bundle preparation

The protocol described below is common for all the fibers used throughout this thesis. Individual fiber bundles were cut to a length of approximately 5 cm. They were placed in a holder and polished with different films on the fiber polisher. After polishing, each fiber bundle was cleaned with ethanol and dried under air.

500 µL of 1 N hydrochloric acid was diluted in a glass vial with 19.5 mL DI water to 0.025 M. Four fiber bundles were mounted vertically on a plastic cap and partially immersed in the acid solution. Fibers were etched for 115 s, while being stirred using a magnetic stirrer. The different speeds of etching between the fiber cores and cladding produce a uniform array of wells with a volume of 46 fL and variation of 3.9% (Figure 2.4, A, B). After etching, fiber bundles were washed with 2-propanol and immersed in 0.5 M EDTA for 30 minutes to remove any heavy metals, which might be present in the glass composition. In the single molecule experiments it is very important to remove any metals, which could inhibit the activity of the enzyme. Next, the fiber bundles were washed in 2-propanol followed by water and finally air-dried. They were stored at room temperature.

Fiber bundle modification

It is well known that proteins can interact with unmodified glass surfaces. Non-specific binding of the enzyme to the surface can affect the results. When single molecule experiments are performed, the high surface area to volume ratio increases the chance of surface-enzyme interactions. To minimize nonspecific binding we used several techniques, which differed depending on the specific experiment being performed (e.g. heated or room temperature experiment) and depending on the particular enzyme. Here, we present three general techniques, which we applied throughout experiments mentioned in this thesis.

a) *Bovine Serum Albumin (BSA)*

   BSA is a small 66.5 kDa protein that is commonly used to prevent adhesion of enzymes to surfaces. Its presence can stabilize or have no effect on the studied enzyme. The BSA molecule binds to both hydrophobic and hydrophilic surfaces. BSA binding to

hydrophobic surfaces occurs as a single step and the adhesion of BSA to hydrophilic surfaces consists of two steps.(*18*) Surface passivation is performed using 0.02% BSA solution. The dry, etched fiber is immersed in the solution for 30 min prior to the experiment. The fiber is sonicated and washed with the buffer that will be used for that particular experiment. The PDMS sheet is washed with the BSA solution and air-dried. In figure 2.22, parts A and C show kinetics profiles of single β-galactosidase molecules performed on a BSA-modified fiber and a non-modified fiber

b) Poly-l-lysine

Poly-l-lysine is a small natural homopolymer containing lysine monomers. With a pKa of 10.5 for the side chain amine group, lysine has a positive charge in most of the buffers used in our experiments. This polymer is used mostly for fiber modification when highly positively charged RNase A was used. To modify the fiber surface with poly-l-lysine, a 0.1% (v/v) solution (Sigma Aldrich) was diluted to 0.01% in DI water in a vial. Fiber bundles were partially immersed for 30 minutes and dried under nitrogen. Fiber bundles were used just after modification. Longer exposure resulted in a great amount of surface contamination.

Ethoxysilanes

A few different ethoxysilanes were used in this thesis. 3-aminopropyl triethoxysilane was used for the β-galactosidase experiments described in chapters 3 and 4, as well as for the RNase A experiments described in Chapter 6. 2-methyl-2-methoxysilane was used for the lipase experiments. The standard surface modification procedure was performed on four fibers at the same time. A glass vial containing 14.75 mL of anhydrous ethanol (Sigma Aldrich) and 0.75 mL of distilled water was purged for 30 min with nitrogen gas. The

fibers were plasma treated for 60 s in the expanded plasma cleaner (Harrick Plasma, Ithaca, NY). After plasma treatment, fibers were placed in the ethanol/water solution prepared previously and 150 µL of silane was added. The fibers were immobilized for 30 min and washed with anhydrous ethanol several times. After washing, fiber bundles were dried under vacuum inside a desiccator for an hour. The resulting fiber bundles were placed in a nitrogen gas filled container at 80 °C for 30 min. Figure 2.23 shows the activity traces for β-galactosidase measured in fibers with different surface modifications.

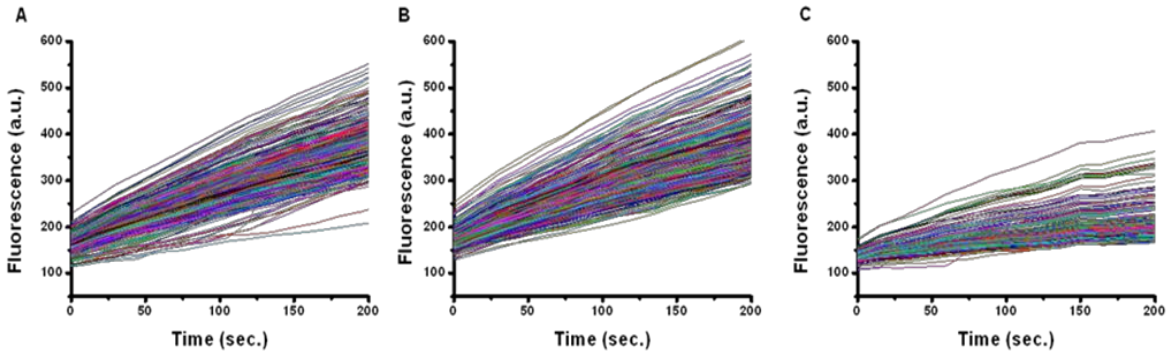

Figure 2.23. Activity traces of single β-galactosidase enzyme molecules for different surface modifications of the fiber. (A) and (B) represent modifications with BSA blocking buffer and silane respectively; (C) is an un-modified fiber.

Sealing integrity

The addition of temperature fluctuations can have negative consequences for sealing integrity. We have used several fiber modifications, which did decrease nonspecific binding, but for which the integrity of the seal was compromised (Figure 2.24).

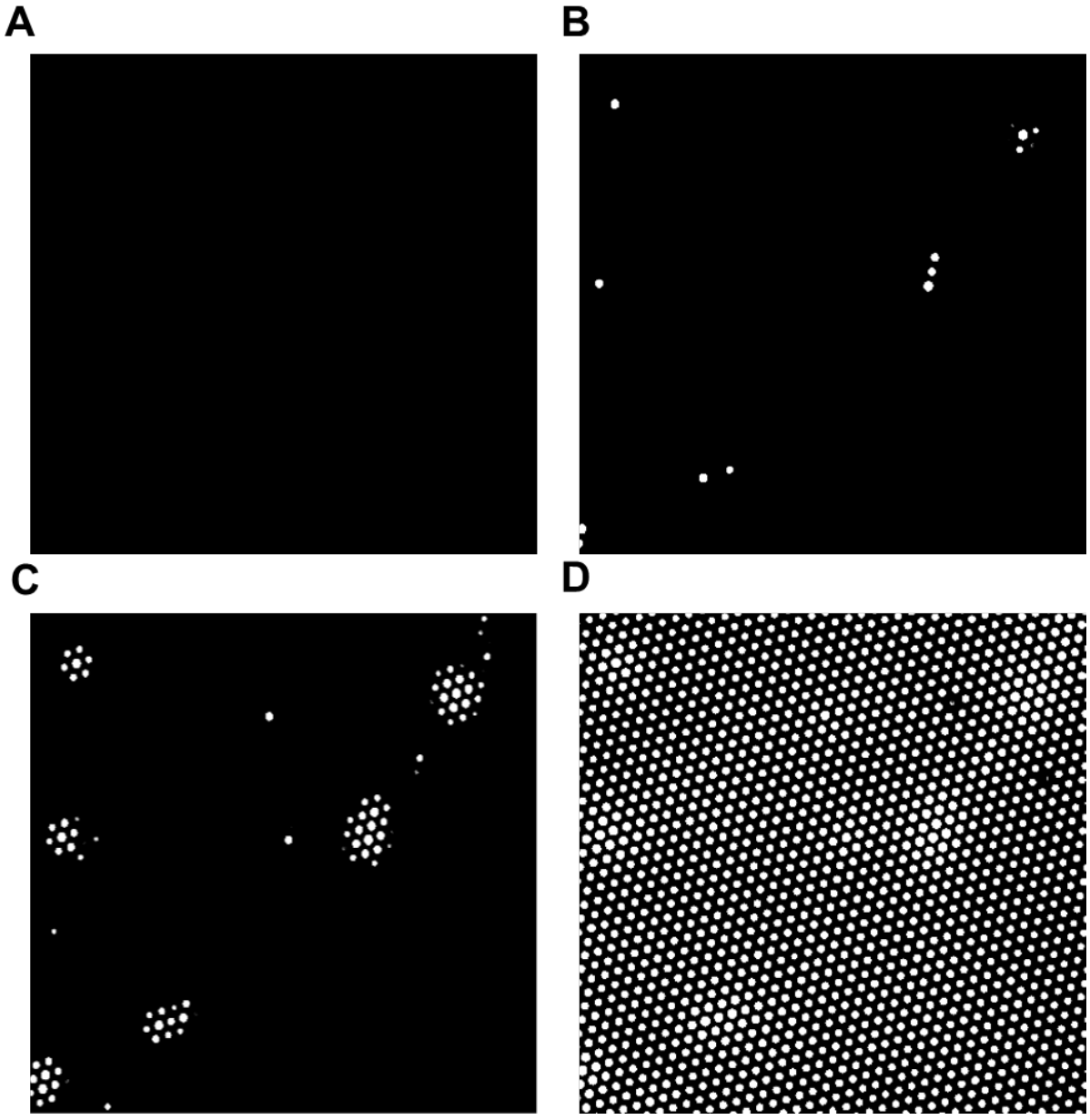

Figure 2.24. Heating experiment on single β-galactosidase molecules performed on a BSA-modified fiber. (A) Image taken at the beginning of the experiment. (B) Image taken before heating pulse. (C) Immediately after the heating pulse. (D) 30 s after the heating pulse. The sealing integrity is clearly compromised.

Protein based blocking agents need to be avoided due to their ability to aggregate due to elevated temperature. For example, we could not perform heating experiments with BSA-treated surfaces instead the silane-based fiber surface modifications were used.

To measure sealing integrity, a solution of 10 μM resorufin in deionized (DI) water was enclosed in the individual wells. High intensity light was used to illuminate a small portion of the array for 20 min to photobleach the resorufin. A full view image was taken and no significant leakage was observed. An additional image was taken after 15 min to confirm the integrity of the seal (Figure 2.25).

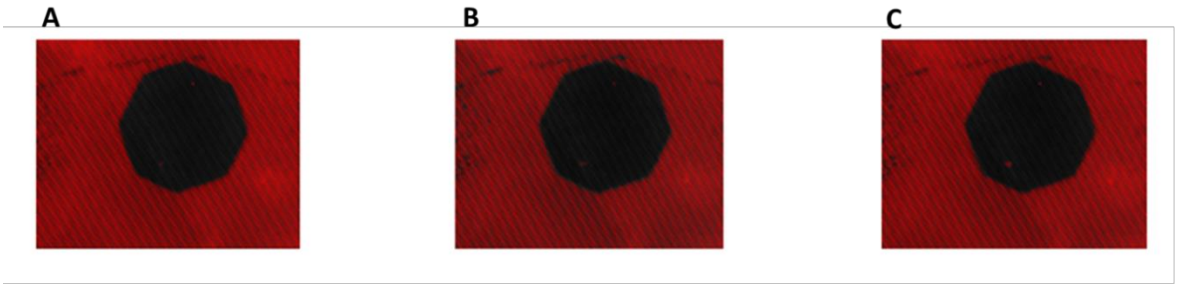

Figure 2.25. Fluorescent images taken after photobleaching of 10 μM resorufin. Images taken (A) before heating pulses, (B) after introducing six heating pulses, and (C) 15 min after the pulses show that the seal remains intact.

2.6 Summary

The fiber bundles described in this chapter have several advantages over other techniques used to study single enzyme kinetics. The most important feature is that the enzyme does not need to be immobilized to the surface. In addition, hundreds to thousands of single molecules can be observed simultaneously. The observed kinetics results only from intrinsic enzyme properties. Another advantage is that the fluorescent signal is locally concentrated inside the fiber well and no custom optics are necessary; hence, the single molecule system is relatively inexpensive and simple. With the addition of the heating platform, we expanded our abilities to study enzymes not only over time, but over changing temperatures as well. This feature allows us to focus our

research on the conformations, thermodynamic constants, or even folding behaviors of individual enzymes. The main limitations are the thermal stability of the substrates or fluorescent products.

2.7 References

1. D. R. Walt, Fibre optic microarrays. *Chem Soc Rev* **39**, 38 (2010).
2. D. M. Rissin, D. R. Walt, Digital concentration readout of single enzyme molecules using femtoliter arrays and Poisson statistics. *Nano letters* **6**, 520 (Mar, 2006).
3. D. M. Rissin, D. R. Walt, Digital concentration readout of single enzyme molecules using femtoliter arrays and Poisson statistics. *Nano letters* **6**, 520 (Mar, 2006).
4. J. W. Lichtman, J. A. Conchello, Fluorescence microscopy. *Nat Methods* **2**, 910 (Dec, 2005).
5. J. R. Lakowicz, *Principles of fluorescence spectroscopy*. (Springer, 2007).
6. N. Turro, M. M. Photochemistry, Benjamin/Cummings. *Menlo Park, CA*, 317 (1978).
7. M. Quaranta, S. M. Borisov, I. Klimant, Indicators for optical oxygen sensors. *Bioanalytical reviews* **4**, 115 (Dec, 2012).
8. B. Valeur, M. N. Berberan-Santos, *Molecular fluorescence: principles and applications*. (John Wiley & Sons, 2013).
9. www.olympusamerica.com.
10. http://zeiss-campus.magnet.fsu.edu.
11. D. Litwiller, CMOs vs. CCD: Maturing technologies, maturing markets. *Photon Spectra* **39**, 54 (Aug, 2005).
12. D. Litwiller, How an imaging sensor feeds off light. *Photon Spectra* **38**, 96 (May, 2004).
13. http://www.tetech.com.
14. H. F. Arata, Y. Rondelez, H. Noji, H. Fujita, Temperature alternation by an on-chip microheater to reveal enzymatic activity of beta-galactosidase at high temperatures. *Anal Chem* **77**, 4810 (Aug 1, 2005).
15. S. Yoshioka, Y. Aso, K. Izutsu, S. Kojima, Is Stability Prediction Possible for Protein Drugs - Denaturation Kinetics of Beta-Galactosidase in Solution. *Pharmaceutical research* **11**, 1721 (Dec, 1994).
16. D. B. Craig, E. R. Nichols, Continuous flow assay for the simultaneous measurement of the electrophoretic mobility, catalytic activity and its variation over time of individual molecules of Escherichia coli beta-galactosidase. *Electrophoresis* **29**, 4298 (Nov, 2008).
17. D. B. Craig, L. N. Chase, Arrhenius plot for a reaction catalyzed by a single molecule of beta-galactosidase. *Anal Chem* **84**, 2044 (Feb 21, 2012).
18. B. Sweryda-Krawiec, H. Devaraj, G. Jacob, J. J. Hickman, A new interpretation of serum albumin surface passivation. *Langmuir : the ACS journal of surfaces and colloids* **20**, 2054 (Mar 16, 2004).

Chapter 3: Origins of Static Heterogeneity of Enzymes

3.1 Abstract

There are two possible reasons why the initial activities of enzymes exhibit heterogeneity. First, the enzyme molecules may possess different conformations, and consequently different activities, even with the same primary sequence. A second possibility is that the enzymes vary in primary sequence due to errors in transcription and translation. This chapter addresses both these possibilities. The chapter is composed of two sections. In the first section we describe the effect of heating on the activity of enzymes. We carried out these studies using a commercially available enzyme, B-galactosidase, using the heating stage described in detail in **Chapter 2, Section 3**. The second section of the chapter describes the effects of random error in genetic sequence resulting in amino acid substitutions on the distribution of enzyme activity. The presented work was performed on enzyme samples obtained from the laboratory of Prof. Sigal Ben-Yehuda from the Hebrew University of Jerusalem. In this section we use the eight fiber imager developed at Quanterix and described in **Chapter 2, Section 3**. The aim of both sets of experiments described in this chapter is to understand the origins of the static heterogeneity of activities observed in enzymes.

3.2 Introduction to Static Heterogeneity

Enzymes exhibit both fast changes and long-lived differences in activity.(*1-7*) Fast changes give rise to what is called "dynamic heterogeneity" in which relatively low energy barriers (compared to the Boltzmann energy (k_BT)) enable rapid interconversion between different conformations at ambient temperature.(*8*) These dynamic changes are relatively fast and are the result of a wide range of internal motions, such as fluctuations within a group of atoms, within sub-domains, or within the entire protein.(*9-11*) Previous experiments indicate that enzymes can also exhibit long-lived activity differences at room temperature resulting in a distribution of activities between ostensibly identical molecules, termed "static heterogeneity".(*2, 3, 12*) This static heterogeneity arises either from different conformations of the enzyme and/or different primary sequences between molecules, with the latter possibility resulting from errors in transcription and translation.(*11, 13-15*) When a nascent protein folds, it is possible that each molecule becomes trapped in a local energy minimum and many different local minima, i.e. different conformations, may be populated, with each conformation exhibiting a different activity. Moreover, if different enzyme molecules differ in their primary sequence, they could also exhibit a distribution of activities.(*16, 17*) The commercially available β-galactosidase used in this experiment (Sigma Aldrich) is expressed in E. coli and therefore it is expected that both transcription and translation processes are not error-free. Transcription errors (such as polymerase slippage and nucleotide misincorporation) and translation errors (such as amino acid misincorporation, frame-shifts, tRNA misacylation, etc.) account for 14% and 29% respectively of the population of proteins having one or more errors. The probability of a β-galactosidase tetramer molecule (465 kDa) existing without any errors is only 25%. The rest of the population contains one or more errors in primary sequence. These changes in primary structure might have

an influence on the conformational dynamics or energetics, resulting in altered activity of individual enzymes.(*18, 19*)

3.2.1 Observing Single Molecules Interconvert between Activity States upon Heating

3.2.1.1 Introduction

In this section, we demonstrate that single enzyme molecules of β-galactosidase interconvert between different activity states upon exposure to short pulses of heat. We show that these changes in activity are the result of different enzyme conformations. Hundreds of single β-galactosidase molecules are trapped in 46-femtoliter reaction chambers and the individual enzymes are subjected to short heating pulses. When heating pulses are introduced into the system, the enzyme molecules switch between different activity states. Furthermore, we observe that the changes in activity are random and do not correlate with the enzyme's original activity. This study demonstrates that different stable conformations play an important role in the static heterogeneity reported previously, resulting in distinct long-lived activity states of enzyme molecules in a population.

3.2.1.2 Materials and Methods

Materials and Bulk Solutions Preparation

Lyophilized β-galactosidase (Grade VIII) from Escherichia coli was purchased from Sigma-Aldrich, St.Louis, MO. β-galactosidase (1.3 mg) was dissolved in 1.4 mL 1:1 solution of autoclaved 1x PBS/1 mM $MgCl_2$ and glycerol to a final enzyme concentration of 2 μM. Aliquots

of 10 μL were stored at -80 ˚C. The 2 μL of enzyme stock solution was diluted in 1x PBS/1 mM $MgCl_2$ buffer to 360 pM immediately before analysis. Resorufin β-D-galactopyranoside (RBG) and resorufin were purchased from Invitrogen, Carlsbad, CA. Resorufin β-D-galactopyranoside was dissolved in DMSO to a concentration of 100 mM and aliquots of 5 μL were stored at -20°C and diluted to 10 mM in DMSO before each experiment. 10 mM RBG was further diluted in 1x PBS/1 mM $MgCl_2$ buffer to a final concentration of 100 μM. 396 μL of 100 μM RBG substrate was mixed with 4 μL of 360 pM enzyme, giving the working solution of 3.6 pM β-galactosidase. 10x PBS buffer (pH 7.4) was purchased from Ambion, Foster City, CA.

Bulk experiments

Thermal stability experiments of the RBG substrate and the resorufin product were performed on an Infinite M200 microtiter plate reader (Tecan AG, Mannedorf, Switzerland). The RBG substrate (100 μM) was exposed to different temperatures (40°C, 45°C and 50°C) for 1 min and cooled to room temperature. Each sample was used for an enzymatic assay and compared to an unheated RBG enzymatic assay. The average turnover rate of the enzyme was calculated from these experiments. Both heated and unheated substrates were used, with no difference in enzyme activity observed, indicating that the substrate did not degrade substantially by heating (Figure 3.1). A similar experiment was performed on resorufin where 100 μM concentrated product was heated at different temperatures (40°C, 45°C and 50°C) for 1 min and cooled to room temperature.

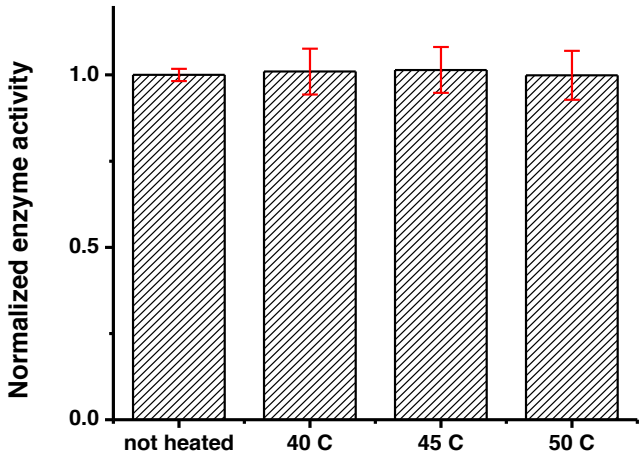

Figure 3.1. Normalized average activities of the enzymes. The enzymatic assay was performed with unheated substrate and substrate that was exposed to different temperatures (40°C, 45°C, 50°C) for 1 min. and then cooled to room temperature. The activity was normalized against the unheated substrate assay. Error bars correspond to three different experiments. The blank experiments where only substrate was present showed no change in fluorescence.

The fluorescence intensity (Ex. 558 nm/Em. 590 nm) was recorded over 10 min and compared with unheated product, and no difference in fluorescence intensity was observed. In addition, the product's stability was studied on the microscope stage where 10μM product was trapped in the 46 fL microchambers. The fluorescence intensities were measured and no significant difference in fluorescence intensity was observed before and after heating pulses at 47°C and 55°C (Figure 3.2).

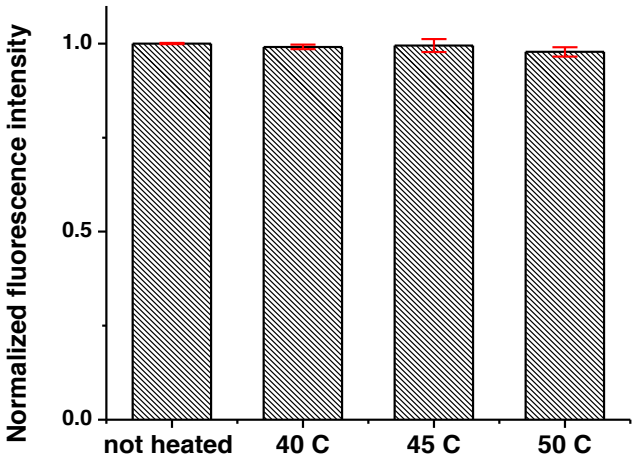

Figure 3.2. Normalized average product fluorescence intensities**.** 100 μM fluorescent product was heated at different temperatures (40°C, 45°C, 50°C) for 1 min and cooled to room temperature. The fluorescence intensities were measured every 30 s over 10 min. The results were averaged and normalized against the fluorescence of unheated product. Error bars correspond to three different measurements of the fluorescence intensities.

Activities of the enzymes at varying temperatures were measured for the system. The heated stage was equilibrated to a specific temperature and single molecule experiments were performed as previously described. For each temperature, the activities of 1000 molecules were obtained and averaged and then plotted against the temperature. The optimum temperature of the enzyme for maximum activity was obtained and found to be 55°C. Beyond this temperature enzyme activities decreased (Figure 3.3, B). In addition, the conformational stability of the enzyme was studied via circular dichroism, using a JASCO J-720 spectropolarimeter, with a Peltier pump attached. The readings were performed at 222 nm with a temperature ramp of 1°C per min. (Figure 3.3, A).

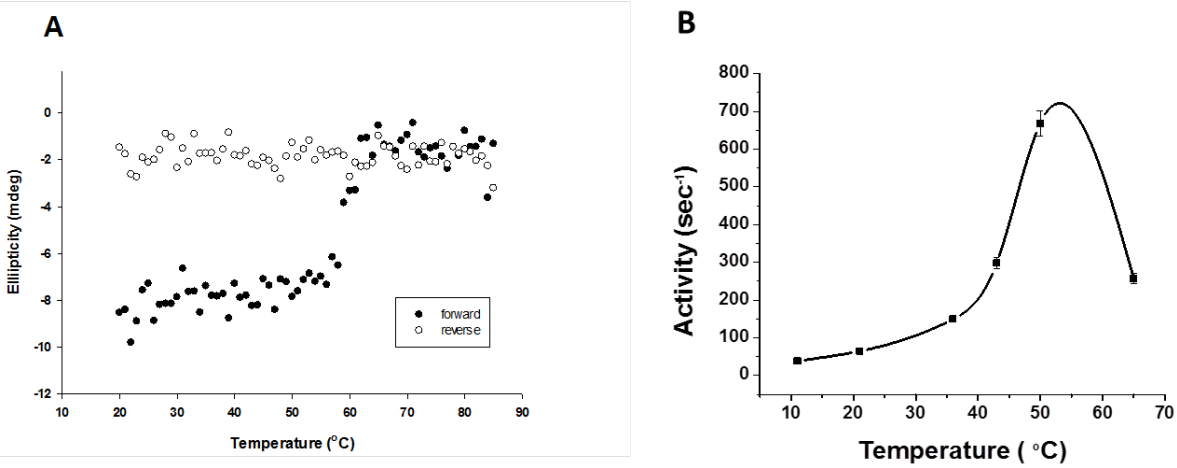

Figure 3.3. Thermal denaturation of β-galactosidase. (A) Circular dichroism spectrum of the enzyme sample as a function of temperature. The experiment was performed on a JASCO J-720 spectropolarimeter with an attached Peltier pump. The readings were obtained at 222 nm with a temperature ramp of 1°C per minute. Both forward and reverse temperature measurements were acquired. (B) Change in the activity of the enzyme molecules with respect to temperature. The heating stage was equilibrated to a specific temperature and the activities of the trapped enzymes were obtained. Each temperature point corresponds to the average activity of about 1000 enzymes.

Microarray preparation

Custom made optical fiber bundles of ~50,000 4.5 μm diameter optical fibers purchased from Schott North America Inc. Elmsford, NY were cut to lengths of 4.5 cm. Both sides of the bundles were polished using a fiber polisher from Allied High Tech Products Inc, Rancho Dominguez, CA. One end of the fiber bundle was etched in 0.025 M HCl for 115 s. The differential rate of etching between the core and the cladding results in an array of 2.5 μm deep wells of 46 fL volume.(*20*) The bundles were washed several times with EDTA and ethanol followed by plasma treatment for 60 s in an Expanded plasma cleaner from Harrick Plasma, Ithaca, NY. The surface of the wells was silanized for 30 min with 150 μL silane from Gelest Inc, Morrisville, PA in 15 mL of ethanol. The silanized fiber bundles were washed with ethanol and dried under low pressure for 1 hour. The resulting fiber bundles were placed in a nitrogen-

filled container at 80°C for 30 min. The detailed description of the silanization is included in **Chapter 2**. The fiber bundles were stored under nitrogen in a dessicator and used within two days. Room temperature single molecule experiments on modified fibers were compared with experiments on non-modified fibers and fibers treated with BSA. No difference in activity was observed between BSA-treated and silane-treated fibers, and the average activity was comparable to the bulk activity. However, since the variation in BSA passivation properties upon heating are unknown, only silane-passivated fibers were used. Additionally, the sealing proficiency of modified fibers was confirmed by photobleaching experiments as described in **Chapter 2**.

Microscope/stage description

An upright Olympus B64 microscope with an attached short arc mercury lamp as an excitation light source was used. The excitation source and fluorescence emission are filtered through a filter cube (Ex. 577 nm, Em. 620 nm, dichroic 585 nm LP) from Chroma Technology Corp, Bellows Falls, VT. The emission light was detected by a CCD camera from Sensicam QE, Cooke Corporation, Romulus, MI and captured images were analyzed using IPLab software from BD Bioscience, Rockville, MD. The setup used to seal the assay solution within the fiber wells is described in **Chapter 2**. In addition to that setup, a flat Peltier heating plate with an attached thermocouple was installed between the heat sink and the PDMS sheet. The Peltier plate and thermocouple are controlled and the temperature is recorded by a computer via LabView from National Instruments, Austin, TX. The heating plate was calibrated prior to each experiment. The temperature variations within a single experiment did not exceed more than 0.5°C. By changing the current (3.0 A), voltage (4.0 V) and pulse duration (3 s) it was possible to heat a sample to 47°C in 4 s and cool it back to 20°C within 20 s.

Image processing, normalization, and data analysis

20 µL of 3.6 pM enzyme solution and 100 µM of RBG substrate were placed on the PDMS sheet on the heating Peltier plate. A fiber bundle containing 50,000 wells was sealed against the heating Peltier plate to create 46 fL reaction vessels. It takes approximately 30 s from the onset of mixing the enzyme with the substrate to the time we acquire the first image. Each individual well contains 1 or 0 enzyme molecules with a ratio of a single enzyme molecule per 10 empty wells (Figure 3.4, A).(*21*)

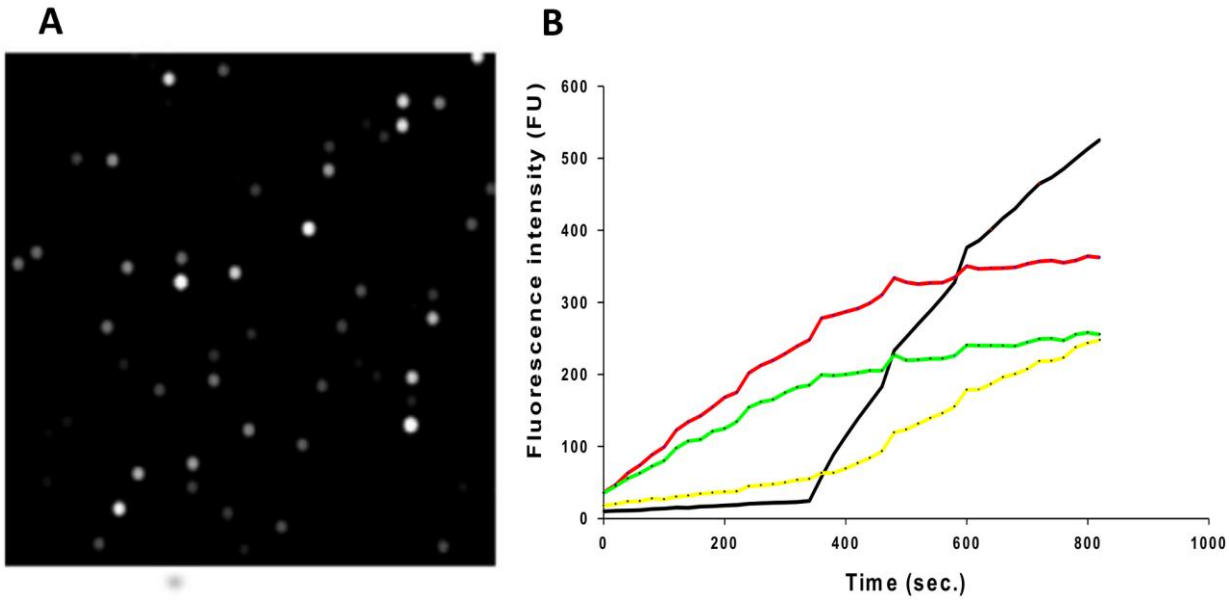

Figure 3.4. Single enzymes trapped in wells and raw intensities of the trajectories**.** (A) Image of fiber bundle with trapped active enzymes. Each enzyme generates a high local concentration of fluorescent resorufin. (B) Raw fluorescence intensities of the trajectories of individual β-galactosidase molecules.

Moreover the probability of a well containing more than one molecule is around 0.45%. To obtain initial enzyme activities, six images were taken 20 seconds apart and the fluorescence signal was obtained for each well containing an active enzyme molecule (Figure 3.4, B). Next,

five heating pulses were introduced and six images were taken between each pulse. Only five images were analyzed–the first image after heating was not considered for data analysis to ensure that the system had returned to ambient temperature. The raw fluorescence intensities of the trajectories were multiplied by a calibration factor that converted fluorescence into concentration, and were background corrected (Table 3.1).

	# of product molecules	
Time (sec.)	Enzyme I	Enzyme II
0	12669	10362
20	16577	14164
40	20067	17106
60	22644	19982
80	26329	23785
100	29744	27121
Heating pulse 1		
120	37164	34408
140	39757	37184
160	43767	40140
180	48834	42813
200	52030	46067
220	56862	49514
Heating pulse 2		
240	64750	56367
260	67836	58389
280	69930	58931
300	71727	60059
320	75003	60850
340	77854	61995
Heating pulse 3		
360	88597	68902
380	90973	71040
400	94250	72113
420	98096	74679
440	100916	77126
460	105401	79826
Heating pulse 4		
480	116057	88474
500	115614	88565
520	118063	90372
540	120429	92366
560	121640	93596
580	123608	97396

Table 3.1. Calculated number of fluorescent product molecules per active well for two randomly picked enzymes. The raw fluorescence intensities were obtained from individual wells (average intensity of 81 pixels per well). Intensities were plotted with respect to time. The intensity of 50 non-active wells per fiber were collected and averaged as a background signal. The active enzyme intensities were corrected with respect to background and multiplied by the standard factor of 320 molecules per fluorescence intensity unit. The standard factor was obtained from a standard curve generated using known concentrations of fluorescent product. The data highlighted in yellow are not included in the analysis as they were collected directly after the heat pulse and before the temperature had settled.

The substrate turnover was calculated for each enzyme before and between heating pulses using the equation $S(t) = F'(t) + k_{ph} \times F(t)$, where S(t) is substrate turnover in s^{-1}, F(t) is fluorescence intensity as a function of time, F'(t) is the fluorescence intensity time derivative and k_{ph} is a photobleaching rate (Table 3.1 and 3.2).(*20*) The photobleaching rate was determined by trapping 10 μM of fluorescent product and monitoring the fluorescence decrease every 20 s with an exposure of 2 s over 1 hour (Appendix 1).

	Enzyme I					Enzyme II				
	Slope F'(t)	St. error	Adj. R-squere	$F(t)*k_{ph}$	S(t)	Slope F'(t)	St. error	Adj. R-squere	$F(t)*k_{ph}$	S(t)
Before heating	167	4	0.997	15	182	165	4	0.998	13	178
After pulse 1	212	7	0.995	31	243	153	4	0.997	30	183
After pulse 2	125	8	0.982	51	176	46	3	0.985	42	88
After pulse 3	178	7	0.994	69	247	123	3	0.998	52	175
After pulse 4	98	7	0.982	84	182	99	2	0.998	64	163

Table 3.2. Linear regression analysis for enzymes I and II for all periods between the pulses**.** The number of product molecules were plotted against time and fitted using a linear regression tool. Each slope F'(t) is corrected for photobleaching. The final rate S(t) is calculated from the equation $S(t) = F'(t) + F(t) \times k_{ph}$.

3.2.1.3 Results and Discussion

The presented assay consists of an array of surface-passivated sealed microwells containing a single active enzyme and a high concentration of the fluorogenic substrate resorufin β-D-galactopyranoside (RBG). Upon enzymatic reaction, RBG is cleaved and the fluorescent product resorufin is produced and builds up in the microwells. The surface modification (described in more detail in **Chapter 2**) minimizes any interaction of the trapped enzyme with the surface of the fiber wells. In previous papers, we have described the heterogeneity observed in the activities

of individual enzymes, and definitively demonstrated that different initial activities are not caused by surface interactions. (*20*)

In this section, we employed a heating stage to introduce thermal pulses to perturb the conformation of the enzyme molecules. In our system, we observe the activity changes resulting from conformational changes; however, we cannot observe individual protein conformations directly. If conformational differences are the cause of static heterogeneity, we would expect that heat pulses would convert some of the molecules into different conformations and we would observe changes in activity from the initial activity state after cooling. On the other hand, if sequence differences are the primary determinant of activity, then heating would not be expected to change the activity.

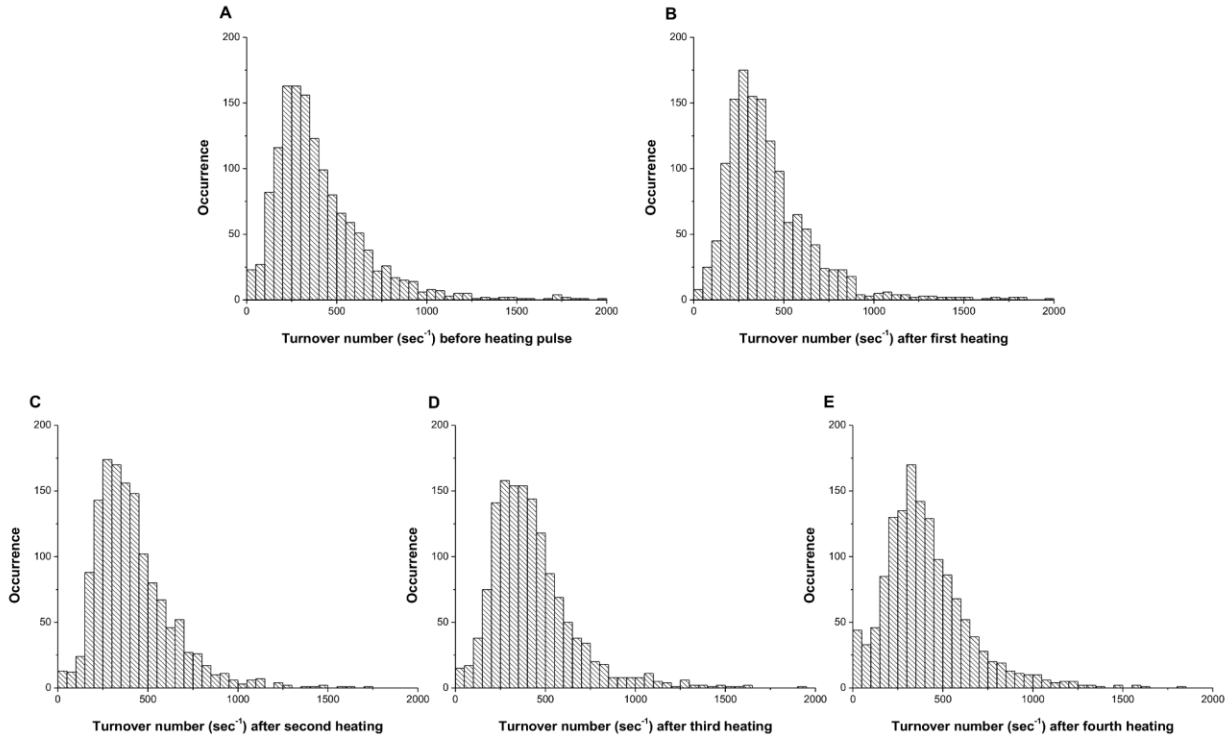

Figure 3.5. Histograms of activity distribution for single β-galactosidase molecules after each heating cycle. (A) Activity distribution of single β-galactosidase molecules before heating. The mean turnover number for the population of single β-galactosidase molecules of the enzyme population is calculated as 420 s^{-1}. (B,C,D,E) Activity distribution of single enzyme molecules after each sequential heating pulse. The mean turnover numbers are 426 s^{-1}, 418 s^{-1}, 427 s^{-1} and 411 s^{-1} respectively. The bin size for all the histograms is 50 s^{-1}. Measurements were made at 20 °C.

After obtaining the initial activity of the enzyme molecules, five short heating pulses were introduced (Chapter 2, Figure 2.3) and the activities were measured after each pulse (Table 3.1 and 3.2). When populations of enzymes were exposed to pulses of heat, the activity distributions narrowed slightly after the first two heating pulses. After the second heating pulse, the activity distributions did not change. Importantly, the average activities after each heating pulse were similar to the average activities prior to heating (Figure 3.5, A-E).

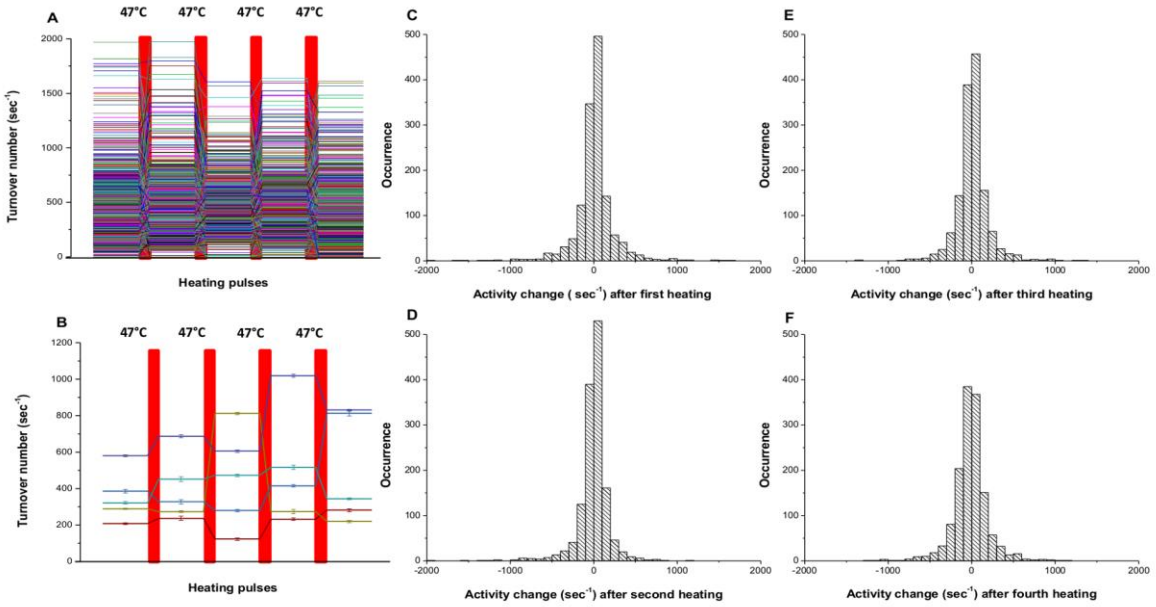

Figure 3.6. Activity traces and changes in individual β-galactosidase molecules between heat pulses. (A) Activity traces of all the individual β-galactosidase molecules taken from a single experiment. Six images were taken between each heating pulse and the activity was obtained (R^2 = 0.9 or greater). (B) Only four individual enzyme activity traces are shown to make it clear how the activities change after each heating pulse. The error bars correspond to linear fitting of data between heating pulses. (C, D, E, F) Histogram of the activity changes resulting from heat pulses. Negative values correspond to a decrease in the activity and positive values correspond to an increase in the activity after a heat pulse. The average changes in activity are 4 s^{-1}, -10 s^{-1}, 9 s^{-1}, and -15 s^{-1} respectively for C, D, E and F.

When the activities of individual β-galactosidase enzymes were studied, the turnover rates of individual enzymes changed randomly upon introducing a heat pulse and then remained constant during the period between heat pulses (Figure 3.6, A, B Figure 3.7).

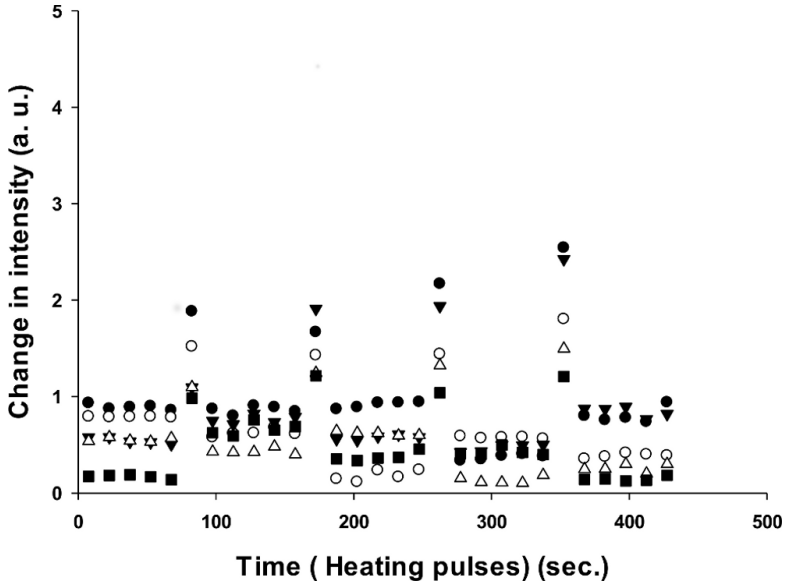

Figure 3.7. The first derivative plot of raw intensities of individual molecules with respect to time. The activities of the enzymes are relatively stable between the heating pulses. The sudden increases of the activities observed in the graph are due to the heating pulse when the solution did not have time to reach room temperature. Those frames are excluded from the analysis.

Enzyme activity was stable ($R^2 > 0.9$) during the 120 s (6 frames) between the heat pulses (Table 3.1). After each heating cycle, the activity of each individual enzyme molecule changed randomly from its prior activity, with approximately 50% of the population gaining activity and 50% losing activity (Figure 3.6, C-F, Figure 3.8, Figure 3.9, B). Considering the error associated with linear fitting, a maximum of 12 % of the enzyme population may have unchanged activity after a given pulse.

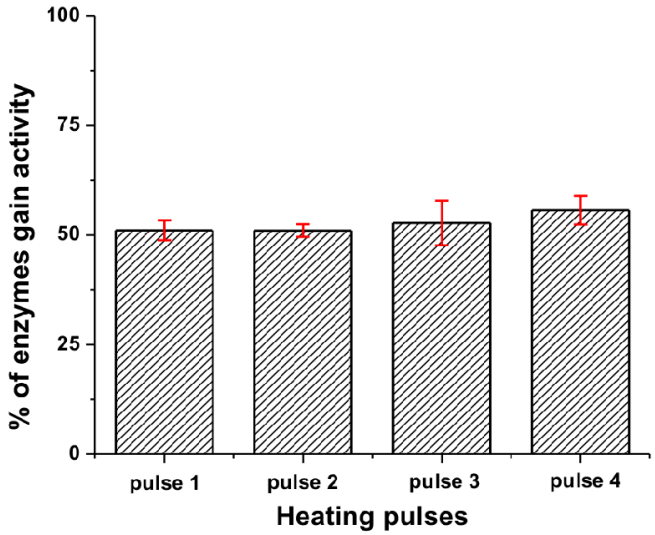

Figure 3.8. Bar graph representing the percentage of enzyme population gaining activity after each heating pulse. The error bars represent variations from four different experiments.

There are several possible results that may be expected to occur upon heating an enzyme. First, if the activation barrier is too high for the molecule to convert to a different local minimum, the enzyme will fall back into the same local minimum, maintain its original conformation, and there will be no change in the reaction rate after heating. Second, if the enzyme overcomes the energy barrier, it may convert to a new stable conformation. The new conformation may have either a faster or slower reaction rate. The changes in activity could also be a result of the tetramer-dimer-monomer equilibrium. At the single molecule level, however, the tetramer-dimer-monomer equilibrium is shifted to the monomer form due to the low concentration of monomer in the microwells such that if the tetramer dissociates, we would expect an irreversible loss in enzyme activity—a phenomenon we observe for a small number of enzyme molecules in these experiments. Narrowing of the distribution after the first heating pulse may be caused by kinetic traps that have slightly higher energy barriers and are only accessible when the nascent protein folds; thus some enzymes cannot return to their previous states upon re-heating at 47°C. No

correlation between the activities of enzymes before and after heating was observed, suggesting that enzymes have no 'memory' of any previous conformations before the heating pulse was introduced (Figure 3.9, A).

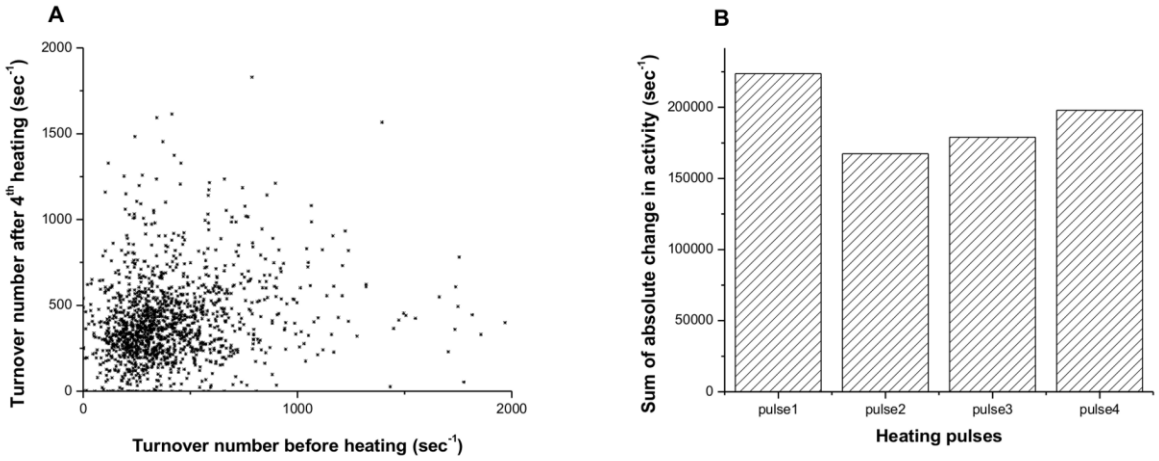

Figure 3.9. Observations of enzyme activities before and after heating (A) Plot of the turnover number of enzymes before heating vs. turnover number after the fourth heating. No correlation between activities was observed. (B) Bar graph of sum of absolute activity changes for all enzymes after each heating pulse. No dramatic change is observed between different heating pulses.

The change in activity of each enzyme was random as well, i.e., it did not correlate with its initial activity. Each enzyme exhibits an equal probability of either gaining or losing activity through all heating periods (Figure 3.6, C-F, Figure 3.8). As temperature increases, a protein molecule is expected to gain enough energy to overcome an energy barrier and convert to a new conformation that has a different activity (Figure 3.10). If conformational differences between different enzyme molecules are the cause of the broad activity distribution, then the activities of the individual molecules should redistribute after each heating pulse, which is what we observe (Figure 3.6 A, B). On the other hand, if sequence differences are the sole basis for the activity distribution, then upon heating, each enzyme molecule should revert to its original activity. Our results clearly show that virtually all the enzyme molecules redistribute their activity when

heated, demonstrating the importance of conformations in static heterogeneity. It is important to note that both conformation *and* sequence may contribute to the activity distribution because enzyme molecules with different sequences will also interconvert between conformations upon heating. Moreover, enzymes with different primary sequences may display varying kinetic responses upon heating (Figure 3.6 A, B).

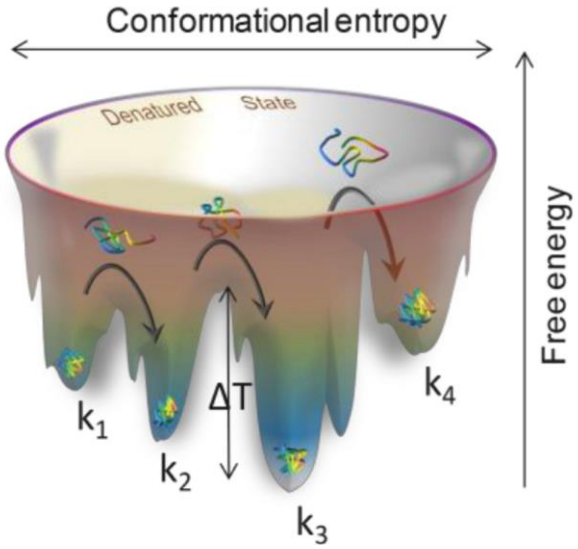

Figure 3.10. Depiction of the energy landscape. An enzyme with a characteristic rate k_1 is trapped in a local minimum. When a heat pulse is introduced (ΔT), the enzyme changes its conformation and relaxes into a different minimum. The new conformation exhibits a different rate (k_2). After sequential pulses, the enzyme can adopt different conformations leading to different rates (k_3, k_4).

In addition to the observed change in activity due to conformational changes, irreversible denaturation of some enzyme molecules occurred, which is likely the reason for some loss in activity when activity is measured in bulk solution.(*22-25*) The denaturation temperature of β-galactosidase was calculated to be 55^{o}C by CD experiments and confirmed by kinetic measurements (Figure 3.3), which agrees well with denaturation temperatures reported in the literature.(*15, 26-28*) In the present experiments, denaturation of the enzymes was minimized by heating only to 47°C, which is below this denaturation temperature. Enzymes that did not show

any activity after three consecutive heating pulses were considered denatured and were not included in the analysis. However, enzymes that lost activity after a heat pulse and gained activity in a subsequent heat pulse were not considered to have denatured. An additional fifth heat pulse was used to determine if the enzyme was denatured. When sufficient energy is introduced, an active enzyme (A) should denature and lose activity (D) based on a denaturation rate k_d (Eq. 3.1) and should follow first order reaction kinetics with respect to the heat pulses. (Figure 3.11) The rate of denaturation, (k_d), is calculated using Eq. 3.2, where the number of active molecules, (N), changes with respect to the heat pulse number, (Hp),

$$A \xrightarrow{k_d} D \quad \text{(Eq. 3.1)}$$

$$-\frac{dN}{dHp} = k_d N \quad \text{(Eq. 3.2)}$$

and is equal to 0.6% of the population per heating pulse. The total number of enzymes that denatured during the experiment was minimal.

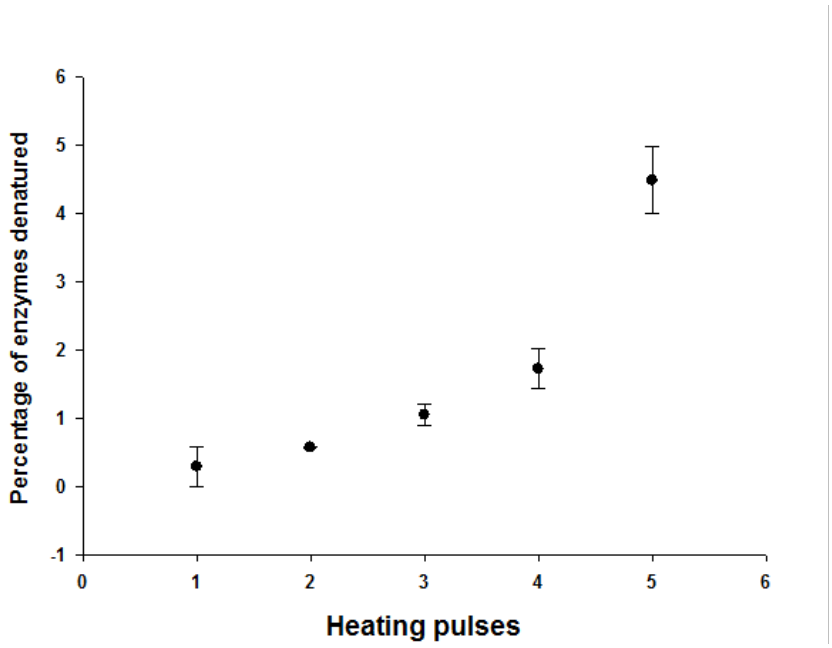

Figure 3.11. First order relationship between heating pulses and natural logarithm of the number of denatured molecules. A denatured molecule is defined as a molecule that does not show any activity after a heating pulse. Molecules that are not active but gain activity after a heating pulse are not considered denatured. The calculated rate of denaturation is equal to 0.6% of the total population per heating pulse with an R^2 value of 0.98.

There are three major denaturation pathways: aggregation, dissociation, and irreversible conformational changes. Since the enzyme is trapped inside the well, aggregation is ruled out as a possibility. We performed a native gel bulk analysis of the unheated and heated enzyme and only observed bands corresponding to the tetramer for the unheated enzyme. On the other hand, the heated enzyme showed bands corresponding to the monomer as well as the tetramer (Figure 3.12). This analysis shows that dissociation of the enzyme into monomers occurs under our experimental conditions but reassociation would be virtually impossible as the collision frequency in the microwells is extremely low due to the very low concentration of the four monomers.

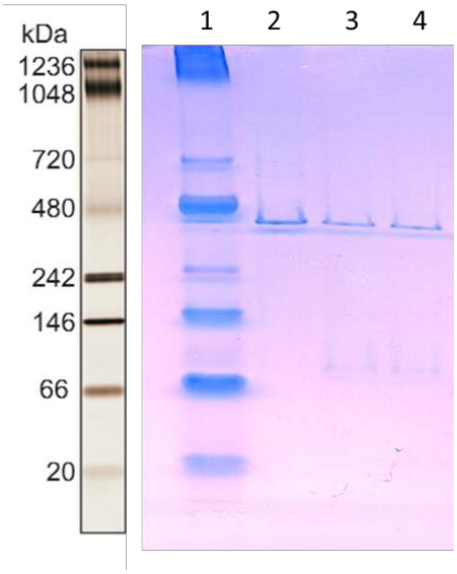

Figure 3.12. Native Novex® Tris-Glycine polyacrylamide gel of β-galactosidase**.** Lane 1 is a ladder, lane 2 is purified β-galactosidase, lanes 3 and 4 are enzymes heated at 47°C for 2 min and 4 min.

Finally, the third possible denaturation pathway, irreversible conformation changes, has not been ruled out as a possibility, but we do not include any enzyme molecules that exhibit irreversible denaturation in the analysis. It is also plausible that a single enzyme molecule's activity is below the detection limit of 5 s^{-1}, which is only 1% of the average activity for β-galactosidase. No correlation between a particular enzyme activity and its rate of denaturation was observed.

3.2.2 Sequence based heterogeneity studies

3.2.2.1 Introduction

In the previous section we showed that stable protein conformations are responsible for the activity distribution of β-galactosidase. However, differences in primary structure among individual molecules could also affect the activity distribution. In this section, we present single molecule studies of β-galactosidase expressed by *Bacillus Subtilis*. The enzyme was expressed at two different temperatures (23°C and 36°C). As previously reported, mutations in the protein stemming from errors in transcription and translation can be altered by changes in the environment such as temperature or type of medium.(*29*, *30*) Recent studies by Prof. Sigal Ben-Yehuda *et*. *al*. showed that the error level in expressed protein increases at lower temperature.(*31*) We were able to obtain samples from the Ben-Yehuda lab of two populations of the enzyme having different percentages of random errors. Our aim was to perform single molecule experiments and compare the activity distributions of both populations of enzymes. If the errors contribute greatly to the distribution of the activity, we should be able to observe a different distribution for different populations of the enzyme containing a different rate of random errors.

3.2.2.2 Materials and Methods

Materials and Bulk Solution Preparation

The β-galactosidase enzyme was expressed in *Bacillus Subtilis* at different incubation temperatures (23°C and 36°C) in Prof. Sigal Ben-Yehuda's lab at the Hebrew University of Jerusalem in Israel. The proteins were purified and shipped in dry ice. The samples contain 50

mM NaH_2PO_4, 300 mM NaCl, 250 mM imidazole, and 100 mM ABSEF inhibitor. The concentrations of the samples were evaluated by the Bradford assay (Appendix 1) as 0.59 μM for the protein expressed at low temperature (23°C) and 1.75 μM for the protein expressed at high temperature (39°C). Aliquots of 10 μL were stored at -80°C. The enzyme stock solution was diluted in 1x PBS/$MgCl_2$ buffer to 360 pM immediately before analysis. The substrate resorufin β-D-galactopyranoside (RBG) and the product resorufin were purchased from Invitrogen, Carlsbad, CA. The substrate was prepared as described in the previous section.

Bulk Experiments

Bulk experiments were performed on an Infinite M200 microtiter plate reader from Tecan AG, Mannedorf, Switzerland. 20 μL of 36 pM enzyme solution was directly added to 180 μL of 100 μM substrate solution. To obtain the kinetic data, commercially available enzyme and two enzyme mutants expressed in bacteria were mixed with different concentrations of the substrate (0, 10, 25, 50, 75, 100 μM of final substrate concentration). The fluorescence intensity (Ex=558 nm, Em=590 nm) was monitored in the plate reader at 30 sec. intervals for 1 hour.

Microarray preparation

Eight custom made optical fiber bundles were joined together by silicone elastomer Sylgard 184 strip described in details in **Chapter 2** (Figure 3.14). Both sides of the bundles were polished using a fiber polisher from Allied High Tech Products Inc., Rancho Dominguez, CA with a custom made fiber holder. One end of the strip was etched in 0.025 M HCl for 115 s. The differential rate of etching between the core and the cladding results in an array of 2.5 μm deep wells of 46 fL volume.

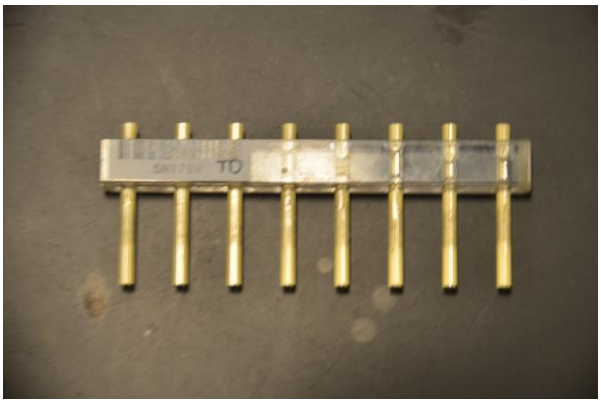

Figure 3.13. Photograph of the fiber strip. The strip contains 8 individual fiber bundles, with 50,000 fibers per fiber bundle.

The strip was washed several times with EDTA and ethanol followed by plasma treatment for 60 sec in a plasma cleaner from Harrick Plasma, Ithaca, NY. The surface of the wells was silanized following the protocol described in **Chapter 2**. The silanized fiber strips were washed with ethanol and dried under low pressure for 1 hour. The resulting fiber strips were placed in a nitrogen-filled container at 80°C for 30 min. The fiber bundles were stored under nitrogen in a desiccator.

Microscope/stage description

Single molecule enzymatic assays were performed on a custom designed imager from Quanterix, Lexington, MA described in detail in **Chapter 2**. The imager is equipped with a 200 Watt metal arc lamp from Prior Scientific, Rockland, MA. The excitation source and fluorescence emission are filtered through a filter cube (Ex. 559 nm, Em. 630 nm, dichroic 585 nm LP) from Semrock, Rochester, NY. Emission was detected by a CCD camera Infinity4-11 from Lumenera, Ontario, Canada and captured images were analyzed by the MATLAB software from MathWorks. Natick, MA. The optical fiber strip was fixed on the custom stage of an upright microscope such that the

non-etched end of the bundle was facing the objective (10x, LU PlanFluor, from Nikon, Japan). 8 25 µL droplets of the substrate solution (100µM) containing the diluted enzyme (3.6 pM) were placed on a well-cleaned PDMS gasket on a glass slide directly under each fiber. The z-direction stage was then used to mechanically seal the reaction solution within the optical fiber wells.

Image processing, normalization, and data analysis

Images were obtained every 30 sec. by collecting the fluorescence from the entire fiber with an exposure time of 2 sec. (Figure 3.15).

The same fiber was used to calculate the standard curve for the product concentration and for the photobleaching experiment. Activities of individual enzymes were calculated as previously described.(*32*)

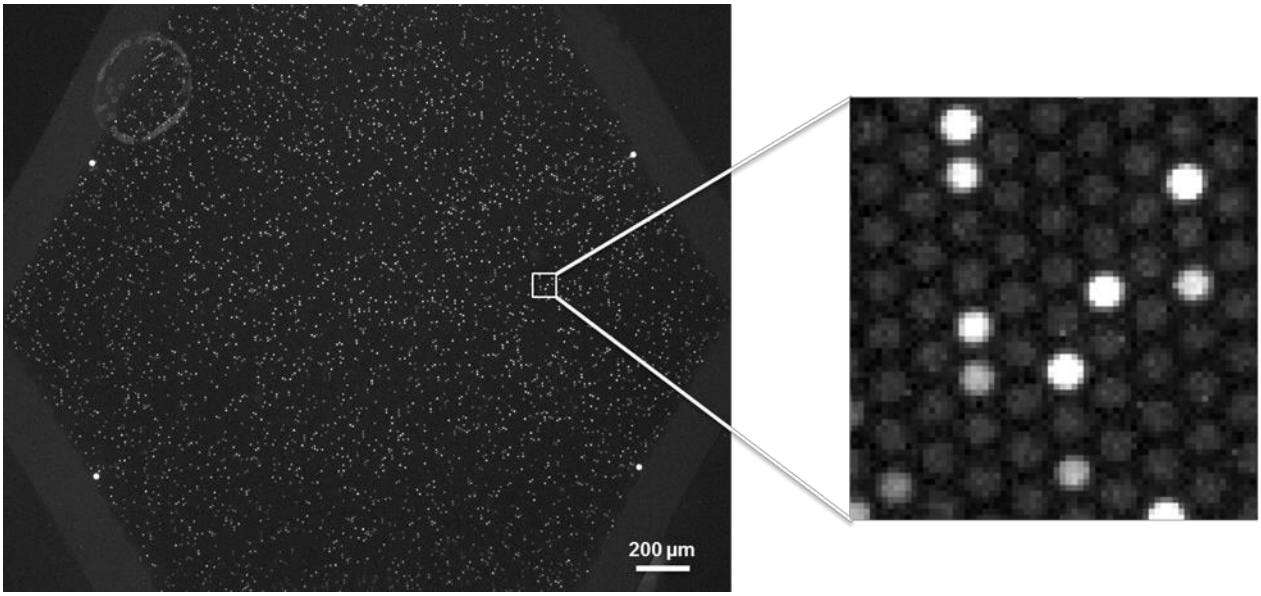

Figure 3.14. Fluorescence image of a fiber bundle. Each fluorescent well contains an individual active enzyme.

3.2.2.3 Results and Discussion

The kinetic progression curves of the two enzyme samples expressed in *Bacillus Subtilis* that had been grown at 23°C and at 36°C as well as a sample of commercially available β-galactosidase were obtained from the bulk studies and compared (Figure 3.16). The turnover number calculated from bulk experiments is 264 s^{-1} for the commercially available enzyme, 14 s^{-1} for the enzyme expressed at 23°C and 10 s^{-1} for the enzyme expressed at 36°C.

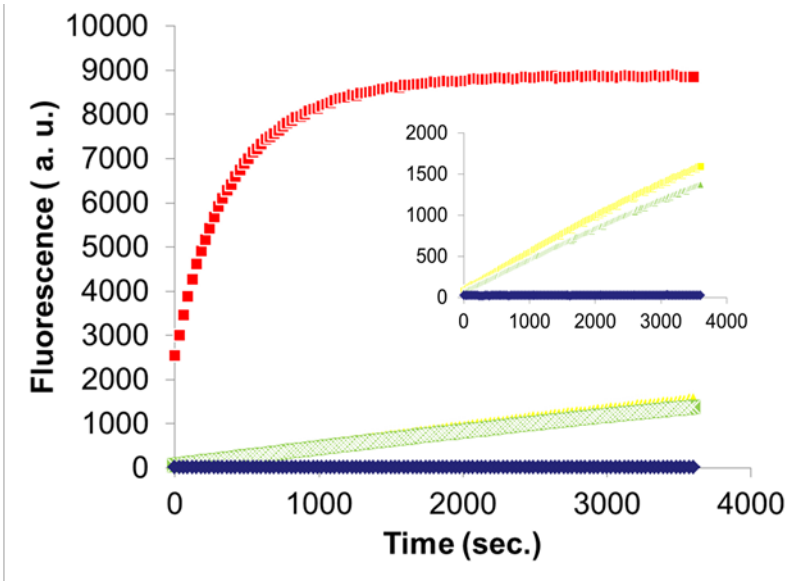

Figure 3.15. Progress curves of enzymatic reaction of the β-galactosidase enzyme. Kinetics of 360 pM commercially available enzyme (red), enzyme expressed at 23°C (yellow), and enzyme expressed at 36°C (green) were interrogated. An enzymatic assay was run for 60 min. Data show the kinetics curves for the 100 μM concentration of the substrate. Inset: Zoom of the y-axis where the small difference in the activity of less active enzymes is visible. Background is shown in blue.

Moreover we also performed single molecule experiments on the enzymes expressed in bacteria that had been grown at 23°C and at 36°C. According to previous studies, the enzymes obtained from the bacteria grown at low temperature or in an extreme environment should have more errors (Figure 3.16).(*31*)

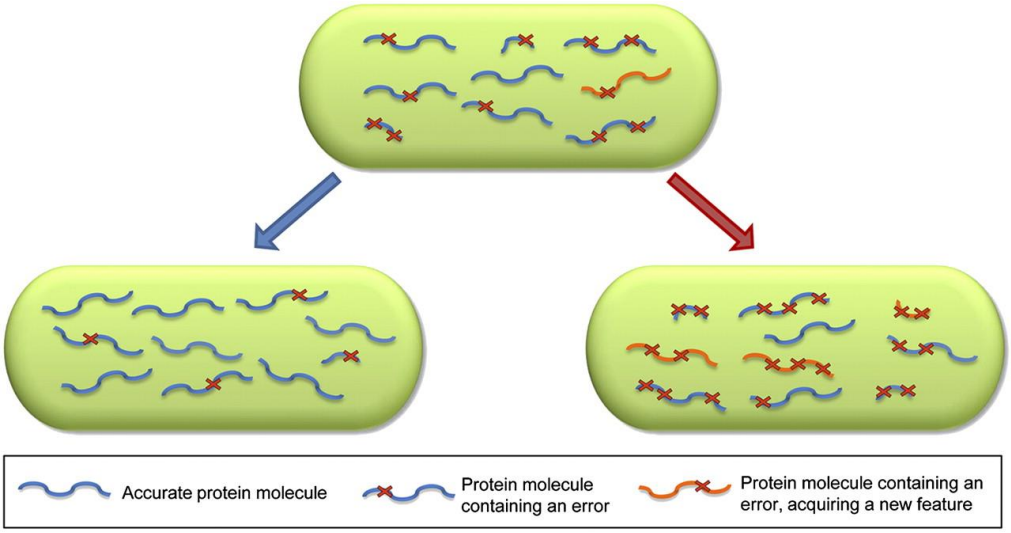

Figure 3.16. Heterogeneity of protein expression of bacterium. Schematic representation of the protein molecules produced by a single gene. Under normal growth conditions, the bacterial cell contains a mixture of different protein species. During certain conditions, such a high temperature, gene expression is more accurate and the proteins are more homogenous. (Lower left) During stress conditions, such as starvation or low temperature, the heterogeneity of produced proteins increases. (Lower right) Figure from ref. 31.

Previous studies showed that gene expression at the higher temperature is more accurate resulting in more homogenous protein structures.(*31*) During low temperature conditions or other challenging conditions, an increase in errors expands the variety of protein structures; hence more proteins with more amino acids substitutions are produced (Figure 3.16). These substitutions can potentially increase the robustness of the bacterium under stress. If errors in the primary structure play an important role in the static heterogeneity of the activity, the distribution of activities for enzymes expressed in the bacteria at lower temperature should be more diverse. From a single molecule perspective we would expect a broader distribution of the enzymatic activities within the population of proteins expressed at the lower temperature. When we obtained both distributions and compared the activities, we observed that both distributions looked similar.

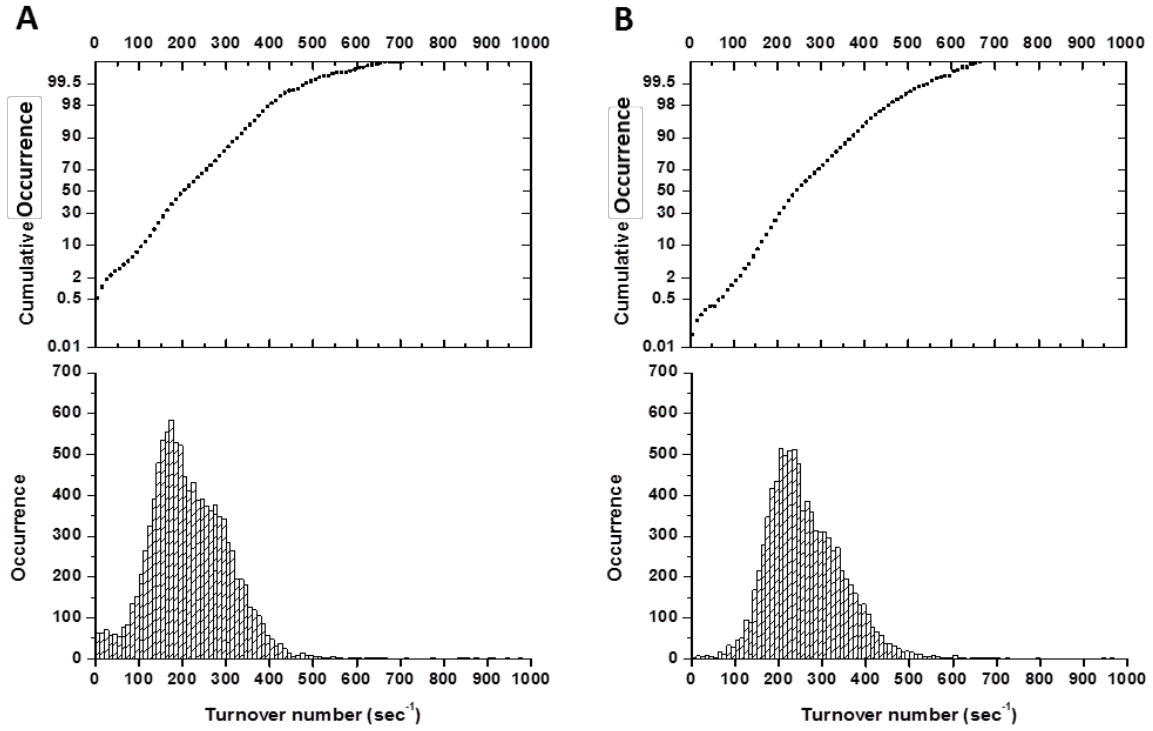

Figure 3.17. Activity distributions of single β-galactosidase enzymes. Distribution of the activity of A) β-galactosidase expressed at 37°C and B) β-galactosidase expressed at 23°C. Upper graphs correspond to normalized cumulative occurrence of increasing activities. The studies were performed on more than 11000 individual molecules on the 8 fiber strip using the Quanterix optical instrument. The binning is 10 molecules per second. The average turnover number for (A) is 212 s^{-1} and for (B) is 260 s^{-1}.

The average turnover numbers obtained in the single-molecule studies were relatively close to the turnover number obtained from bulk studies for the commercially available enzyme. The mean activity of the enzymes expressed in bacteria at high temperature is 212 turnovers per second, and for the enzymes expressed at low temperature the mean activity is 260 turnovers per second, whereas for the commercially available enzymes the mean activity measured in bulk is 264 turnovers per second. However, we observe a large difference between the bulk and single molecule experiments in the enzymatic activities for the enzymes expressed at high and low temperature (14 s^{-1} and 10 s^{-1} vs. 212 s^{-1} and 260 s^{-1}, respectively). This discrepancy can be

explained by the presence of enzymes that do not have activity because of the high concentration of errors per molecule. The bulk experiments are based on the total concentration of the protein (active and non-active). However, the single molecule experiments measure only active proteins; hence, the presence of non-active enzymes will decrease the mean activity in bulk measurements but will not influence the mean activity measured at the single molecule level. The calculated coefficient of variation (CV) is 56% for the enzymes expressed at high temperature and 33% for the enzymes expressed at low temperature. These results agree with the bulk experiments for the commercially available enzyme (33%). The observed difference between the activity distributions for enzymes expressed at high and low temperature is most pronounced at the low enzyme activity region. To eliminate any bias related to the analysis, we compared the background intensities of inactive wells in the two experiments and used a thresholding technique to make sure that comparable lower-activity enzymes are included in the analysis of both experiments. Above this low activity region the distributions of both populations are not distinguishable from each other (Figure 3.18).

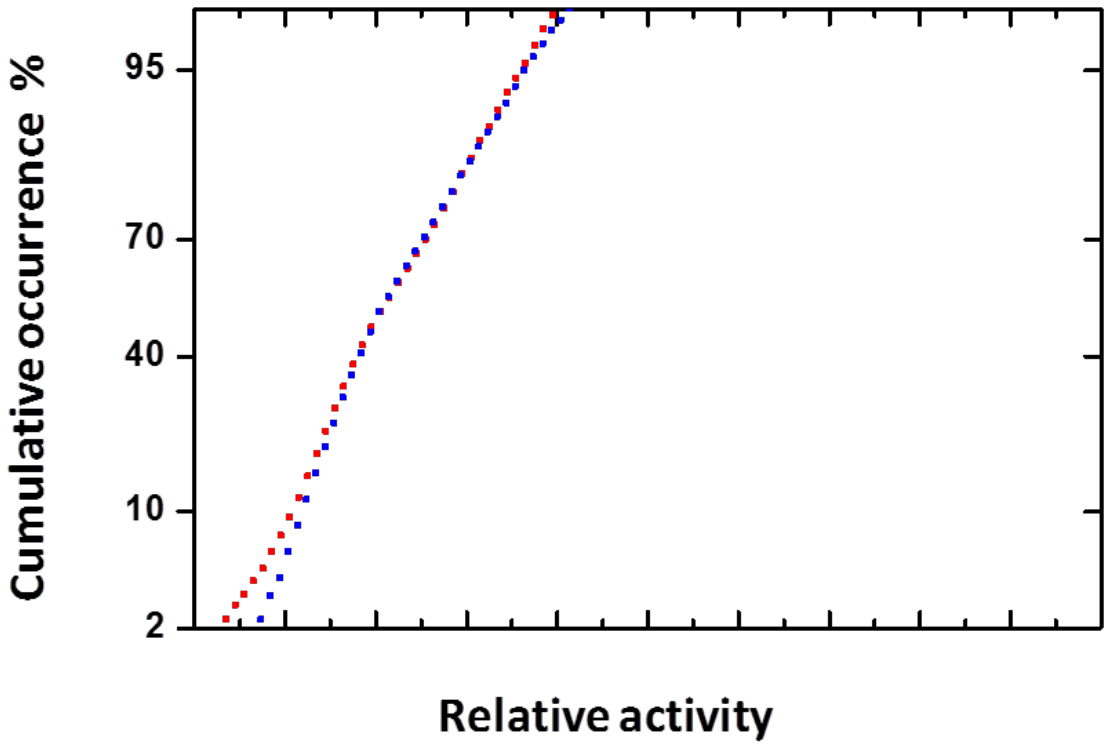

Figure 3.18. Relative activity of the two enzyme populations. Cumulative occurrence for enzymes expressed in bacteria at low temperature (blue) and high temperature (red) plotted against relative activity. The 2% of the enzymes with the highest and the lowest activities were omitted from this graph. (i.e., activities within 2 standard deviations of the mean are included.) The activity distributions for both populations only differ in the low activity range.

One possibility is that for enzymes expressed under stressed conditions, additional errors are imposed on the top of the usual random error rate, and that these added errors either enhance or have no effect on the activity. However, there may exist some maximum error rate at which the enzyme loses its activity. This hypothesis is consistent with the obtained results. First, enzymes at the lower activity region already have a high number of errors and any additional change in primary structure causes complete loss of activity. However, in the previous section we proved that activity values are influenced by enzyme conformation, and that activity values do not correspond to changes in primary structure of the protein. Recall that low activity enzymes can

switch to a high activity state when a heat pulse is introduced. Second, the increase of errors may be beneficial for enzymes up to some critical threshold, leading to either no change, or an increase in average activity. However, some enzymes will completely lose their activity due to errors if an error threshold is exceeded. This "all or nothing" possibility is supported by the bulk and single molecule average activity data. For both single molecule experiments we use the same protein concentration of the enzymes. However, when the active molecules were counted, the sample expressed at low temperature had 75% of the number of active molecules found in the sample expressed at high temperature. This result agrees with the trend observed in bulk studies (The average activity of the low temperature sample was 71% that of the high temperature sample.). These data suggest that additional errors will either increase the enzyme activity or leave it unchanged, or will completely abolish the enzyme activity. (In other words, it is not possible for these errors to modulate the activity downward without completely turning it off). It would be beneficial to know the error ratio between the two populations and check whether this ratio supports our hypothesis.

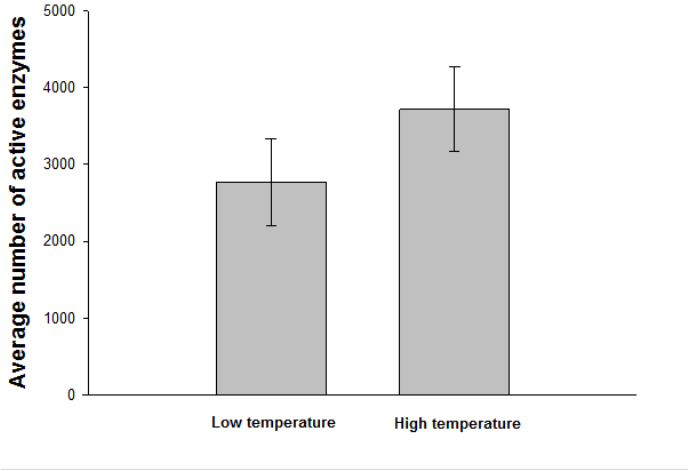

Figure 3.19. **The enzyme occurrence bar graph**. The average number of active enzymes detected at the single molecule level. Standard deviations correspond to triplicate measurements.

3.3 Conclusion

In the first section of this chapter, we presented a platform capable of observing the activities of thousands of single enzyme molecules and perturbing them using thermal energy. Using this platform, we observed that individual β-galactosidase molecules have numerous stable activity states that can be interconverted by providing thermal energy to the system. This work proves that these activity changes are the result of conformational changes. We demonstrated that static heterogeneity of an enzyme population is caused by the existence of many different yet stable conformations. The ability to perturb enzyme conformation using thermal energy provides a new tool for studying single enzyme molecules that can lead to new insights into fundamental biochemistry. The second section of this chapter supports the data presented in the first section. We showed that introduced errors do not greatly change the distribution of the activities; hence they play a marginal role in the activity differences observed in single enzyme kinetics studies. However, we do not eliminate the possibility that sequence differences between molecules may also lead to some heterogeneity in activity. The β-galactosidase structure has many available conformations due to its size, and any changes in activity influenced by the changes in primary structure could be hidden by those caused by conformational changes. Hence, we can only observe extreme cases such as "all or nothing" type activity changes of individual enzymes with respect to error content. In future work we would suggest using a much smaller enzyme to study the relationship between activity changes due to errors and due to conformation.

3.4 References

1. B. P. English *et al*., Ever-fluctuating single enzyme molecules: Michaelis-Menten equation revisited. *Nature chemical biology* **2**, 87 (Feb, 2006).
2. D. M. Rissin, H. H. Gorris, D. R. Walt, Distinct and long-lived activity states of single enzyme molecules. *J Am Chem Soc* **130**, 5349 (Apr 16, 2008).
3. W. Min *et al*., Fluctuating enzymes: lessons from single-molecule studies. *Accounts of chemical research* **38**, 923 (Dec, 2005).
4. H. H. Gorris, D. M. Rissin, D. R. Walt, Stochastic inhibitor release and binding from single-enzyme molecules. *Proc Natl Acad Sci U S A* **104**, 17680 (Nov 6, 2007).
5. Q. F. Xue, E. S. Yeung, Differences in the Chemical-Reactivity of Individual Molecules of an Enzyme. *Nature* **373**, 681 (Feb 23, 1995).
6. D. B. Craig *et al*., Differences in the average single molecule activities of E-coli beta-galactosidase: Effect of source, enzyme molecule age and temperature of induction. *J Protein Chem* **22**, 555 (Aug, 2003).
7. H. P. Lu, L. Y. Xun, X. S. Xie, Single-molecule enzymatic dynamics. *Science* **282**, 1877 (Dec 4, 1998).
8. D. D. Boehr, R. Nussinov, P. E. Wright, The role of dynamic conformational ensembles in biomolecular recognition (vol 5, pg 789, 2009). *Nature chemical biology* **5**, 954 (Dec, 2009).
9. K. Henzler-Wildman, D. Kern, Dynamic personalities of proteins. *Nature* **450**, 964 (Dec 13, 2007).
10. F. Schotte, J. Soman, J. S. Olson, M. Wulff, P. A. Anfinrud, Picosecond time-resolved X-ray crystallography: probing protein function in real time. *J Struct Biol* **147**, 235 (Sep, 2004).
11. L. C. James, D. S. Tawfik, Conformational diversity and protein evolution - a 60-year-old hypothesis revisited. *Trends Biochem Sci* **28**, 361 (Jul, 2003).
12. A. C. Dyck, D. B. Craig, Individual molecules of thermostable alkaline phosphatase support different catalytic rates at room temperature. *Luminescence* **17**, 15 (Jan-Feb, 2002).
13. D. A. Drummond, C. O. Wilke, The evolutionary consequences of erroneous protein synthesis. *Nature reviews*. *Genetics* **10**, 715 (Oct, 2009).
14. A. M. van Oijen *et al*., Single-molecule kinetics of lambda exonuclease reveal base dependence and dynamic disorder. *Science* **301**, 1235 (Aug 29, 2003).
15. D. B. Craig, E. R. Nichols, Continuous flow assay for the simultaneous measurement of the electrophoretic mobility, catalytic activity and its variation over time of individual molecules of Escherichia coli beta-galactosidase. *Electrophoresis* **29**, 4298 (Nov, 2008).
16. J. N. Onuchic, P. G. Wolynes, Theory of protein folding. *Curr Opin Struc Biol* **14**, 70 (Feb, 2004).

17. E. Z. Eisenmesser *et al*., Intrinsic dynamics of an enzyme underlies catalysis. *Nature* **438**, 117 (Nov 3, 2005).
18. D. A. Drummond, C. O. Wilke, The evolutionary consequences of erroneous protein synthesis. *Nature Reviews Genetics* **10**, 715 (Oct, 2009).
19. D. B. Craig, T. Schwab, R. Sterner, Random mutagenesis suggests that sequence errors are not a major cause of variation in the activity of individual molecules of beta-galactosidase. *Biochemistry and Cell Biology-Biochimie Et Biologie Cellulaire* **90**, 540 (Aug, 2012).
20. D. M. Rissin, H. H. Gorris, D. R. Walt, Distinct and long-lived activity states of single enzyme molecules. *J Am Chem Soc* **130**, 5349 (Apr 16, 2008).
21. D. M. Rissin, D. R. Walt, Digital concentration readout of single enzyme molecules using femtoliter arrays and Poisson statistics. *Nano letters* **6**, 520 (Mar, 2006).
22. M. E. Peterson, R. M. Daniel, M. J. Danson, R. Eisenthal, The dependence of enzyme activity on temperature: determination and validation of parameters (vol 402, pg 331, 2007). *Biochemical Journal* **403**, 615 (May 1, 2007).
23. R. M. Daniel, M. Dines, H. H. Petach, The denaturation and degradation of stable enzymes at high temperatures. *Biochemical Journal* **317**, 1 (Jul 1, 1996).
24. E. Jurado, F. Camacho, G. Luzon, J. M. Vicaria, Kinetic models of activity for beta-galactosidases: influence of pH, ionic concentration and temperature. *Enzyme Microb Tech* **34**, 33 (Jan 5, 2004).
25. T. M. Thomas, R. K. Scopes, The effects of temperature on the kinetics and stability of mesophilic and thermophilic 3-phosphoglycerate kinases. *Biochemical Journal* **330**, 1087 (Mar 15, 1998).
26. S. Yoshioka, Y. Aso, K. Izutsu, S. Kojima, Is Stability Prediction Possible for Protein Drugs - Denaturation Kinetics of Beta-Galactosidase in Solution. *Pharmaceutical research* **11**, 1721 (Dec, 1994).
27. A. Muga, J. L. R. Arrondo, T. Bellon, J. Sancho, C. Bernabeu, Structural and Functional-Studies on the Interaction of Sodium Dodecyl-Sulfate with Beta-Galactosidase. *Archives of biochemistry and biophysics* **300**, 451 (Jan, 1993).
28. H. F. Arata, Y. Rondelez, H. Noji, H. Fujita, Temperature alternation by an on-chip microheater to reveal enzymatic activity of beta-galactosidase at high temperatures. *Anal Chem* **77**, 4810 (Aug 1, 2005).
29. M. Ballesteros, A. Fredriksson, J. Henriksson, T. Nystrom, Bacterial senescence: protein oxidation in non-proliferating cells is dictated by the accuracy of the ribosomes. *Embo Journal* **20**, 5280 (Sep 17, 2001).
30. P. H. Ofarrell, Suppression of Defective Translation by Ppgpp and Its Role in Stringent Response. *Cell* **14**, 545 (1978).
31. M. Meyerovich, G. Mamou, S. Ben-Yehuda, Visualizing high error levels during gene expression in living bacterial cells. *P Natl Acad Sci USA* **107**, 11543 (Jun 22, 2010).

32. M. J. Rojek, D. R. Walt, Observing Single Enzyme Molecules Interconvert between Activity States upon Heating. *Plos One* **9**, (Jan 21, 2014).

Chapter 4: Measuring the Thermodynamic Properties of Single Enzyme Molecules

4.1 Abstract

In this chapter we demonstrate the ability to measure activation energies for many individual enzyme molecules within a population. Hundreds of non-immobilized single β-galactosidase molecules were trapped in femtoliter reaction chambers and the activities of individual enzymes were measured at different temperatures. The average activation energy of the entire population was determined to be 52 kJ mol^{-1} with a broad distribution of activation energies from 5 kJ mol^{-1} to 115 kJ mol^{-1} for individual enzyme molecules. In addition to the activation energies, the entropies and enthalpies of individual enzyme molecules were obtained.

4.2 Introduction

The origins of enzymatic rate acceleration remain incomplete.(*1*) In **Chapter 3** we showed that individual enzymes have different reaction rates that might be associated with different stable conformations. (*2-4*) Furthermore, several studies showed that the activation energies of single molecules are heterogeneous.(*2, 5-8*) However, none of the previous studies explored the relationship between activation energy and the turnover rates of individual enzymes. Enzymatic reactions follow the Arrhenius relationship and demonstrate an increase of activity with increasing temperature. Beyond a critical temperature, enzymes also undergo thermal denaturation resulting in a loss of activity.(*9, 10*) Due to the correlation between temperature and enzyme activity, it is of great interest to study the activity of single enzyme molecules over a broad temperature range. Moreover, knowing the values of the reaction rate constants and the

activation energies of the catalytic steps can provide insight into the molecular basis of static heterogeneity observed in an enzyme population.(*11*) Earlier thermal studies were performed on 2000 enzymes per well(*12*) or were using capillary electrophoresis based assays and were restricted to kinetic measurements for short time intervals at a maximum of three different temperatures.(*5*) (*2, 13*) Here, we present a method for simultaneously interrogating the activity of hundreds of individual enzyme molecules across a temperature range of 11°C to 65°C thereby enabling us to study conformation-induced kinetic changes and determine the thermodynamic properties of single enzyme molecules.

4.3 Materials and Methods

Materials.

Lyophilized β-galactosidase (Grade VIII) from *Escherichia coli* was purchased from Sigma-Aldrich (St. Louis, MO). The enzyme was purified by the size exclusion chromatography and reconcentrated to 2 μM in 1:1 solution of autoclaved 1xPBS/1mM $MgCl_2$ and glycerol. To confirm purity and chemical homogeneity of the enzyme, the LC/MS/MS analysis was performed. Trypsin and chymotrypsin digested protein analysis was conducted with the Agilent 6550 Q-TOF MS (Santa Clara, CA) and Thermo-Fisher LTQ-Orbitrap (San Jose, CA) instruments (Appendix 2). Aliquots of 10 μL were stored in a –80 ˚C freezer. The enzyme stock solution was diluted to 3.6 pM in 1xPBS/1mM $MgCl_2$ buffer just before the experiments. Resorufin β-D-galactopyranoside (RBG) and resorufin were purchased from Invitrogen (Carlsbad, CA). Resorufin β-D-galactopyranoside was dissolved in DMSO to a concentration of 100mM and 5 μL aliquots were stored at -20 °C and diluted to 10 mM in DMSO before each experiment. 10x PBS buffer (pH 7.4) was purchased from Ambion (Foster City, CA).

Bulk experiments

Thermal stability experiments at six different temperatures (11ºC, 22ºC, 36ºC, 41ºC, 50ºC, 65ºC) of the substrate RBG and the resorufin product were performed on the Infinite M200 microtiter plate reader from Tecan AG (Mannedorf, Switzerland). 100 µL of 100 µM RBG substrate was exposed to different temperatures (11ºC, 22ºC, 36ºC, 41ºC, 50ºC, 65ºC) on a dry bath from Lab-net Inc. (Woodbridge, NJ) for 1 min. and cooled to room temperature. The fluorescence intensity (Ex. 558nm/Em. 590nm) was measured for all substrate samples and the background intensities were compared. In addition, each sample was used for a standard enzymatic assay and data were compared with unheated RBG substrate. No differences in fluorescent signals were observed for heated and unheated substrates. A similar experiment was performed with the resorufin product (100µM), which was heated for 1 min. in a dry bath and cooled to room temperature. The fluorescence intensity (Ex. 558nm/Em. 590nm) was recorded over 10 min. for all samples and compared with the fluorescence of the unheated product.

Microarray preparation

Custom made optical fiber bundles (2 mm diameter) composed of 50,000 fibers of 4.5 µm diameter purchased from Schott North America Inc. (Elmsford, NY) were cut to a length of 4.5 cm. Both sides of the bundle were polished using a fiber polisher from Allied High Tech Products Inc (Rancho Dominguez, CA.). One end of the fiber was etched in 0.025 M HCl for 115 sec. Differential etching between the core and the cladding results in an array of 2.5 µm deep wells of 46 fL volume.(*3*) The volume distribution of the wells is within 4% and does not have an effect on the observed activities. The bundles were washed several times with EDTA and ethanol followed by plasma treatment for 60 sec in Expanded plasma cleaner from Harrick Plasma (Ithaca,

NY). The surface of the wells was silanized for 30 min with 150 μL of a slightly hydrophobic silane from Gelest Inc (Morrisville, PA) in 15 mL of ethanol. The silanized fiber bundles were washed with ethanol and dried under vacuum for 1 hour. The resulting fiber bundles were placed in a nitrogen gas filled container at 80°C for 30 min. The fiber bundles were stored under nitrogen in a dessicator and used within two days. To minimize any data misinterpretation due to non-specific binding, we performed several experiments with different types of surface modification. In addition, a photobleaching experiment was performed for each fiber modification where the solution of 10 μM resorufin in deionized (DI) water was enclosed in the individual wells. High intensity light was used to illuminate a small region of the array for 20 min to photobleach the resorufin. A full field of view image was taken, followed by another image after short temperature bursts and no significant leakage between adjacent wells was observed. An additional image was taken after 15 min to confirm the integrity of the seal. (**Chapter 2**)

Microscope/stage description.

An upright Olympus B64 microscope with an attached short arc mercury lamp as an excitation light source was used. The excitation and emission light were filtered through a filter cube (Ex. 577/10x, Em. 620/60m, dichroic 585LP) from Chroma Technology Corp (Bellows Falls, VT). The emitted fluorescence light was detected by a Sensicam QE CCD camera, from Cooke Corporation (Romulus, MI) and the captured images were analyzed using IPLab software from BD Bioscience (Rockville, MD). The setup used to seal the assay solution within fiber wells is described elsewhere.(*3*) In addition, a flat Peltier heating plate with an attached thermocouple was installed between the heat sink and the PDMS sheet (**Chapter 2**). The temperature of the Peltier plate was monitored by a thermocouple and controlled by a computer. The plate was calibrated before each experiment. The temperature of the plate was controlled between 11°C and 65°C by

modifying the power applied to the plate. The temperature stayed constant for 2 min during each heating period and the temperature fluctuations did not exceed 0.5°C.

Image processing, normalization, and data analysis.

Single β-galactosidase molecules and 100 μM non-fluorescent substrate were captured in the 46 fL microwell reaction chambers located on the end of an optical fiber bundle.(*3, 14*) The concentration of the enzyme was calculated using the Poisson equation; at an enzyme concentration of 3.6 pM, the ratio of empty wells to filled wells is expected to be 10:1. At this ratio the probability of having more than 1 enzyme per well is 0.0045 and is considered negligible.(*14*) A fiber bundle containing 50 000 wells was sealed against the Peltier plate cooled to 11°C to randomly trap individual enzymes in the 46 fL wells. To obtain initial enzyme activities, six images were taken 15 seconds apart and the fluorescence signals were obtained for each well containing an active enzyme molecule. Next, the temperature of the Peltier plate was increased stepwise from 22°C to 36ºC, 41ºC, 50ºC and 65ºC with 75 s between each new temperature increase. Five images were obtained for each temperature. The raw fluorescence intensities of the trajectories were multiplied by a calibration factor and background corrected. The substrate turnover rate of each enzyme molecule was calculated before and between heating pulses using the equation $S(t) = F'(t) + k_{ph} \times F(t)$, where S(t) is the substrate turnover rate in sec^{-1}, F(t) is the fluorescence intensity as a function of time, F'(t) is the fluorescence intensity time derivative and k_{ph} is the photobleaching rate.(*3*) The photobleaching rate was determined by trapping 10 μM of fluorescent product and monitoring the fluorescence decreases every 15 second with a 2 second exposure over 1 hour. The activities were obtained by linear fitting of five points for each temperature. The error due to the fitting was ± 5 s^{-1}. The final errors of the activation energy and enthalpy were less than 5 kJ/mol and for entropy were less than 15 J/mol*K.

4.3 Results and discussion

Measurements of individual β-galactosidase molecule activities were performed by using different fiber modifications. We compared activities of the single molecules trapped in unmodified fibers, with fibers blocked with BSA and modified with a hydrophobic silane. (Discussed in detail in **Chapter 2**)

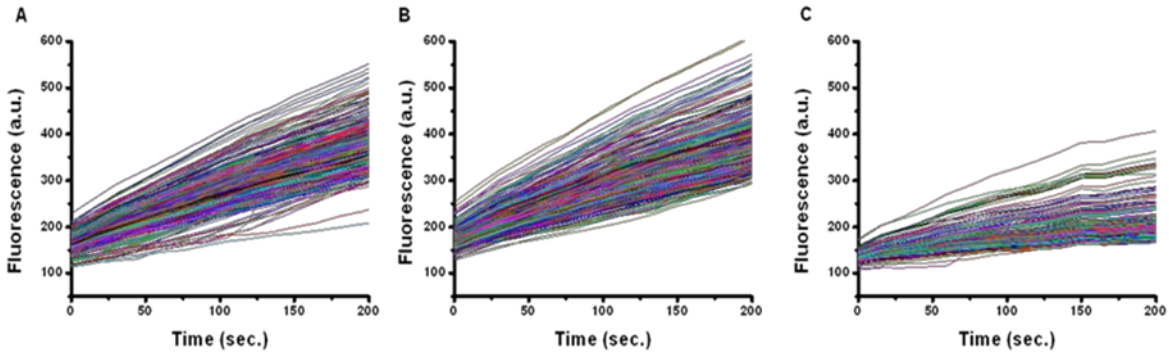

Figure 4.1. Activity traces of single β-galactosidase enzyme molecules for different surface modifications of the fiber. A and B represent modifications with BSA blocking buffer and silane respectively; C is an unmodified fiber.

The average turnover rates for each enzyme were obtained and compared with bulk experiments. The data obtained from BSA and hydrophobic silane-modified fibers showed similar results when compared with both bulk assays and unmodified fibers. However using the silane improved sealing, which was confirmed by photobleaching experiments (**Chapter 2**, Figure 2.25).

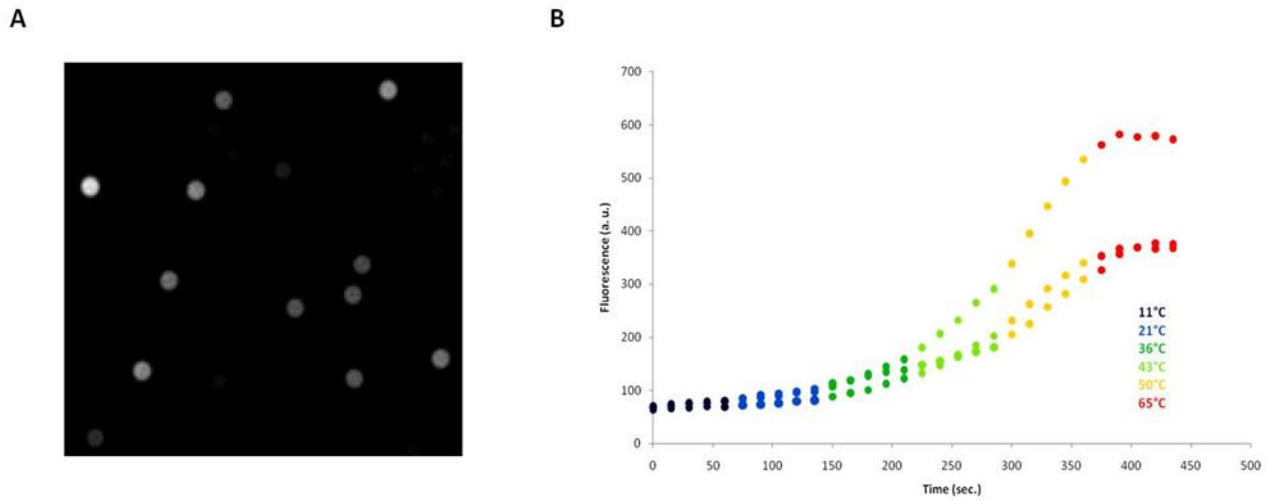

Figure 4.2. Single molecule activity experiment. (A) Fluorescence image of the fiber array with single β-galactosidase molecules trapped in 46-fL chambers (B) Fluorescence intensity traces as a function of temperature and time for individual enzyme molecules. The temperature of the array was kept steady for 75 sec (5 frames) and then was increased by approximately 10°C and stabilized within one frame time (15 sec). The temperature was increased in 10°C steps from 11°C to 65°C.

The activities of single β-galactosidase molecules trapped inside femtoliter chambers (Figure 4.2, A) were monitored as a function of temperature (Figures 4.2, B, 4.3, 4.4, A, B). While heating, the average activity of the molecules increased according to the Van't Hoff rule, and reached a maximum at 50 °C. (Figure 4.4, A) Similar results were previously reported for bulk studies of β-galactosidase.(*12, 15, 16*) We also observed a small population of enzymes (12%) that had lower thermal stability, however they were indistinguishable from the rest of the enzymes with respect to their activity.

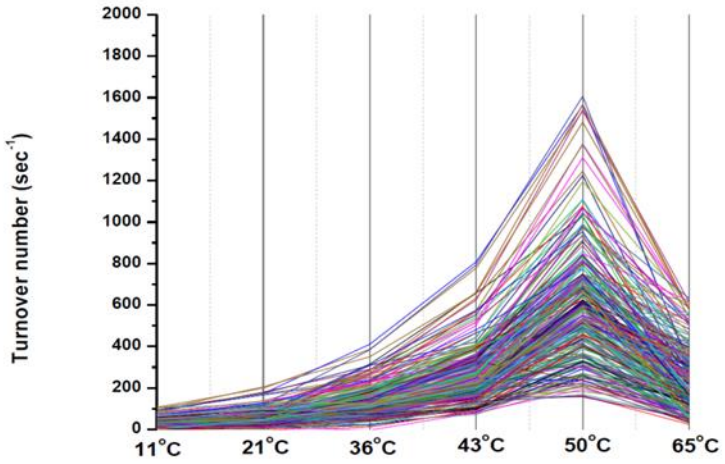

Figure 4.3. Graph of activities of hundreds of individual enzyme molecules as a function of temperature.

Both the individual enzyme activation energies and the average activation energy of the populations were calculated from the Arrhenius equation (Equation 4.1),

$$k = Ae^{-\left(\frac{E_a}{RT}\right)} \quad \text{(Eq. 4.1)}$$

where k is the rate of the reaction, E_a is the activation energy, R is the gas constant, T is the temperature in Kelvin and A is the frequency factor. The calculated average activation energy of 52 ±3 kJ/mol agrees well with the literature value of 55 ± 6 kJ/ mol for bulk experiments (Figure 4.4, B).(*13*)

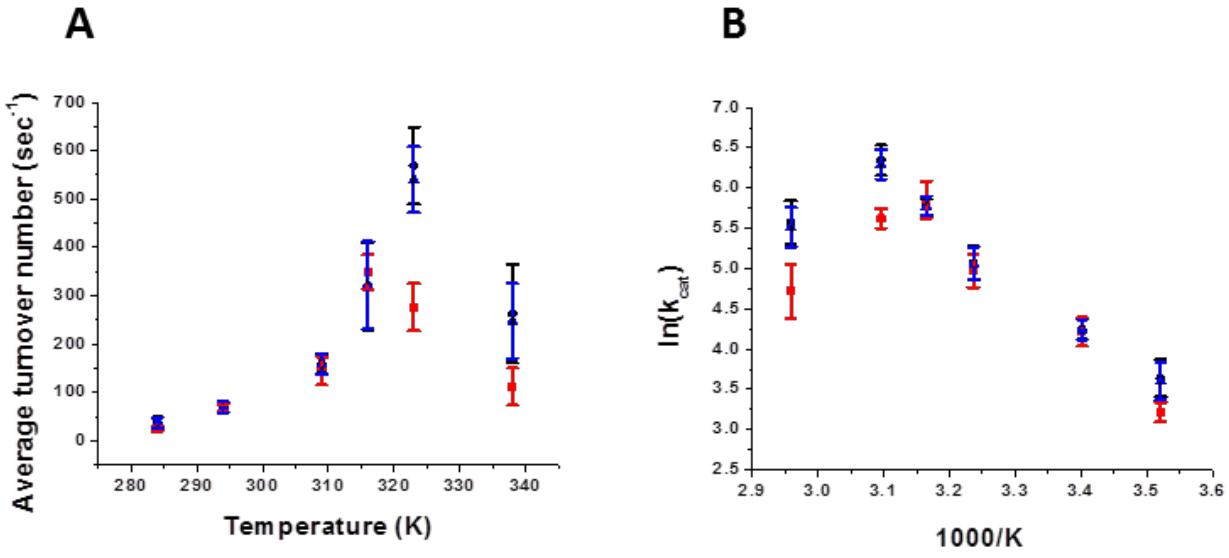

Figure 4.4. Single enzyme activities with respect to temperature. A) Average activity of thousands of β-galactosidase molecules as a function of temperature for more thermostable enzymes (black) and less thermostable enzymes (red). The average activity for the total population is in blue (B) Linear Arrhenius plot corresponding to Figure 2A. The calculated activation energy is equal to 52 ±3 kJ/mol and R^2=0.985. (52 ±3 kJ/mol for black and 57 ±6 kJ/mol for red). The error bars were obtained from four experiments with different fibers.

In addition, activation energies were calculated for individual enzymes and ranged from 5 to 115 kJ/ mol. (Figure 4.5, A) Values of activation energy for each individual enzyme molecule were plotted as a function of the initial activity of β-galactosidase (Figure 4.5, B). As expected, the activation energy decreased with respect to the initial activity. It should be noted that Equation 4.1 was derived for elementary steps and not for more complex enzyme reactions so it is not possible to obtain an absolute value for the free energy of activation.(*17*) Since ΔG_{act} and ΔH_{act} are directly linked to changes between the ground state and the transition state, we can use the Eyring-Polanyi Equation 4.2 to extract those values.(*18, 19*) Eyring analysis was performed to extract the activation entropy and enthalpy of the enzymatic reaction for the entire population and also for individual enzyme molecules. Although using the Eyring equation to obtain the magnitude of activation enthalpy is sufficient, determining the corresponding activation entropy

depends on the magnitude of the transmission coefficient. In most cases the transmission coefficient is treated as unity, (*20, 21*) however it is not theoretically justified. (*21*) Since it is impossible in our case to separate the transmission coefficient from the entropy of activation, the calculated entropy should be considered to be the "apparent" activation entropy. The thermodynamic parameter values of activation enthalpy $\Delta H^{\ddagger}$ and apparent activation entropy $\Delta S^{\ddagger}$ were obtained from Equation 4.3:

$$k = \frac{k_B T\kappa}{h} exp - \left(\frac{\Delta G^{\ddagger}}{RT}\right) \qquad \text{(Eq. 4.2)}$$

$$k = \frac{k_B T\kappa}{h} exp\left(-\frac{\Delta H^{\ddagger}}{RT} + \frac{\Delta S^{\ddagger}}{R}\right) \quad \text{(Eq. 4.3)}$$

where k, R, k_B and h are the overall reaction rate constant, gas constant, Boltzmann constant, and Planck constant, respectively, κ is the transmission coefficient and $(k_B T\kappa/h)$ exp $(\Delta S^{\ddagger}/R)$ corresponds to the pre-exponential factor A in the Arrhenius Equation 4.1. Both thermodynamic parameters, $\Delta H^{\ddagger}$ and $\Delta S^{\ddagger}$, and the activation energy E_a were calculated for the average population (Figure 4.4, B) and for individual enzyme molecules (Figure 4.5, A and Figure 4.6, A,B). The average enthalpy of activation of 50 kJ/mol and average apparent activation entropy of –49 J/mol*K for β-galactosidase are similar to the values reported in previous experiments (54 ± 3 kJ/mol for $\Delta H^{\ddagger}$ and -64.9 ± 4 J/mol*K for $\Delta S^{\ddagger}$). (*16, 22*)

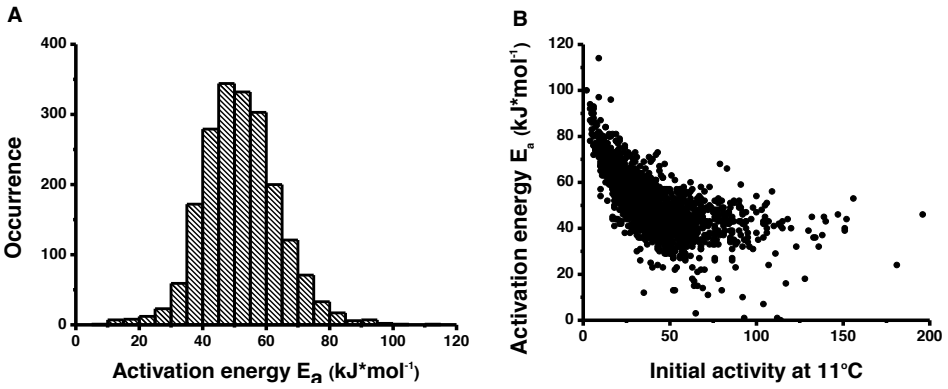

Figure 4.5. Single molecule histograms. (A) Activation energy distribution with a 5kJ/mol bin width. (B) Plot of the initial turnover numbers for individual enzymes at 11°C vs. their activation energies. At 11 °C the activity of the enzyme is strongly correlated to the activation energy. As expected, no high turnover enzyme has a high activation energy.

Taking advantage of the single molecule assay, we were able to calculate E_a, $\Delta H^{\ddagger}$ and $\Delta S^{\ddagger}$ for each individual enzyme molecule. When single enzyme molecules are analyzed separately, the activation energies differ from molecule to molecule and the distribution varies from 5 kJ/mol up to 115 kJ/mol with similar wide ranges for both $\Delta H^{\ddagger}$ (5 – 110 kJ/mol) and $\Delta S^{\ddagger}$ (-200 – 170 J/mol*K) (Figures 4.5, A, 4.6, A, B).While the single molecule turnover velocity distributions are in agreement with previously reported experiments and confirm the heterogeneity within the population, wide distributions of activation energies, enthalpies, and entropies are also observed (Figure 4.5, A, Figure 4.6, A, B). Figure 4.5, B shows a plot of the activation energy of individual enzyme molecules against their initial turnover rates at 11°C. As expected, a negative correlation between the activation energy and the activity of the enzyme can be seen—i.e. enzymes with a high turnover number have a low activation energy and vice versa. It is noteworthy that some of the enzymes with similar activation energies in the low activation energy regime have different turnover numbers ranging from tens to hundreds of turnovers per second.

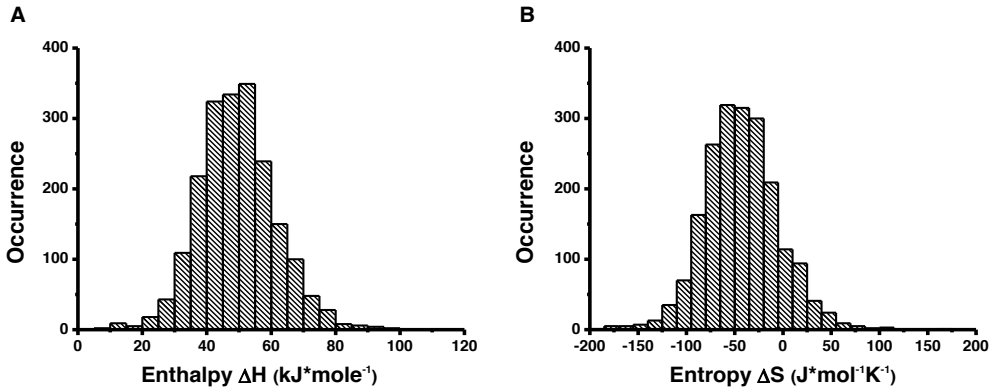

Figure 4.6. Single molecule histograms. (A) Enthalpy distribution of individual β-galactosidase molecules. The bin width is 5 kJ/mol. (B) Entropy distribution histogram with the 15 J/mol*K bin width.

In **Chapter 3**, we showed that individual enzyme molecules have stable conformations and that different conformations are primarily responsible for the observed distribution of enzyme activities.(*3, 4*) It is possible that enzymes with different conformations have different activities but have similar activation energies; however, enzymes might also be present that have different conformations and similar activities but have different activation energies (Figure 4.5, B).

The distribution of activation energies might be due to the changes in conformation near the active site and those changes may or may not be beneficial for enzyme activity. Moreover, a wide distribution of entropies and enthalpies is observed for individual molecules, yet the entropy-enthalpy relation is linear for the entire population. The likely reason for the distribution of entropies and enthalpies among ostensibly identical enzyme molecules is their different stable conformations.(*3, 23, 24*) Conformational changes during catalysis will generate different transition state structures. Those transition states might differ between individual molecules. When the entropies of individual enzymes are plotted with respect to the initial turnover numbers at 11°C, the positive values of entropy are associated with less active enzymes and the negative values are

associated with more active enzymes (Figure 4.7). The negative entropies suggest that the transition state is more ordered than the ground state.(*25*)

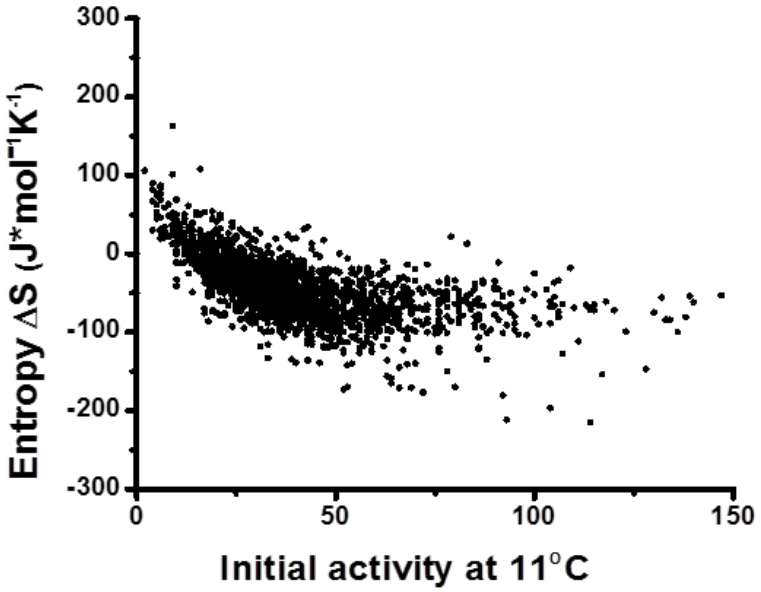

Figure 4.7 Plot of the initial activities of single enzyme molecules with their entropies. The entropy changes from positive values for low activity enzymes to negative values for high activity enzymes. The average entropy for the entire population is negative.

Entropy of activation of an enzymatic reaction may be positive or negative and reflects the difference in the number and character of the translational, rotational and vibrational degrees of freedom between the transition state and the reactant. Factors determining the size and magnitude of $\Delta S^{\ddagger}$ include changes in polarity at the reaction center, changes in solvation, changes in the conformation of the enzyme and associated changes in the structure of ordered networks of bound water molecules.(*26*) The formation of new hydrogen bonds would decrease entropy; however, the melting of water will increase entropy. One possible explanation for differences in the entropy in these single molecule experiments (both positive and negative) can be explained

by differences in enzyme conformations that affect water structure. Association of the correctly folded enzyme with the substrate results in release of the previously bound water and an increase in entropy. Formation of the well-ordered transition state $ES^{\ddagger}$ complex decreases entropy. The total change in entropy for the enzymatic reaction is negative if the enzyme is in the native conformation (Figure 4.8, A). On the other hand, if the enzyme is not in its native conformation it may still be able to bind to the substrate (E'S), but cannot directly proceed to $ES^{\ddagger}$. The molecule may need to change from its ground state conformation to the native conformation. The enzyme may undergo conformational changes where additional water is lost to form ES. The positive ΔS might correspond to E'S → ES instead of to ES→ $ES^{\ddagger}$ (Figure 4.8, B). In our data, we observe that for single β-galactosidase molecules, the entropy of activation is broadly distributed and ranges between negative and positive values. Furthermore, entropy of activation shows an inverse relationship with respect to turnover number, i.e., molecules with positive entropy have a low turnover number and molecules with negative entropy have a high turnover number. This inverse relationship between entropy and turnover number (Figure 4.7) suggests that the enzyme conformation changes are directly coupled to catalysis and that these changes play a dynamic role in the catalysis.

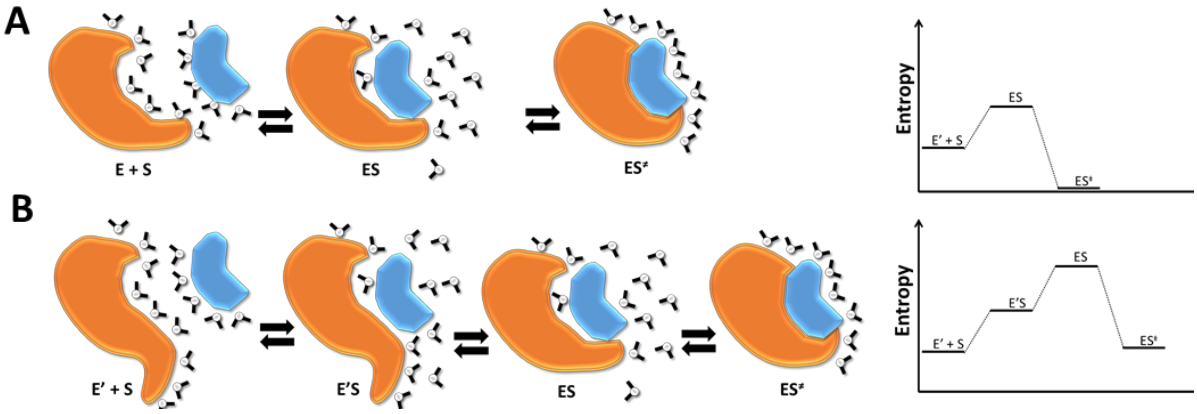

Figure 4.8 Schematic representation of the enzyme-substrate complex. The top row (A) represents the native enzyme (E) interacting with substrate (S) (blue). The binding of enzyme and substrate (ES) results in the release of ordered water resulting in an increase in entropy. Formation of the well-ordered transition state ($ES^{\ddagger}$) is accomplished by a conformation change that fits the substrate and is characterized by a decrease in entropy. In this case, the ΔS is negative. The bottom row (B) represents the enzyme in a non-native conformation (E'). The substrate binds to the enzyme, however the enzyme-substrate complex (E'S) cannot proceed to the transition state complex ($ES^{\ddagger}$) but needs to go through additional conformational changes where additional water is lost before it can form ES. The ΔS for this pathway is positive.(*27*)

The observed changes in the apparent activation entropy cannot be explained only by protein–solvent interactions. Any change in apparent activation entropy due to structuring of water molecules around the enzyme's exposed residues should be similar for all enzyme molecules. The most plausible basis for the wide distribution of apparent activation entropies is likely the differences in internal structure of the enzyme. Slight differences in primary structure or between alternative stable conformations can account for these entropy differences. The enzymes exhibiting low activities probably have conformations with less optimized transition state structures. It is important to note that activation energies were calculated from the Arrhenius equation. The assumption in these calculations is that E_a does not change with respect to temperature. This assumption is only valid when considering molecules that have an identical mechanism and transition state. If different enzymes have different conformations as is the case here, this assumption

is not entirely valid but it underscores the importance of conformation in determining the activities of individual enzyme molecules.

We also observed two different populations of the enzymes, where one population contains both thermostable (88%) enzymes and less thermostable (12%) enzymes. No difference in the thermodynamic parameters was observed between these two populations and both populations are indistinguishable with respect to activity. It is possible that enzymes that denature at lower temperatures contain more primary structure changes (amino acid differences due to errors in transcription and translation) that make them less stable. This difference in stability might be a primary reason for the biphasic Arrhenius plots observed previously.

4.3 Conclusion

In this chapter, we demonstrated that thermodynamic values for single enzyme molecules can be successfully measured. The wide range of temperatures used for the measurements provide more accurate values compared with previously-reported single molecule experiments and the average values for the thermodynamic parameters are in agreement with experimental values obtained from bulk experiments. The ability to analyze many single enzymes per experiment allows for the determination of the distribution of activation energies within a population. We showed that the activation energy, entropy and enthalpy varied significantly between individual enzyme molecules. In our experiments, we showed that single β-galactosidase molecules can have either positive or negative entropies of activation. We suggest that this variation may be due to different enzyme conformations**.** This method would be beneficial to explain the role that conformational changes play in the catalytic activity of enzymes. The method described here could be easily applied to different enzymes as long as the substrates used are thermostable. Moreover, the temper-

ature ramp could be modified so that the number of different temperatures used to collect data can be increased. It also will be beneficial from a bioengineering perspective to understand the basis of the high activity and low activation energy of some enzymes so that one can design enzymes with particular free energy characteristics. Is such high activity caused only by conformational differences or by differences in primary structure due to amino acid substitutions resulting from errors in transcription and translation? Moreover as shown in previous work, stable active conformations are the most important cause of the heterogeneity.(*4, 28*)

4.4 References

1. Z. D. Nagel, M. Dong, B. J. Bahnson, J. P. Klinman, Impaired protein conformational landscapes as revealed in anomalous Arrhenius prefactors. *Proceedings of the National Academy of Sciences of the United States of America* **108**, 10520 (Jun 28, 2011).
2. D. B. Craig, E. A. Arriaga, J. C. Y. Wong, H. Lu, N. J. Dovichi, Studies on single alkaline phosphatase molecules: Reaction rate and activation energy of a reaction catalyzed by a single molecule and the effect of thermal denaturation - The death of an enzyme. *J Am Chem Soc* **118**, 5245 (Jun 5, 1996).
3. D. M. Rissin, H. H. Gorris, D. R. Walt, Distinct and long-lived activity states of single enzyme molecules. *Journal of the American Chemical Society* **130**, 5349 (Apr 16, 2008).
4. M. J. Rojek, D. R. Walt, Observing Single Enzyme Molecules Interconvert between Activity States upon Heating. *Plos One* **9**, (Jan 21, 2014).
5. D. B. Craig, L. N. Chase, Arrhenius plot for a reaction catalyzed by a single molecule of beta-galactosidase. *Anal Chem* **84**, 2044 (Feb 21, 2012).
6. B. P. English *et al.*, Ever-fluctuating single enzyme molecules: Michaelis-Menten equation revisited (vol 2, pg 87, 2006). *Nat Chem Biol* **2**, 168 (Mar, 2006).
7. S. C. Kou, B. J. Cherayil, W. Min, B. P. English, X. S. Xie, Single-molecule Michaelis-Menten equations. *J Phys Chem B* **109**, 19068 (Oct 20, 2005).
8. L. Edman, Z. Foldes-Papp, S. Wennmalm, R. Rigler, The fluctuating enzyme: a single molecule approach. *Chemical Physics* **247**, 11 (Aug 1, 1999).
9. R. M. Daniel *et al.*, The molecular basis of the effect of temperature on enzyme activity. *Biochemical Journal* **425**, 353 (Jan 15, 2010).
10. T. M. Thomas, R. K. Scopes, The effects of temperature on the kinetics and stability of mesophilic and thermophilic 3-phosphoglycerate kinases. *Biochemical Journal* **330**, 1087 (Mar 15, 1998).
11. J. C. Kappelhoff *et al.*, Practical considerations when using temperature to obtain rate constants and activation thermodynamics of enzymes with two catalytic steps: native and N460T-beta-galactosidase (E. coli) as examples. *Protein J* **28**, 96 (Feb, 2009).
12. H. F. Arata, Y. Rondelez, H. Noji, H. Fujita, Temperature alternation by an on-chip microheater to reveal enzymatic activity of beta-galactosidase at high temperatures. *Anal Chem* **77**, 4810 (Aug 1, 2005).
13. D. B. Craig, Heterogeneous Properties of Individual Molecules of beta-Galactosidase from the Thermophilic Bacteria Geobacillus stearothermophilus. *Protein Journal* **29**, 55 (Jan, 2010).
14. D. M. Rissin, D. R. Walt, Digital concentration readout of single enzyme molecules using femtoliter arrays and Poisson statistics. *Nano Letters* **6**, 520 (Mar, 2006).

15. F. C. Chilaka, C. Okeke, E. Adaikpoh, Ligand-induced thermal stability in beta-galactosidase from the seeds of the black bean, Kestingeilla geocarpa. *Process Biochemistry* **38**, 143 (Oct, 2002).
16. M. I. Rajoka, S. Khan, R. Shahid, Kinetics and regulation studies of the production of beta-galactosidase from Kluyveromyces marxianus grown on different substrates. *Food Technol Biotech* **41**, 315 (Oct-Dec, 2003).
17. M. Oliveberg, Y. J. Tan, A. R. Fersht, Negative Activation Enthalpies in the Kinetics of Protein-Folding. *Proceedings of the National Academy of Sciences of the United States of America* **92**, 8926 (Sep 12, 1995).
18. K. Truong, Y. Su, J. Song, Y. Chen, Entropy-Driven Mechanism of an E3 Ligase. *Biochemistry* **50**, 5757 (Jun 28, 2011).
19. S. Hammes-Schiffer, Catalytic Efficiency of Enzymes: A Theoretical Analysis. *Biochemistry*, (Dec 14, 2012).
20. Y. S. N. Day, C. L. Baird, R. L. Rich, D. G. Myszka, Direct comparison of binding equilibrium, thermodynamic, and rate constants determined by surface- and solution-based biophysical methods. *Protein Sci* **11**, 1017 (May, 2002).
21. D. J. Winzor, C. M. Jackson, Interpretation of the temperature dependence of rate constants in biosensor studies. *Analytical Biochemistry* **337**, 289 (Feb 15, 2005).
22. N. Banzet, I. Heiberlanger, J. L. Saldana, P. Lemay, C. Balny, Pressure and Temperature Effect on Activity and Stability of Escherichia-Coli Beta-Galactosidase. *High Pressure and Biotechnology* **224**, 179 (1992).
23. K. Henzler-Wildman, D. Kern, Dynamic personalities of proteins. *Nature* **450**, 964 (Dec 13, 2007).
24. D. D. Boehr, R. Nussinov, P. E. Wright, The role of dynamic conformational ensembles in biomolecular recognition (vol 5, pg 789, 2009). *Nat Chem Biol* **5**, 954 (Dec, 2009).
25. K. Truong, Y. Su, J. Song, Y. Chen, Entropy-driven mechanism of an E3 ligase. *Biochemistry* **50**, 5757 (Jun 28, 2011).
26. G. G. Hammes, Multiple conformational changes in enzyme catalysis. *Biochemistry* **41**, 8221 (Jul 2, 2002).
27. R. B. Loftfield, E. A. Eigner, A. Pastuszyn, T. N. E. Lovgren, H. Jakubowski, Conformational-Changes during Enzyme Catalysis - Role of Water in the Transition-State. *P Natl Acad Sci-Biol* **77**, 3374 (1980).
28. D. B. Craig, T. Schwab, R. Sterner, Random mutagenesis suggests that sequence errors are not a major cause of variation in the activity of individual molecules of beta-galactosidase. *Biochemistry and Cell Biology-Biochimie Et Biologie Cellulaire* **90**, 540 (Aug, 2012).

Chapter 5: Thermal switches

5.1 Abstract

In this Chapter, we present single molecule experiments on two different β-glucuronidase mutants—code named D2 and D4. Both enzymes were obtained from the laboratory of Prof. Andrew Ellington from the University of Texas at Austin. Using the heating stage described in **Chapter 2,** we performed experiments at room temperature and at 37°C. In this Chapter we demonstrate that at the single molecule level a fraction of the individual enzymes behave as thermal switches, where they lack activity at room temperature but become active when treated with a heating pulse.

5.2 Introduction

β-glucuronidase from *E. coli* (GUS) is a glycosidase type enzyme that catalyzes the breakdown of carbohydrates.(*1*) It is a homotetramer with total molecular weight of 280 kDa.(*2*) In **Chapter 3,** we demonstrated that the main contribution to static heterogeneity in enzyme activity is the multiple stable conformations of the enzyme. Furthermore, any heterogeneity in activity distribution resulting from random errors in the protein primary structure that might occur due to translational errors likely overlaps with the activity differences due to the different conformations. However, if the mutation in the primary structure of the enzyme occurs at a specific amino acid, which can disturb the active site of the enzyme, the activity of the mutant might be drastically altered. It was previously shown that site-specific mutations can alter the thermal stability and activity of enzymes.(*3*) Disruption of salt bridges or changes to the metal binding sites can decrease or increase enzyme resistance to environmental factors such as

temperature or pH variations.(*4*, *5*) An increase in the number of disulfide bonds within the enzyme can alter its stability as well as activity. The two mutants obtained from Prof. Andrew Ellington lab have specific mutations, where the cysteine residue is exchanged with different amino acids (Appendix 3). These mutations prevent the enzyme from forming disulfide bridges and hence makes the protein more flexible so that it can access different conformations. Because of this flexibility, the enzyme can be easily switched between different conformations by introducing heat pulses. In this chapter, we demonstrate that the activity of enzymes with specific mutations can be irreversibly increased with a heat pulse, thereby resulting in a unidirectional thermal switch.

5.3 Materials and Methods

β-glucuronidase (GUS) D2 and D4 mutants were obtained from the Ellington laboratory (University of Texas, Austin) and shipped at -20 °C in 50 mM phosphate buffer at pH 7.4 (without any salts or glycerol present). The concentrations of the mutants were determined using the absorbance value at 280 nm (extinction coefficient = 139910$M^{-1}cm^{-1}$) measured using a NanoDrop instrument. The calculated concentrations are 31.4 μM and 19 μM for D-2 and D-4 mutants respectively. The samples were diluted with an equal amount of glycerol, aliquotted and stored at -80°C. The stock solutions were further diluted to 20 pM with 50 mM Na_2PO_4, 0.01% TritonX-100 (pH 6.5) immediately before analysis. Resorufin β-D-glucuronide sodium salt was purchased from Sigma Aldrich (St. Louis, MO) and the product resorufin from Invitrogen (Carlsbad, CA). 5 mM stock solution of Resorufin β-D-glucuronide sodium salt was prepared in DMSO, and aliquots of 5 mM were stored in -20°C. 5 mM Resorufin β-D-glucuronide was further diluted in 50 mM Na_2PO_4, 0.1% TritonX-100, pH 6.5 to a final concentration of 100 μM

for experiments. 1M Sodium phosphate buffer was purchased from Teknova (Hollister, CA) and TritonX-100 was purchased from Thermo Scientific (Waltham, MA).

Bulk experiments

Bulk experiments were performed on an Infinite M200 microtiter plate reader from Tecan AG (Mannedorf, Swithzaland). 100 μM of substrate solution was prepared in 50 mM Na_2PO_4, 0.01% TritonX-100, pH 6.5 reaction buffer. 15 μL of 20 nM enzyme was mixed with 135 μL of 100 μM substrate solution. The fluorescence intensity (λex=558 nm, λem=590 nm) was measured in the plate reader at 1 minute intervals for 30 minutes. To obtained the turnover number data, 20 nM of the enzyme (either D2 and D4—final concentration of 2 nM) was mixed with different concentrations of the substrate (0, 10, 25, 50, 75, 100 μM of final substrate concentration). The experiments were performed at room temperature as well as at 37 °C. Calibration curves of the resorufin product were obtained at both temperatures (Appendix 3).

Single Molecule Experiments

Single molecule experiments were performed using an array of femtoliter-sized wells generated on an optical fiber bundle as described previously.(*6, 7*) Optical fiber bundles consisting of ~ 50,000 individually clad optical fibers (diameter = 4.8μm, length ~ 2 in.) were purchased from Schott North America Inc. (Elmsford, NY) and femtoliter-sized well array fabrication was performed by acid etching of polished fiber bundles. Immediately after etching, the fiber wells surface was modified with silane to reduce the binding of the enzyme to the well surface.(*8*) Surface-modified fibers were used within 2-3 days of silanization (the detailed description is included in **Chapter 2**).

Isolation of single enzyme molecules in the femtoliter array is described in Figure 5.1. 100 µM of substrate solution was prepared in the reaction buffer (50 mM Na_2PO_4, 0.01% TritonX-100, 10 mM EDTA). The enzyme was diluted into the 100 µM substrate solution to a concentration of 2 pM and immediately sealed within the optical fiber wells. At a concentration of 2 pM, the probability of finding one molecule per well is 4.7 % with the majority of wells empty (95.1%). The probability of having 2 enzymes in a well is negligible. As a result each well has either 0 or 1 enzyme. The kinetics of the single enzyme molecule can be followed by recording the fluorescent signal generated due to the enzyme-catalyzed reaction, which converts the non-fluorescent substrate into a fluorescent product, resorufin.

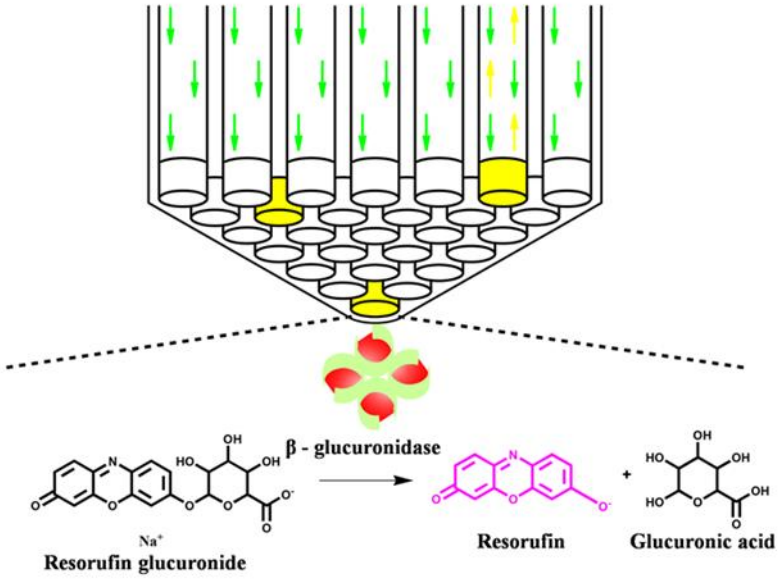

Figure 5.1. Schematic representation of the fiber bundle with individual enzymes trapped inside. When the enzyme is present inside the well it catalyzes the substrate hydrolysis releasing fluorescent product. The wells are sealed such that the released fluorescent product is locally concentrated within the well. When the fiber bundle is illuminated with the excitation light, only wells with the fluorescent product and enzyme will fluoresce.

To study the kinetics of the enzymes at elevated temperature we used the heating platform described in **Chapter 2**. The platform was programmed to maintain a constant temperature of 37°C for the high temperature experiments, and programmed to induce a heat pulse after the 20th frame for the heat pulse experiment. For the heat pulse, the temperature did not exceed 37°C (Figure 5.2).

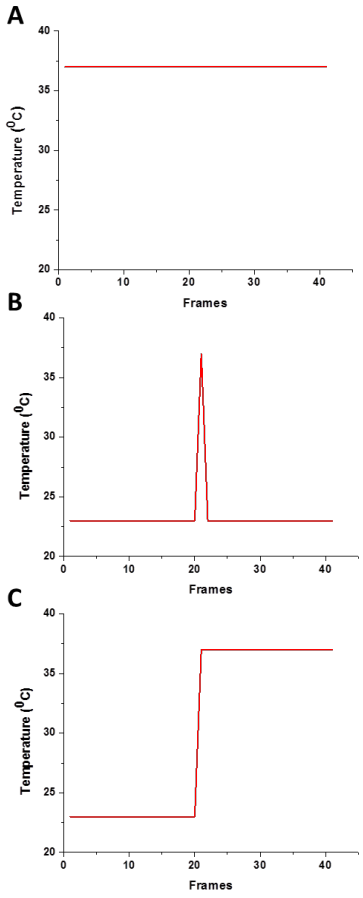

Figure 5.2. Schematic representation of the temperature readings from the heating stage used in this chapter. (A) A constant 37°C temperature was used during the entire experiment. (B) The heating pulse was activated immediately after the 20th frame. (C) Temperature jump from room temperature to 37°C.

Imaging and data analysis

Time lapse imaging of the fluorescent product generated as a result of enzyme catalysis, was performed with an upright Olympus B64 microscope equipped with a short arc lamp from Prior Scientific (Rockland, MA) and a CMOS Orca 4.0 camera (Hamamatsu, Japan). The excitation source and fluorescence emission were filtered through a Texas Red filter cube (Ex. 560/55x, Em. 645/75m, dichroic 595LP) from Chroma Technology Corp. (Bellows Falls, VT). The custom-built sealing stage was equipped with a Peltier plate for temperature measurements. The heating plate was control by a computer via LabView program from National Instruments (Austin, TX). Three different programs were used to perform heating experiments (Figure 5.2). Images of the distal end of the fiber were captured every 30 seconds for a period of 30 minutes. The Images were analyzed using the MATLAB software Image Processing Toolbox.

5.4 Results and Discussion

Bulk kinetic experiments of D2 and D4 were performed at room temperature as well as at 37°C on the microplate reader. The k_{cat} values obtained from bulk experiments are shown in Table 1. The turnover numbers were obtained using SigmaPlot from Systat Software Inc. (San Jose, CA) with a fitting program for the Michaelis-Menten Equation 5.1:

$$V = \frac{V_{max} \times [S]}{K_m + [S]} \quad \text{(Eq. 5.1)}$$

and

$$k_{cat} = \frac{V_{max}}{[E]} \quad \text{(Eq. 5.2)}$$

Where [E] is the total enzyme concentration, [S] is the concentration of the substrate and V is the velocity corresponding to the [S]. The turnover number is obtained from Equation 5.2.

Enzyme type	Measurement	k_{cat} at RT (sec.)	k_{cat} at 37 °C (sec.)
D2	Bulk	16	71
	Avg. Single Molecule	19	178
D4	Bulk	18	82
	Avg. Single Molecule	37	91

Table 5.1. The bulk and average single molecule turnover numbers for D2 and D4 mutants.

The turnover number for the D4 mutant in the bulk experiment was calculated as 18 sec^{-1}. When the experiment was performed at 37°C, the activity increased four-fold (82 sec^{-1}). The enzymatic reaction rate (k_{cat}) should rise with an increase in temperature based on the Arrhenius equation (**Chapter 4**, Eq. 4.1);. From collision theory, in order to convert substrate into product, enzymes must collide with and bind to the substrate at its active site. Increase in the temperature of a system will increase the number of collisions of the enzyme and substrate per unit time, hence the rate of the reaction should increase on average two times per 10°C increase in temperature. However the increase in activity in the D4 mutant is much higher. This unexpected increase in activity was also observed on the single molecule level. The calculated average activities of enzymes from the single molecule experiments are 37 and 91 sec^{-1} for room temperature and for 37°C respectively. By applying the single molecule experiments we showed that the number of active enzymes increased 5x at 37°C for the same working concentration of 2 pM. The results obtained from single molecule experiments suggest that some of the enzymes that are not active at room temperature within the population and gain activity when the temperature increased.This

additional increase of the population of new active enzymes it is a main reason for non Arrhenius increase in activity observed at bulk as well as at single molecule level experiments. Moreover, based on previous results obtained in experiments described in **Chapter 4** we would expect that the activity distribution at elevated temperature is similar to one at room temperature. Distributions should only differ by the shift to higher values as well slightly greater standard deviation. When the activity distribution was obtained for D4 mutant at the elevated temperature and compared to room temperature activity, two peaks of activity distribution become more distinguishable and do not resemble results obtained at room temperature (Figure 5.3). Data suggest that enzymes which become active after the heating greatly influence the activity change, however the origins of these populations need to be investigated further.

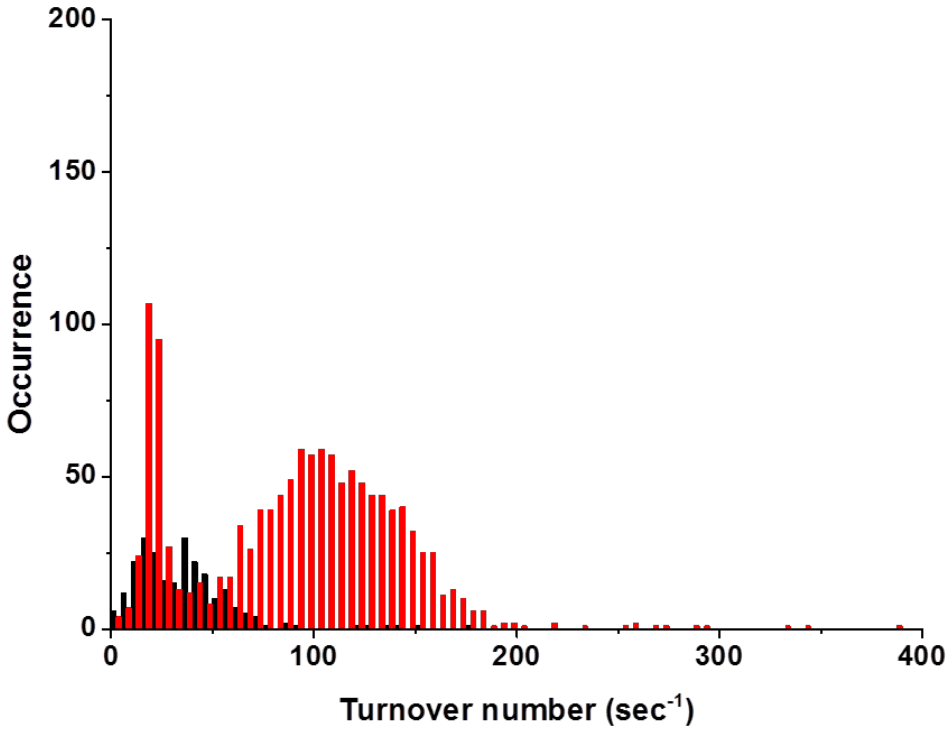

Figure 5.3. The activity distributions for the D4 mutant obtained from the experiments performed at room temperature (black) and at 37°C (red).

The observed switch from non-active to active enzyme might be reversible, and suggests that some conformational changes in enzyme's tertiary structure are involved. To elaborate more on this "on-off" activity behavior of the enzymes, we performed the heat pulse experiment (Figure 5.2, B), where the enzyme activity was recorded at room temperature, followed by a 10 second heat pulse at 37°C and back to room temperature. From the previous experiments performed in **Chapter 3**, we should expect random changes in the activity when the enzyme is subjected to a short heat pulse. Hence, the distribution of the enzyme should look similar before and after the pulse. However, when the entire population of the enzymes was exposed to the heat pulse, the activity distribution of enzymes shifted to higher values (Figure 5.4).

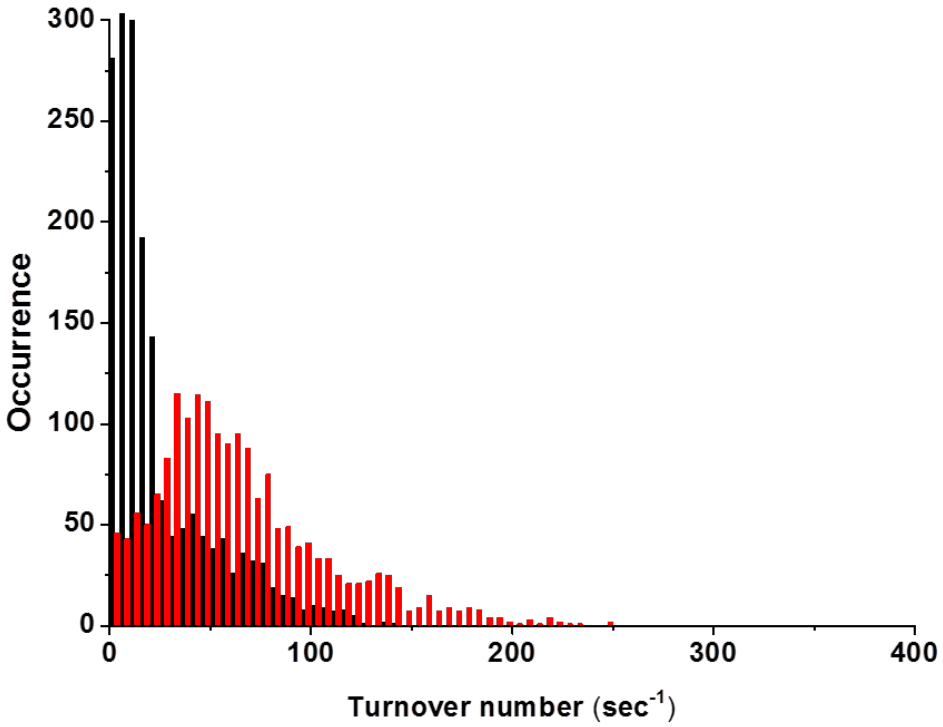

Figure 5.4. The distribution of activities of the D4 mutant before (black) the heating pulse and after (red) the heating pulse.

The average activity of the enzymes increased from 28 sec^{-1} to 61 sec^{-1}. It is noticeable that the distribution of the D4 mutant before heating in this experiment differs from the distribution showed in Figure 5.3. However the differences can be explained by the fact that the analysis performed in Figure 5.4 includes non-active enzymes that gained activity after the pulse. The average turnover number of enzymes that were active before the heat pulse is 33 sec^{-1}, which is comparable to the 37 sec^{-1} turnover number obtained from Figure 5.3.

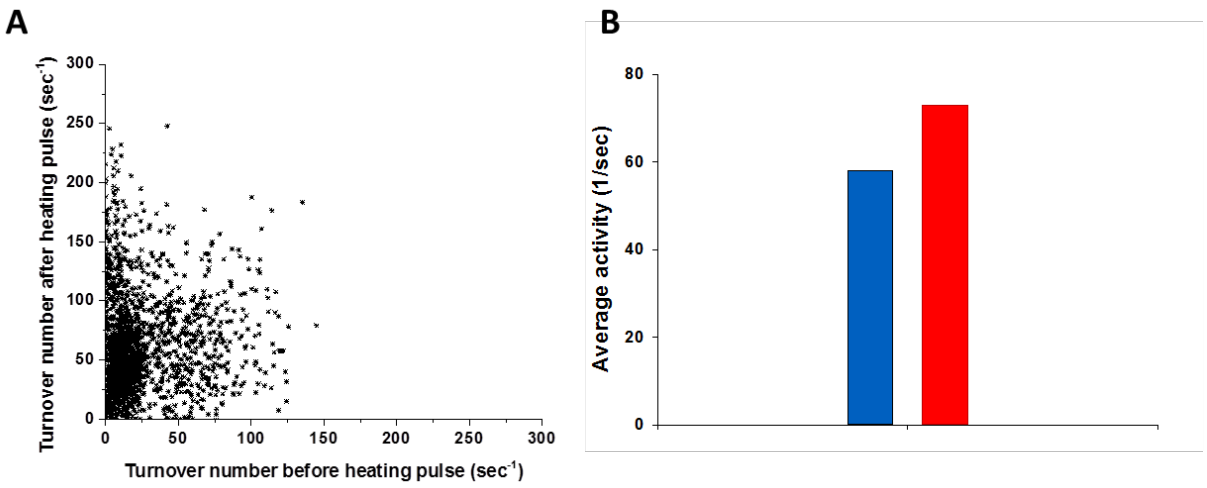

Figure 5.5. (A) The activity correlation graph before and after the heating pulse. (B) The average activities of the single molecules obtained after the heating pulse. The blue bar corresponds to the enzymes that were previously active. The Red bar represents enzymes that gained activity after the pulse but were not active before.

When the activity of individual enzymes before and after the pulse are compared, the activity of the majority of the enzymes increased, however the enzymes that were previously non-active gained activity above the average (Figure 5.5, A, B). It is interesting to note that after the enzyme activity increased due to the heat pulse, it did not revert when the system was cooled down. It is possible that some mutants were trapped in the stable but non active conformation at room temperature, before the heat pulse was administered. When the heat pulse was introduced to the system, the enzymes can overcome the energy barrier to go to the active conformation. Moreover this active conformation seems to be more stable than the non-active conformation and none of the active enzymes become non-active after the pulse.

Data obtained from both experiments suggest that there are two components associated with D2 temperature behavior. First, the activity increases with temperature as one would expect. In other cases, the enzymes isolated from the preparation do not exhibit any activity. Only when they heated above freshold temperature (in this case 37°C) they turn on. The average activities obtained from room and 37°C differ on average of 4 fold. However when the heating pulse is applied the average activity differs only 2 fold. We can conclude that the difference of two coming from Arrhenius relation and the additional difference is due to thermal switching hence any obtained average activity at 37°C temperature should be a multiplication of two.

The single molecule experiments described above were performed on the D2 mutant as well. An interesting feature of the D2 mutant is its activity gain at 37°C. The expected change in activity with respect to temperature is defined by the Arrhenius relationship where for every 10°C increase of the temperature the activity should increase two fold. However, from the bulk studies we observe that the activity increases four times for a 10°C increase in temperature. When single molecule experiments were performed, this rate difference increased to nine fold. The dramatic increase of the rate suggests that the temperature increase is turning on previously non active enzymes. Moreover the distribution of activity of individual enzymes observed at elevated temperature is wider (Figure 5.6).

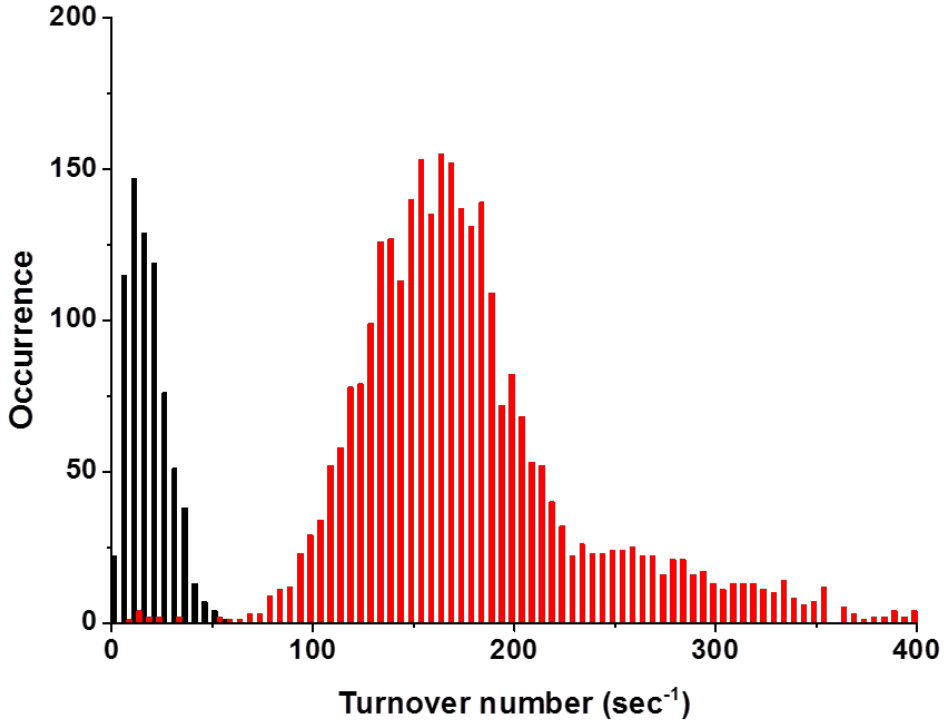

Figure 5.6 The activity distribution of the D2 mutant. The black bars correspond to the room temperature studies, and the red distribution is obtained from the enzyme at 37°C.

5.5 Future work

The preliminary results presented in this chapter show that the activity of individual enzymes can be switched on when a heating pulse is applied. Additional experiment should be performed on D2 mutant specially the heating pulse. Based on our hypothesis, the average activity after heating pulse should be 4-5 times greater than activity obtained before pulse. This switching efficiency might be correlated to the number of enzymes turning on during heating as well as to the changes in primary structure. More specific studies should be carried out to resolve what part of primary structure is responsible for non-active and active conformation switching. This thermal switch

could be beneficial for developing specific drug carriers, where a thermal pulse would trigger downstream enzymatic reactions.

5.6 Conclusion

In this chapter we present single molecule studies of two different mutants of β-glucuronidase enzyme. We presented that the activities of β-glucuronidase mutants do not follow the Arrhenius relation. However only by using the single molecule approach we were able to show that the previously non active enzymes can be thermally switched on and they are mostly responsible for unexpected increase in activity during the thermal studies.

5.7 References

1. M. Sinnott, *Comprehensive biological catalysis : a mechanistic reference*. (Academic Press, San Diego, 1998).
2. B. D. Wallace *et al*., Alleviating Cancer Drug Toxicity by Inhibiting a Bacterial Enzyme. *Science* **330**, 831 (Nov 5, 2010).
3. H. Flores, A. D. Ellington, Increasing the thermal stability of an oligomeric protein, beta-glucuronidase. *Journal of molecular biology* **315**, 325 (Jan 18, 2002).
4. C. Vieille, G. J. Zeikus, Hyperthermophilic enzymes: Sources, uses, and molecular mechanisms for thermostability. *Microbiol Mol Biol R* **65**, 1 (Mar, 2001).
5. A. Merz, T. Knochel, J. N. Jansonius, K. Kirschner, The hyperthermostable indoleglycerol phosphate synthase from Thermotoga maritima is destabilized by mutational disruption of two solvent-exposed salt bridges. *Journal of molecular biology* **288**, 753 (May 14, 1999).
6. D. M. Rissin, D. R. Walt, Digital concentration readout of single enzyme molecules using femtoliter arrays and Poisson statistics. *Nano letters* **6**, 520 (Mar, 2006).
7. D. M. Rissin, H. H. Gorris, D. R. Walt, Distinct and long-lived activity states of single enzyme molecules. *J Am Chem Soc* **130**, 5349 (Apr 16, 2008).
8. M. J. Rojek, D. R. Walt, Observing Single Enzyme Molecules Interconvert between Activity States upon Heating. *Plos One* **9**, (Jan 21, 2014).

Chapter 6: Single Molecule Anfinsen Experiment. Refolding Studies of Single RNase A Enzyme.

6.1 Abstract

Chapter 6 describes the thermal denaturation of monomeric enzyme and refolding studies performed on the single molecule level. In the majority of my experiments I used high molecular mass multimeric enzymes, which have a relatively large conformational freedom. In this Chapter, I performed single molecule experiments on the small 14 kDa monomeric enzyme, ribonuclease A (RNase A).

6.2 Introduction

In 1961, Anfinsen *et*. *al*. described the full recovery in activity of bovine ribonuclease A (RNase A) after chemical denaturation.(*1*) RNase A is a small extracellular enzyme that contains 124 amino acid residues and four disulfide bonds. The researchers used the reducing agent mercaptoethanol ($HS\text{-}CH_2\text{-}CH_2\text{-}OH$) and 8 M urea to completely unfold and destroy the tertiary structure of the enzyme. In the first phase of the experiment, they used mercaptoethanol to reduce all disulfide bonds and 8 M urea to destabilize the hydrogen bonds. Under these conditions the enzyme became an inactive, flexible polymer without any tertiary structure. The recovery of activity was accomplished by dialysis of urea from solution thereby allowing SH

groups present in the enzyme to slowly re-oxidize. The activity of the enzyme was fully recovered and sequence analysis demonstrated the formation of correct S-S bonds. Formation of native S-S bonds required the protein to explore configuration space thoroughly and only the correct configuration (out of 28 possible) was achieved.(*2*) These results led to the proposal that the information for correct protein secondary and tertiary structures was contained in the sequence itself, i.e. sequence determines structure.

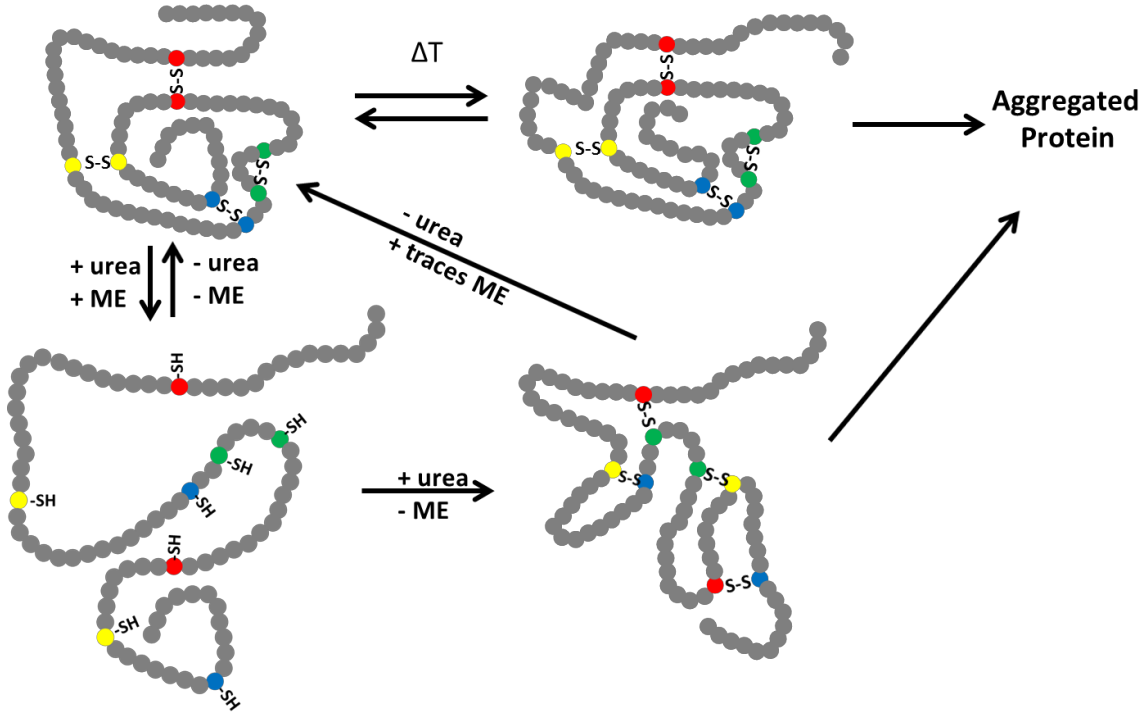

Figure 6.1. Schematic of chemical and thermal denaturation of RNase A. The addition of urea and mercaptoethanol (ME) completely denatures the enzyme. When both are removed the enzyme folds back into its native conformation. When only mercaptoethanol is removed, random disulfide bridges are created. However, when urea is removed and traces of reducing agents are present, the enzyme folds back to its native conformation. The thermal denaturation will change tertiary structure, however, the disulfide interchange may or may not occur.

However, from our previous single molecule experiments we concluded that enzymes can exist in several stable conformations, hence they possess slightly different tertiary structures. By using thermal denaturation we wanted to study refolding pathways of single enzymes. Through heat denaturation and enzyme isolation, we would be able to detect stable intermediates along the pathway or compare the activity before and after refolding. As a result, we would be able to detect any correlation between enzyme activities, refolding times, etc. However, our experimental setup prevents us from introducing any denaturing agents during the experiment. Instead of chemical denaturation, we performed thermal denaturation of the enzyme. Thermal denaturation has similar effects on the enzyme as chemical denaturation would; it disrupts any hydrogen bonding within the molecule (same as urea), triggers disulfide interchange, deaminates asparagine, hydrolyzes aspartic acid, and causes β-elimination of cysteine residues.(*3, 4*) When the enzyme is heated for a prolonged time or if the buffer contains reducing agents, the thermal denaturation might be irreversible preventing the study of activity after heating.(*4-6*) It is important to determine the right conditions so the enzyme can refold back to its active conformation.

6.3 Experimental

Materials

Lyophilized RNase A was purchased from Sigma Aldrich (St. Louis, MO). RNase A was purified in Prof. Ronald Raines laboratory at the University of Wisconsin, Madison by gel filtration chromatography followed by cation exchange chromatography.(*7*) 6 mg of lyophilized enzyme was shipped to our lab on dry ice. The enzyme was kept in a dry container at -20°C and was dissolved in 0.1 M Sodium Phosphate buffer, pH 6.5 from Teknova (Hollister, CA) to a

concentration of 27 μM before experiment. The enzyme was further diluted to a final concentration of 27 pM. The 46 μM RNase A substrate, tetranucleotide 6-FAM-dArUdAdA-6-TAMRA, was synthesized by the Raines lab at the University of Wisconsin, Madison. The substrate was stored at -20°C. The substrate contains 6-carboxyfluorescein (6-FAM) and 6-carboxytetramethylrhodamine (6-TAMRA) fluorescent dyes attached by a tetranucleotide chain (Figure 6.2).(*8*)

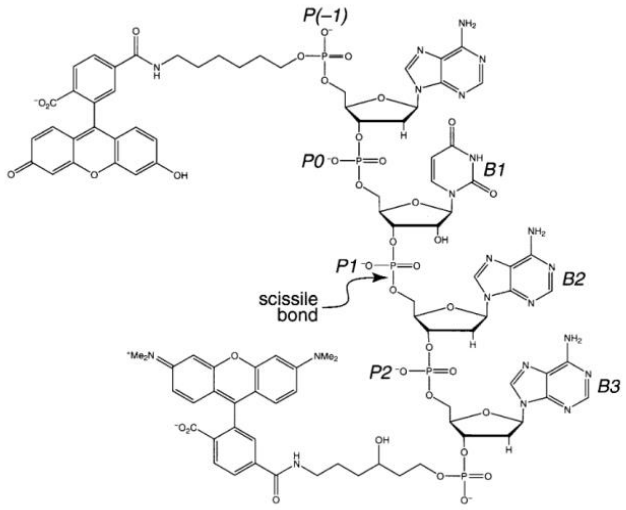

Figure 6.2. Chemical structure of the RNase A substrate.(*8*)

The fluorescence of 6-FAM is efficiently quenched by the 6-TAMRA dye. Upon enzymatic cleavage, the 6-FAM is released and emits a fluorescent signal. 6-FAM was obtained from Molecular Probes (Grand Island, NY) and used to generate the standard curve, the photobleaching rate and for optimizing the microscope filters. The 6-FAM fluorescent spectra under different conditions as well as enzymatic bulk experiments were performed on an Infinite M200 microtiter plate reader from Tecan AG (Mannedorf, Switzerland). To confirm thermal

stability, RNase A substrate and fluorescent 6-FAM product were exposed to 80°C for 1 min and the fluorescent intensities were measured. In addition, the average activity of the enzyme was obtained and compared with heated and unheated substrate. No difference in enzyme activity was observed, indicating that the substrate does not degrade substantially by heating.

Microscope and stage description

An upright Olympus B64 microscope with an attached mercury lamp as described in **Chapter 2** was used for single molecule experiments. A new filter cube (Ex. 475 nm, Em. 540 nm, dichroic 506 LP) from Semrock, Inc. (Rochester, NY) optimized for 6-FAM fluorescent dye was used for light filtering. The emission light was detected by a CMOS Orca 4.0 Flash camera from Hamamatsu (Hamamatsu City, Japan). The images were analyzed using Matlab program from MathWorks (Natick, MA). The stage used to seal the enzymatic assay was described in **Chapter 2**. The heating plate was used to perform the thermal denaturation studies of RNase A. The programmed temperature was above the denaturation temperature of the enzyme. The temperature traces recorded from the heating stage are depicted in Figure 2.22 in **Chapter 2**.

Microarray preparation

The optical fiber bundles were prepared as described in **Chapter 2**. After etching, the distal surface was treated with poly-l-lysine. A 0.1% (v/v) poly-l-lysine solution from Sigma Aldrich (St. Louis, MO) was diluted to 0.01% in DI water in a glass vial. Fiber bundles were partially immersed for 30 minutes and dried under nitrogen. Fiber bundles were used just after modification. In addition, the PDMS sealing sheet was immersed in 0.01% poly-l-lysine solution for 30 minutes and washed with DI water. Extra water was removed with Micro Alpha Swabs from Texwipe (Kernersville, NC).

Bulk experiments and assay optimization

For RNase A experiments we used the fluorescent dye 6-FAM. To maximize the signal to noise ratio a new filter cube was assembled, based on the excitation and emission spectra obtained from measurements with the Infinite M200 microtiter plate reader (Figure 6.3).

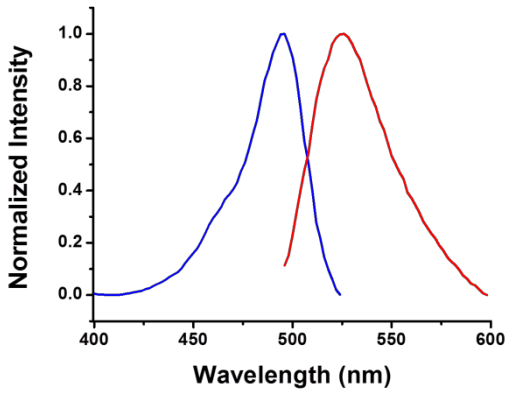

Figure 6. 3. The excitation and emission spectra of 10 µM 6-FAM fluorescent dye diluted in the reaction buffer.

The thermal stability studies of the substrate and product showed that with temperature increases up to 75°C for 1 min. the substrate and product remain unchanged with similar fluorescent intensities before and after heating (Figure 6.4).

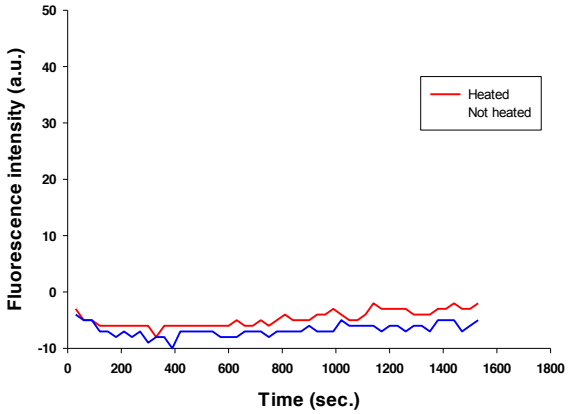

Figure 6.4. Fluorescence intensities of both heated and unheated substrate. 470 nM substrate was heated to 75°C for 10 min. and its fluorescence was compared with unheated substrate on the microplate reader at ex/em of 494/530 nm.

The bulk experiments of the thermal denaturation of the enzyme were performed on a JASCO J-720 spectropolarimeter. 0.5 mg/ mL RNase A was heated up to 90°C with the ramp of 1 degree per minute and cooled down at the same rate. The obtained results confirmed the reversible denaturation of the enzyme, which will enable us to perform refolding experiments on the single molecule level (Figure 6.5). The calculated denaturation temperature from bulk experiment of 70°C was used as a denaturation temperature for single molecule experiments.

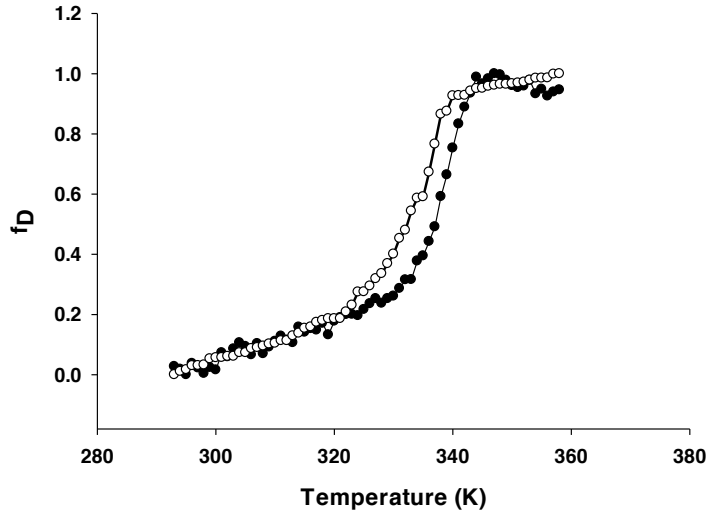

Figure 6.5. Near UV (222 nm) transition profiles for RNase A. Forward (black dots) and reverse (white dots) temperature scans were obtained from the JASCO J-720 spectropolarimeter.

Single molecule experiment results

The single molecule assay consists of surface-passivated microwells containing a single enzyme and a high concentration of the 6-FAM-dArUdAdA-6-TAMRA substrate. Upon enzymatic reaction the substrate is cleaved at a specific recognition site and the fluorescent 6-FAM dye is no longer quenched. Several surface modifications were examined to minimize any interaction of the trapped enzyme within the fiber wells (Figure 6.6, A, B).

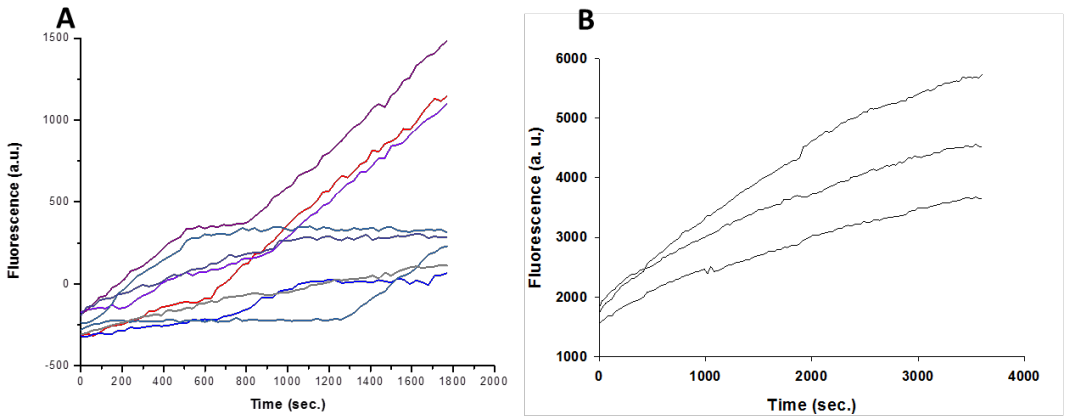

Figure 6.6. The fluorescence intensity traces of individual enzymes. (A) The on and off activity states of single enzymes mostly associated with surface interaction with the molecule. (B) The normal activity traces of the enzyme with the poly-l-lysine modification. Small abrupt changes observed in the traces are due to the image aligment process.

The individual enzyme turnovers were obtained and all the kinetics data were well characterized before denaturation experiments. As expected, the turnover numbers of individual enzymes were distributed over a range but had an average turnover number of 143 molecules per second (Figure 6.7). The distribution of the activities was narrower compared with the single molecule data obtained from β-galactosidase as well as for β-glucuronidase experiments (Chapters 3 and 5).

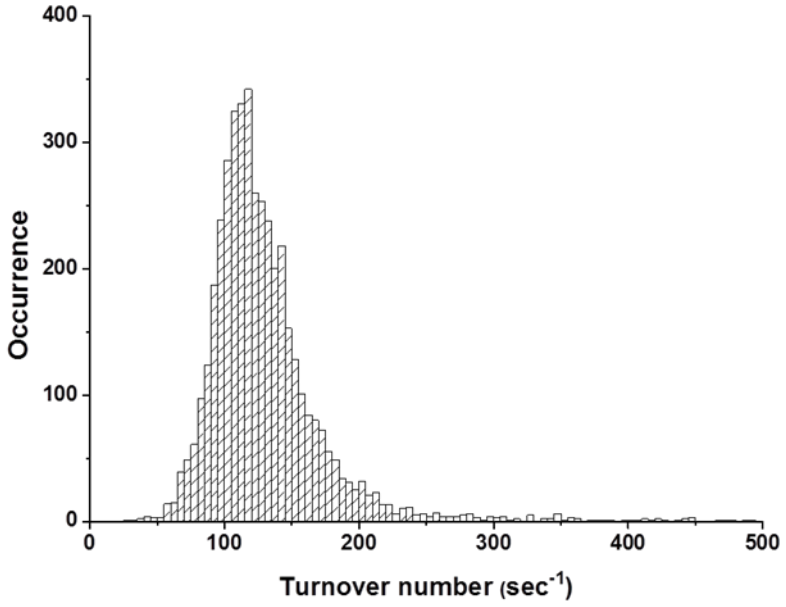

Figure 6.7. The activity distribution of single RNase A molecules. An average turnover number of 143 sec^{-1} was obtained.

As mentioned in Chapter 3, different stable conformations result in the observed static heterogeneity of enzyme activity.(*9*) Because the RNase A is a relatively small enzyme compared to the β-galactosidase and β-glucuronidase, the number of possible stable conformations available for RNase A should be lower, hence the distribution should be narrower which is what is observed. However, the relationship between the molecular size and the activity distribution cannot be obtained from the few enzymes used in this thesis. Further experiments with enzymes of different sizes should be performed.

6.4 Thermal Denaturation Experiments

In this section, we employed a heating stage to introduce a thermal pulse to denature the enzyme molecules. A heat pulse of 70°C for 30 seconds was applied to the system. The heat pulse was sufficient to thermally denature the enzyme molecules; moreover extended heating would lead to evaporation of the solvent through the PDMS sheet. First, the activity traces from individual enzyme molecules were obtained. The experiment at room temperature was performed for 480 seconds (16 frames) to make sure all active enzymes were detected. After the 16^{th} frame, the heat pulse was introduced for 30 sec. and the data acquisition was obtained up to the 73^{rd} frame. The denaturation temperature obtained from the bulk studies suggested that at 70°C all the enzymes should be denatured (Figure 6.5). From bulk studies, thermally denatured enzymes are expected to regain 85% of the activity after equilibrating with room temperature. In the single molecule experiment, the enzyme activity distribution before heating was similar to the single molecule room temperature studies performed in Section 6.3 with an average turnover number of 126 sec^{-1}. However, the average turnover numbers obtained from the enzymes after the heating pulse decreased to 32 sec^{-1} (i.e. only 28% of the average room temperature activity is regained). This result is inconsistent with bulk studies. In the single molecule heating pulse experiment four different responses were observed (Figure 6.8)– enzymes that have decreased activity (51%), enzymes that remain denatured (39%), enzymes that regain activity (9%), and enzymes that demonstrate no change in activity (1%).

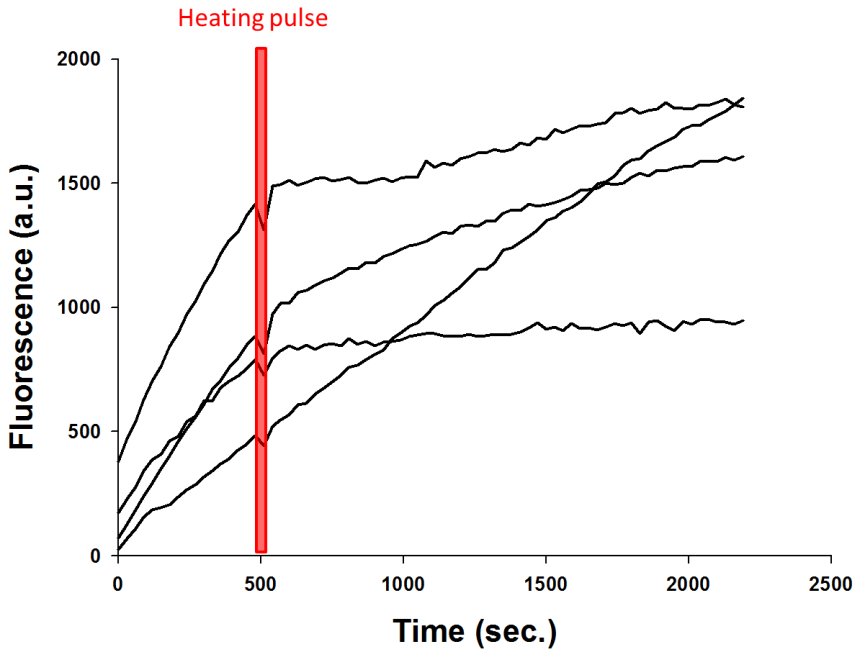

Figure 6.8. Activity traces of individual RNase A molecules. After heating some of the enzymes lost activity for an extend period of time whereas other enzyme molecules regained activity after the heating pulse.

Single molecule data show that denatured enzyme needs about 15 min. on average to regain the activity. However the time differs greatly between individual enzymes. The regained activity is stable and long-lived. For these enzymes, it would be interesting to correlate the regained activity with the refolding times, however, additional data has to be obtained.

The unprecedented loss in activity observed in the single molecule experiments compared with bulk can be associated with the surface interaction between the denatured enzyme and the modified surface. During the heating pulse the refolded enzyme can be irreversibly bound to the surface and the activity of this enzyme would be reduced. Additional experiments with different surface modifications should be performed in the future to determine if the enzyme is inactivated because of surface or because of non-correct refolding.

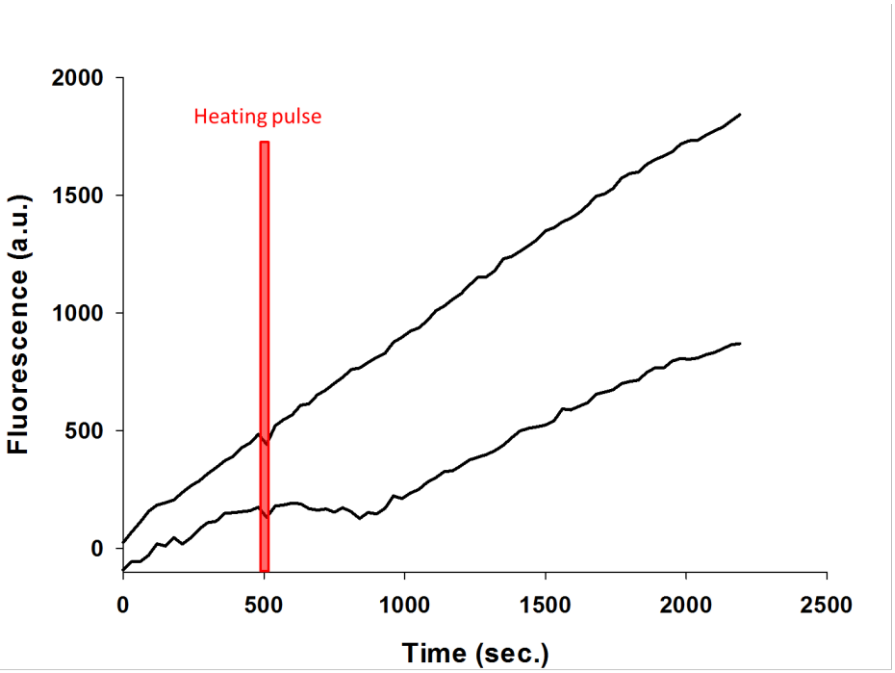

Figure 6. 9 Two different single molecule activity traces, which have the same activity before and after thermal denaturation.

6.5 Conclusions

In this Chapter we showed that using fiber bundles with the heating stage allows us to thermally denature individual enzymes. We show that some enzymes will regain activity after being completely inactive after heating. This proof-of-concept experiment can be successfully used for studying protein folding on the single molecule level without any need for immobilization or modification of the protein.

6.6 Future Work

To better understand the refolding phenomena of individual proteins additional experiments should be performed. In this Chapter we presented the experiments performed on single RNase

A molecules, however, observing other monomeric enzymes would help us to build reasonable and statistically correct theories. There is also room for improvement in our ability to introduce chemical denaturants thereby allowing us to compare thermal and chemical denaturation as well as the ability to study influences of stabilizing and destabilizing agents on the enzyme activity during the experiment. Such experiments would require the development of a permeable film which could allow us to selectively introduce different chemicals.

6.6.1 Different monomeric enzymes

We performed single molecule experiments as well as bulk thermal experiments on several different monomeric enzymes. With respect to the substrate stability and the enzyme activities we chose a few potential candidates for future studies. We have been doing preliminary experiments on lipase, chymotrypsin (FRET substrate) and West Nile virus (WNV) protease (FRET substrate). The denaturation temperatures of each type of enzyme have been measured in bulk using CD (Table 6.1). The obtained temperatures have been used as a reference temperature for thermal denaturation studies performed at the single molecule level.

Enzyme	**Denaturation temperature T_m**	**Reversibility**
Lipase	70-75°C	yes
Chymotrypsin	56-58 °C	yes
RNase A	70°C	yes
WNV protease	N/A yet	N/A yet

Table 6. 1. Tabulated monomeric enzymes which can be used for thermal studies.

6.6.2 Development of permutable film. Chemical denaturation of enzyme

Chemical denaturation allows us to repeat the Anfinsen experiment. In this experiment, two major components must be delivered to the sample: a reducing agent and urea. In order to perform chemical denaturation, a platform using a selectively permeable film must be developed. One of the ideas is to use a hydrogel-based platform. Using such a platform allows for a fiber to be loaded with enzyme and Ca^{2+} ions. After loading, the fiber is quickly washed with an alginate solution followed by oil sealing. A hydrogen membrane is formed when the alginate comes into contact with the Ca^{2+} ions (Figure 6.10). The thickness of the membrane can be controlled by altering the timing between adding the reagents and washing with the alginate solution.

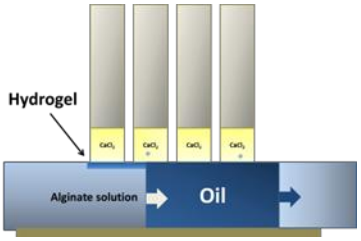

Figure 6. 10. Schematic of the hydrogel based platform. Fiber wells containing Ca^{2}+ ions are washed with an alginate solution.

6.7 References

1. C. B. Anfinsen, E. Haber, M. Sela, F. H. White, Kinetics of Formation of Native Ribonuclease during Oxidation of Reduced Polypeptide Chain. *P Natl Acad Sci USA* **47**, 1309 (1961).
2. G. M. Seddon, R. P. Bywater, Inactivation and reactivation of ribonuclease A studied by computer simulation. *Open Biol* **2**, (Jul, 2012).
3. S. D. Stelea, P. Pancoska, A. S. Benight, T. A. Keiderling, Thermal unfolding of ribonuclease A in phosphate at neutral pH: Deviations from the two-state model. *Protein Sci* **10**, 970 (May, 2001).
4. S. E. Zale, A. M. Klibanov, Why Does Ribonuclease Irreversibly Inactivate at High-Temperatures. *Biochemistry* **25**, 5432 (Sep 23, 1986).
5. S. E. Zale, A. M. Klibanov, Mechanisms of Irreversible Thermoinactivation of Enzymes. *Annals of the New York Academy of Sciences* **434**, 20 (1984).
6. S. E. Zale, A. M. Klibanov, On the Role of Reversible Denaturation (Unfolding) in the Irreversible Thermal Inactivation of Enzymes. *Biotechnology and bioengineering* **25**, 2221 (1983).
7. S. B. Delcardayre *et al*., Engineering Ribonuclease-a - Production, Purification and Characterization of Wild-Type Enzyme and Mutants at Gln11. *Protein Eng* **8**, 261 (Mar, 1995).
8. B. R. Kelemen *et al*., Hypersensitive substrate for ribonucleases. *Nucleic Acids Res* **27**, 3696 (Sep 15, 1999).
9. M. J. Rojek, D. R. Walt, Observing Single Enzyme Molecules Interconvert between Activity States upon Heating. *Plos One* **9**, (Jan 21, 2014).

Appendix 1:

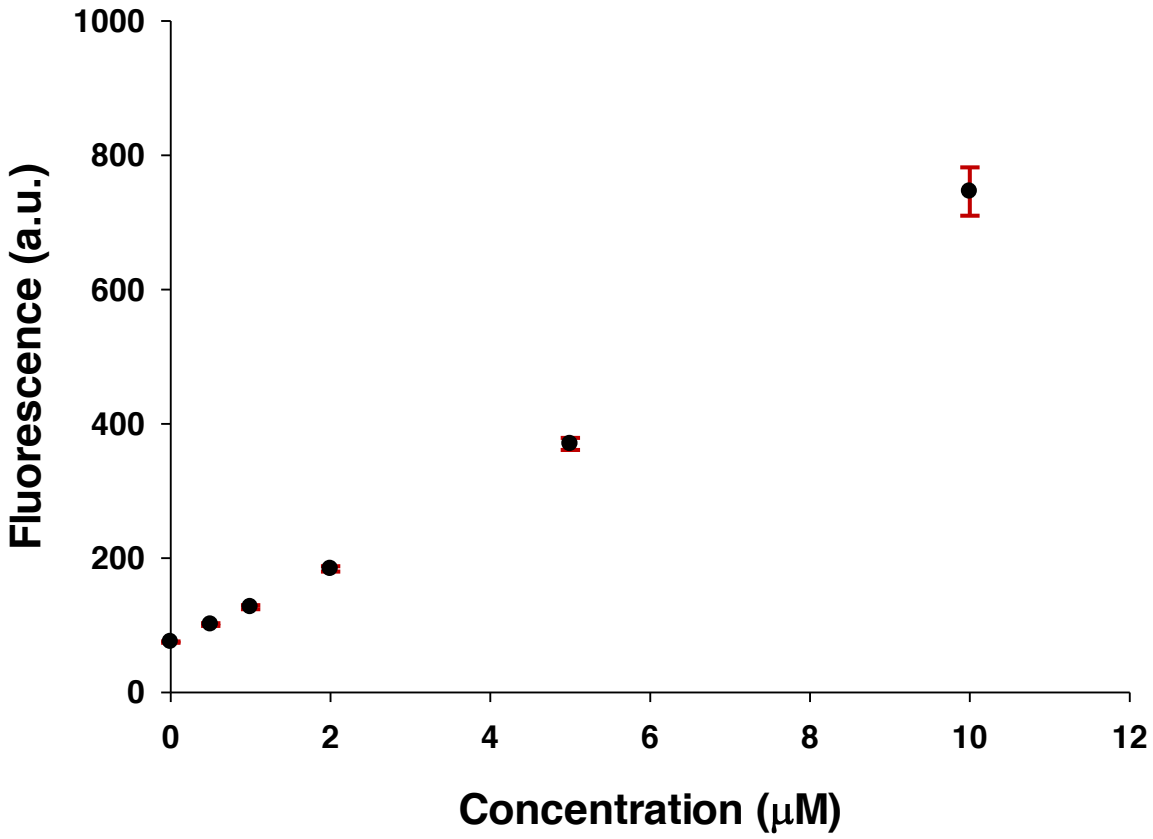

Figure A 1.1. Standard curve of resorufin obtained from upright microscope. One fluorescent unit corresponds to 413 molecules.

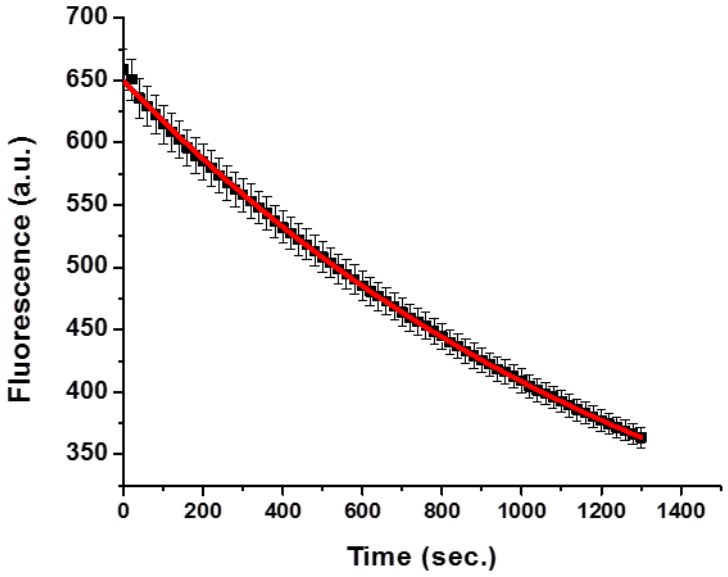

Figure A 1.2. Photobleaching rate of 0.0007 (1/sec.) obtained from the fiber array. Error bars correspond to different intensities of the wells across the fiber array. The calculated SD for the photobleaching rate is equal to 2.0 x 10^{-5}. Data are obtained from more than 2000 wells. The photobleaching rate distribution was equal across the fiber array. Calculations were performed using OriginPro fitting logarithmic decay function.

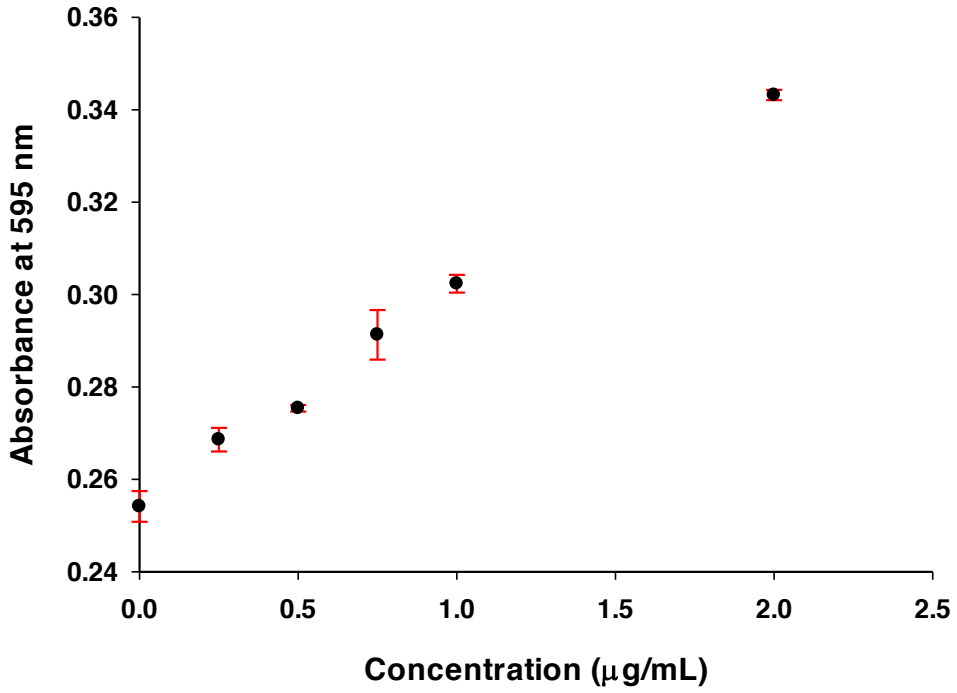

Figure A 1.3. Bradford Assay standard curve for determining the concentration of the β-galactosidase enzyme discussed in Section 3.2.2.

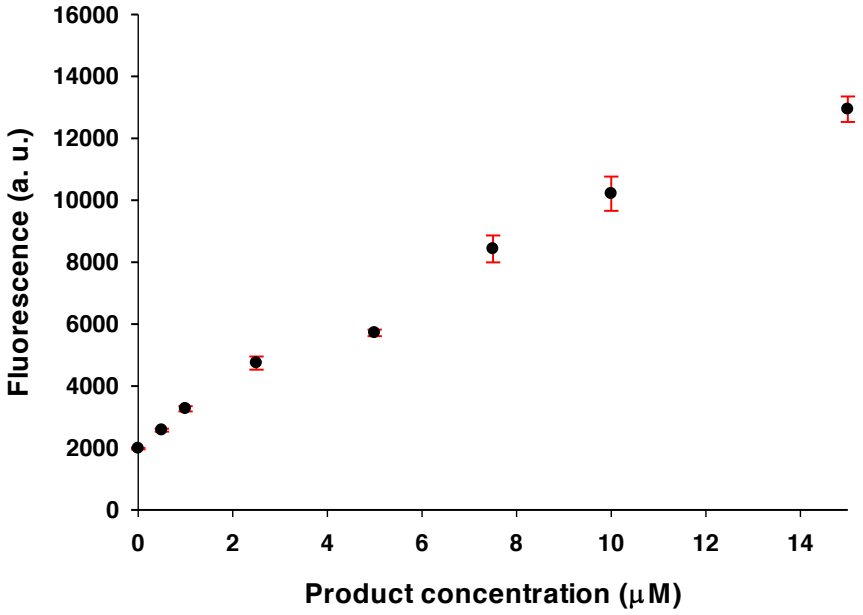

Figure A 1.4. Standard curve of resorufin obtained from the Quanterix imager on fiber strip #772. Calculated fluorescence unit corresponds to 41±2 molecules of the fluorescent product.

Appendix 2:

β-galactosidase mass spectrometry analysis

Performed by Dr. Marianna Budnik and Prof. Catherine E Costello, BUSM CBMS (NIH Research Resource grant P41 GM104603)

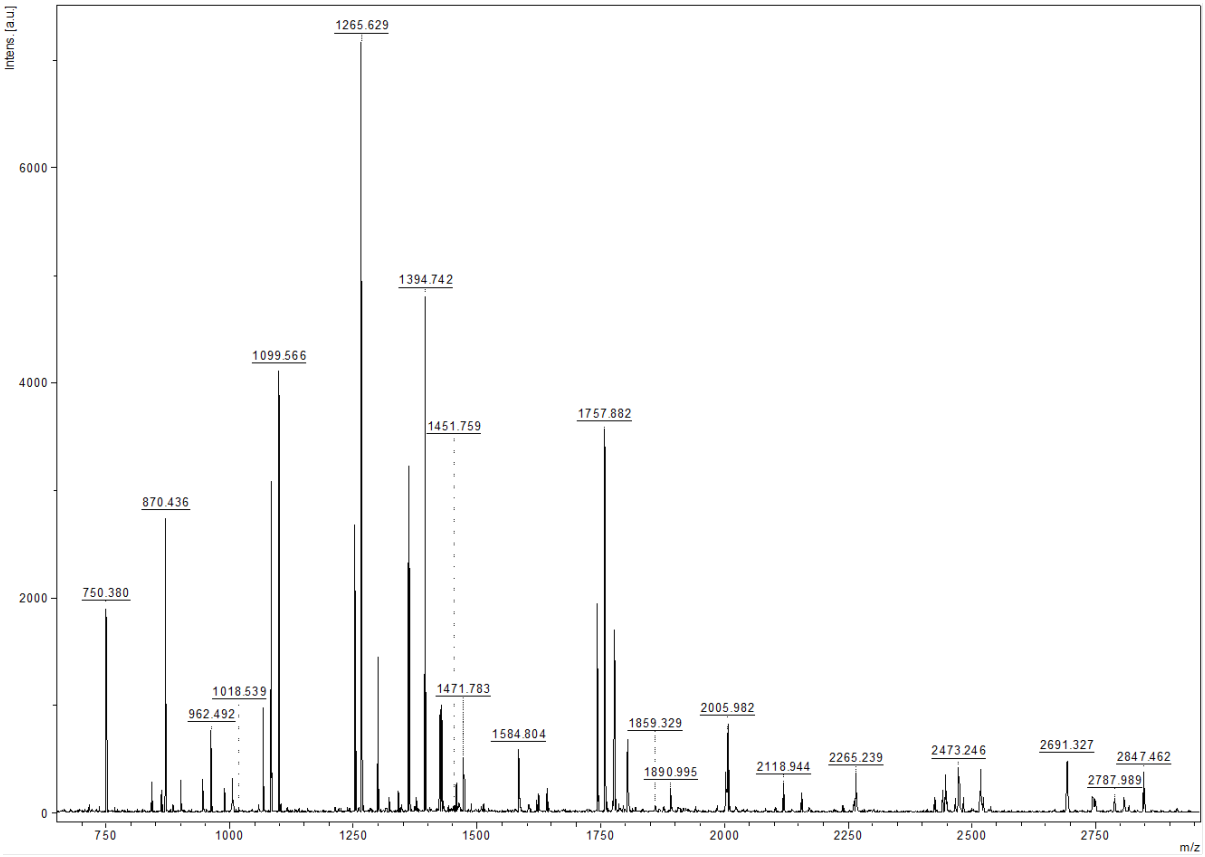

Figure A 2.1. MALDI MS spectrum of trypsin digested β-galactosidase. The analysis was performed on the Bruker UltrafleXtreme TOF/TOF MS, operated in the reflectron mode. The sample was cleaned with a Ziptip™ (EMD Millipore,Billerica,MA) and 1 µl was spotted on DHB (2,5-dihydroxybenzoic acid, Bruker, Billerica,MA) matrix with 1 µl of saturated solution at ~ 1 mg/ml concentration for the digest sample. The obtained data were run against Mascot Search Engine (Matrix Science) with protein sequence coverage of 46%.

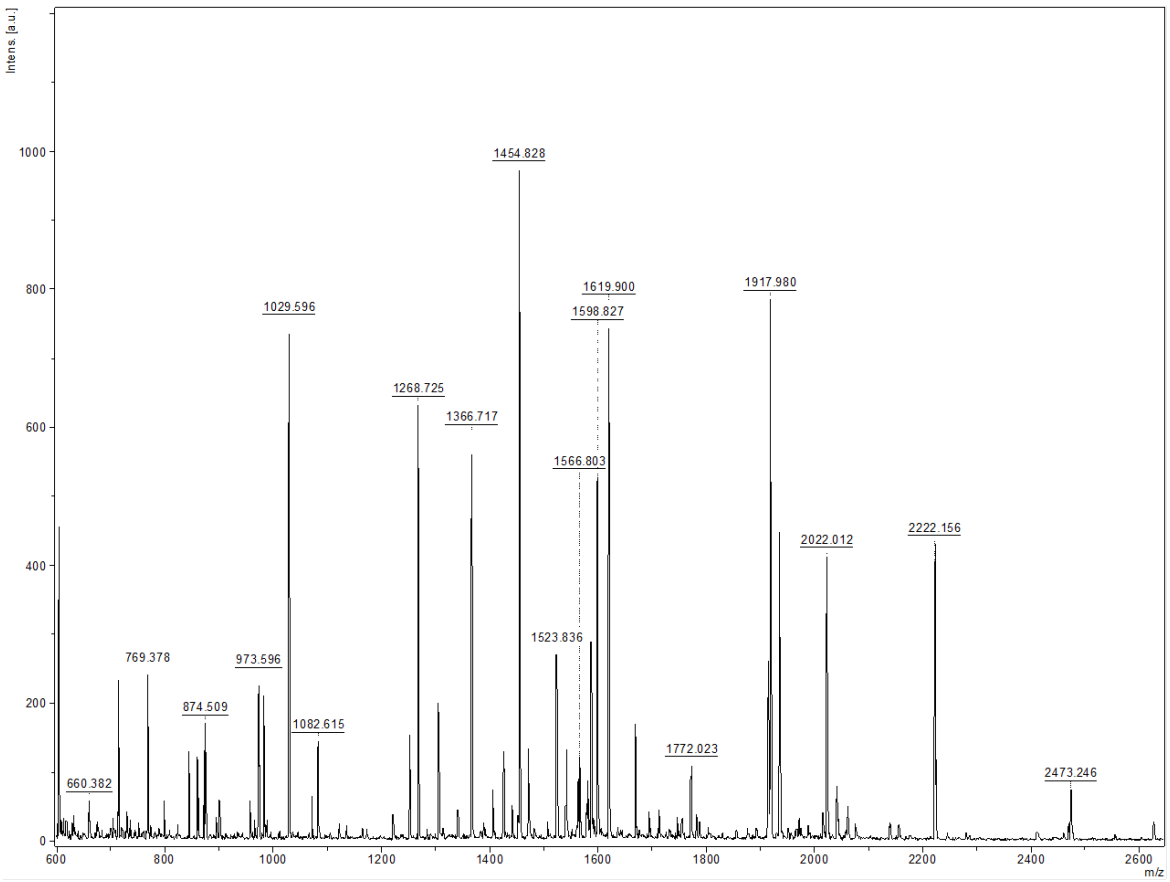

Figure A 2.2. MALDI MS spectrum of chymotrypsin digested β-galactosidase. The analysis was performed on the Bruker UltrafleXtreme TOF/TOF MS, operated in the reflectron mode as previously described. The protein sequence coverage of 38% was obtained.

Agilent 6550 Q-TOF LC/MS/MS

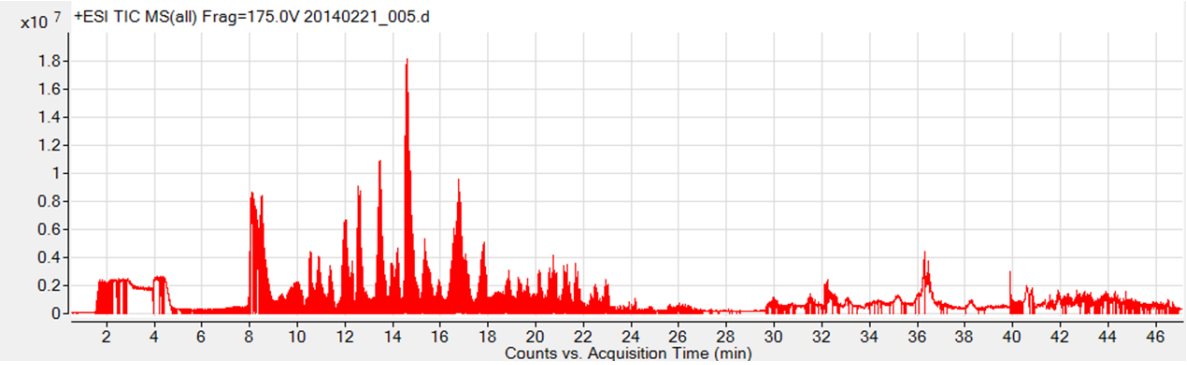

Figure A 2.3. Trypsin-digested β-galactosidase spectrum obtained from an Agilent 6550 Q-TOF mass spectrometer interfaced with an Agilent 1290 Infinity HPLC equipped with Chipcube™. Samples were run on the linear gradient from 2% to 40% buffer B (99% acetonitrile, 1% water, and 0.1% formic acid) for 25 min. with flow rate of 250 nl per minute. Sample was sprayed into the instrument using a Polaris-HR-Chip 3C18. The method of top 6 ions was used for this analysis. Searches were done on Mascot (Matrix Science) with 10 ppm accuracy for the precursor (parent mass) and 50 mmu for fragment ions. The protein sequence coverage of 69% was obtained.

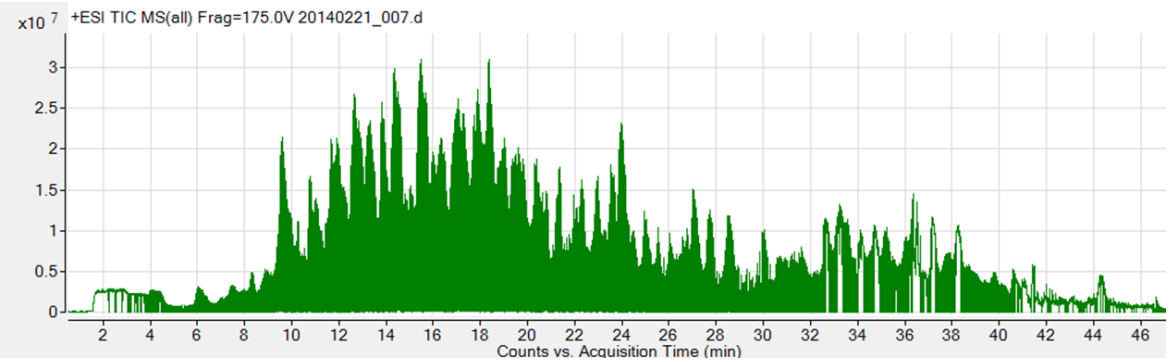

Figure A 2.4. Chymotrypsin digested β-galactosidase spectrum. Data obtained as described in Figure 11. Obtained sequence coverage is 7 %. The total sequence coverage obtained by using the Agilent 6550 for both digestions is 96.4% .

LTQ-Orbitrap analysis of β-Galactosidase

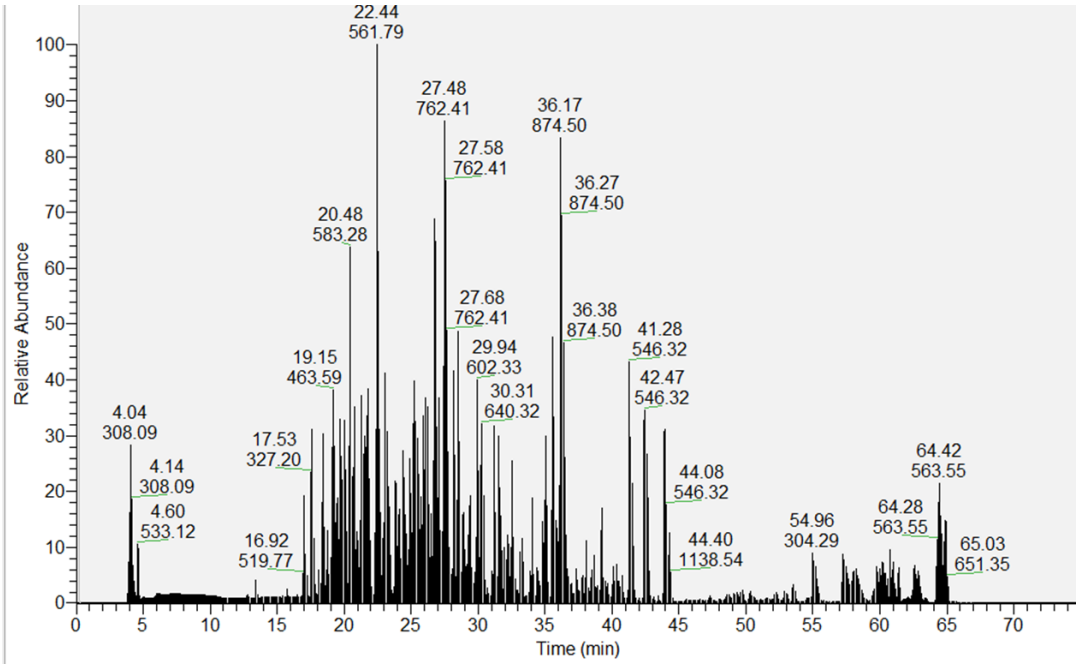

Figure A 2.5. LTQ-Orbitrap spectra for chymotrypsin digested β-galactosidase. Data were searched against E coli database with 20 ppm for parent ion and 0.6 Da for fragment ions.

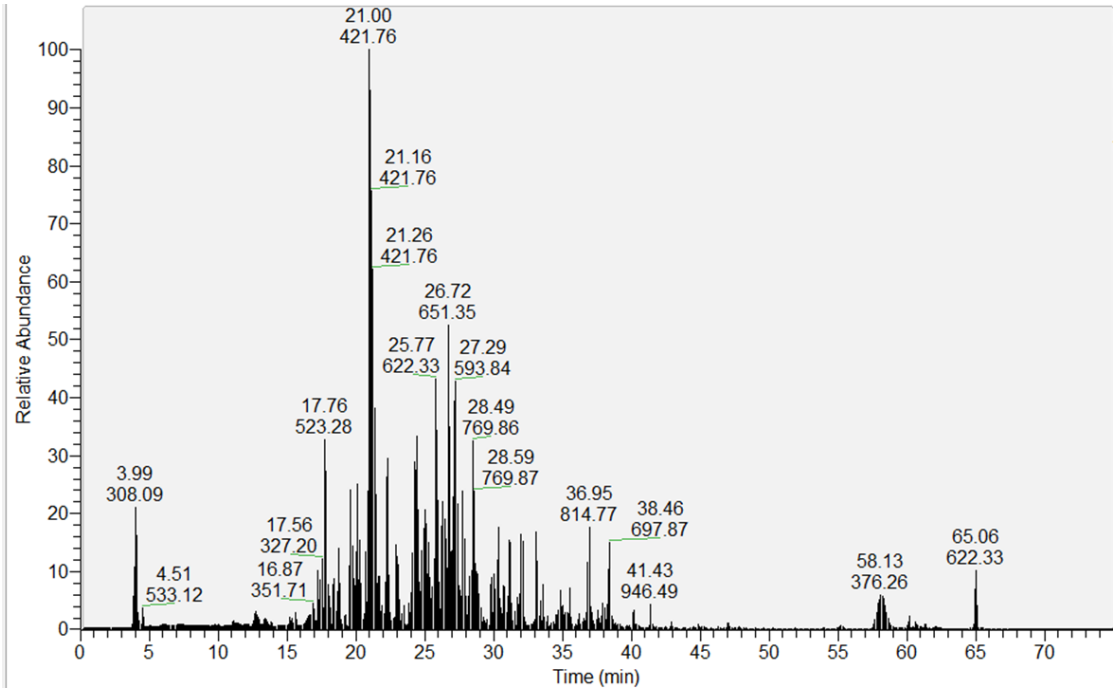

Figure A 2.6. LTQ-Orbitrap spectrum of trypsin digested β-Galactosidase. Data were searched against *E coli* database with 20 ppm for parent ion and 0.6 Da for fragment ions. The total obtained coverage for trypsin and chymotrypsin digestion was 94 %.

Appendix 3:

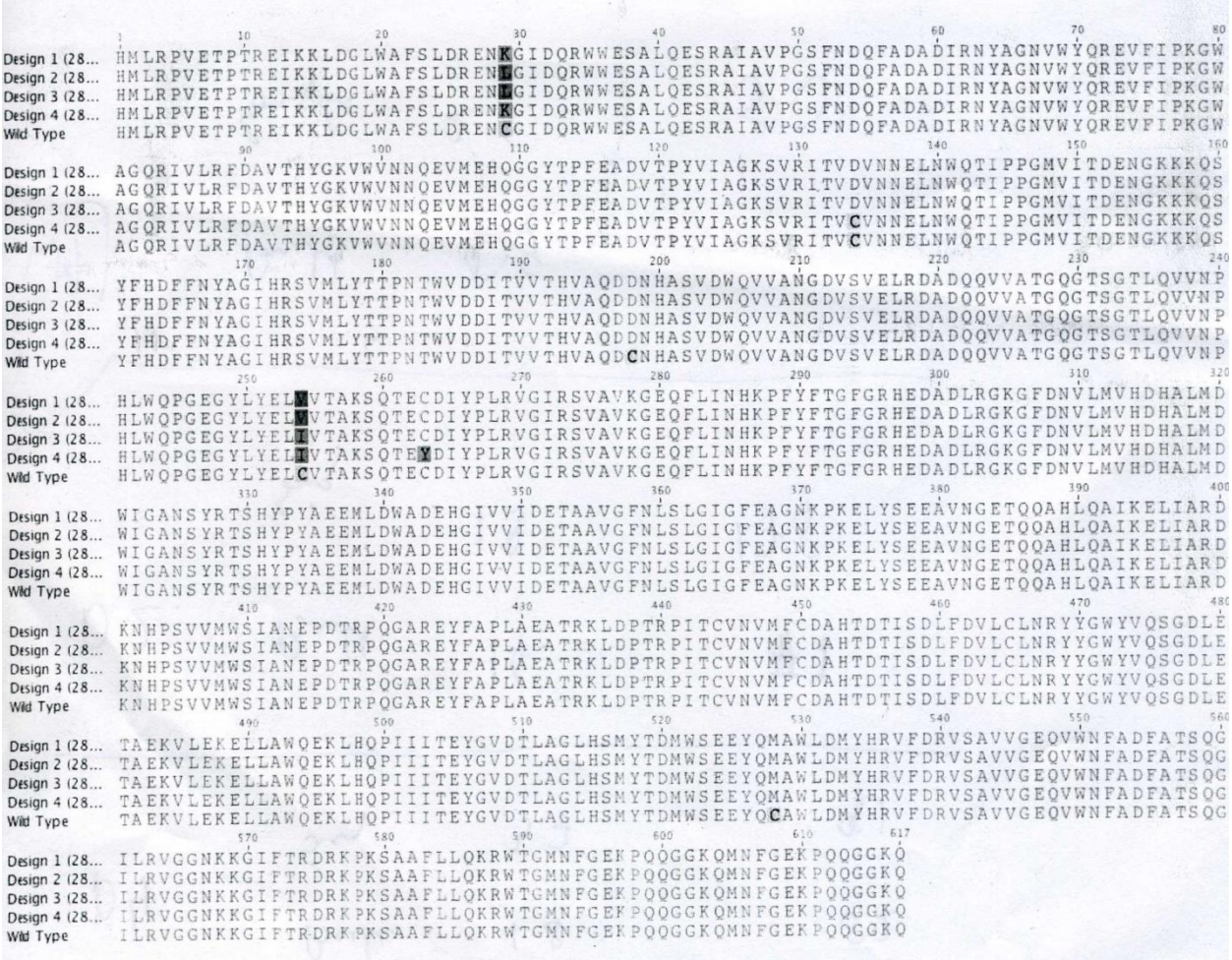

Figure A 3.1. Amino acid sequence of β-glucuronidase mutants. Design 2 (D2) and design 4 (D4) were analyzed in Chapter 5.

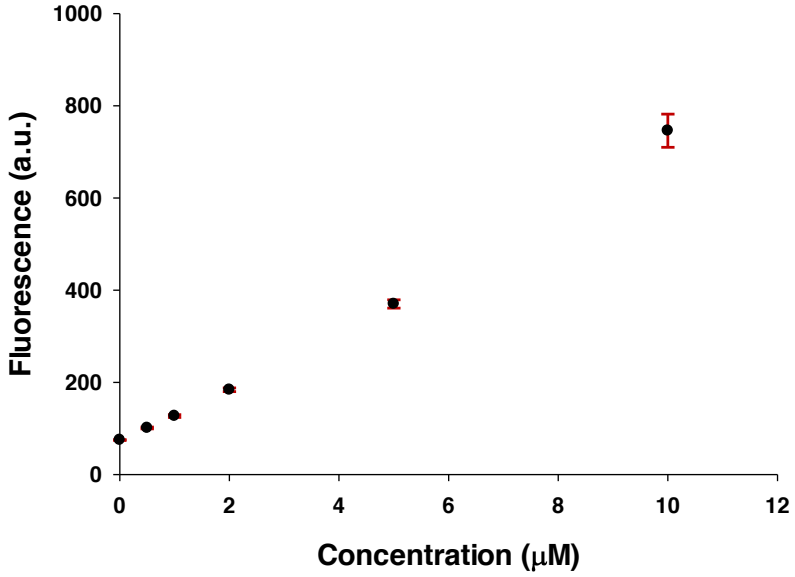

Figure A 3.2. Standard curve of resorufin obtained from upright microscope for experiments described in Chapter 5.